Optimization and Applications of Fluorescence anisotropy assays and Fluorescence Resonance Energy Transfer Measurements

by

Mangala Roshan Liyanage
B.Sc. University of Peradeniya, 2002

Submitted to the Department of Chemistry and the
Faculty of the Graduate School of the University of Kansas
in partial fulfillment of the requirements for
The degree of Doctor of Philosophy

Prof. Carey K Johnson (Chair)

Prof. Robert C. Dunn

Prof. Sue Lunte

Prof. Cindy L. Berrie

Prof. C. Russell Middaugh

Date defended: 04/27/2009

The Dissertation Committee for Mangala Roshan Liyanage
certifies that this is the approved version of the following dissertation:

Optimization and Applications of Fluorescence anisotropy assays and Fluorescence Resonance Energy Transfer Measurements

Committee:

Prof. Carey K Johnson (Chair)

Prof. Robert C. Dunn

Prof. Sue Lunte

Prof. Cindy L. Berrie

Prof. C. Russell Middaugh

Date approved: 04/27/2009

Abstract

Calmodulin (CaM) is a calcium signaling protein that activates over hundred of targets including PMCA. This dissertation mainly focuses on optimizing and applications of fluorescence anisotropy (FA) and FRET experiments for CaM-target interactions. First we evaluated the extent of interaction of fluorophores with CaM upon conjugation. In this study, three dyes were tested for influences of their charges on interaction with CaM. We employed time-resolved and steady state fluoresce anisotropy as well as fluorescence quenching experiments to study these interactions. The positively charged dye turns out to strongly interact with CaM than neutral and negatively charged dyes. Secondly, FA based assays for direct determination of affinities of CaM-target interactions are developed and the results are consistent with previously reported values. Finally, a FRET based methods are used to study the mechanism of activation of PMCA by CaM and found that the results are consistent with previously reported three-state model.

Dedication

This work is dedicated to my loving kids, Vijini and Themiya. You both shed light into my world and gave me enough reasons to dedicate the rest of my life for the advancement of science.

Acknowledgements

Despite my pursuit of a doctoral degree began about six years ago, the entire path for it has a long and silent history. Therefore, I should recognize and acknowledge some people who gave me the guidance and the strength to walk this path. First, I would like to thank Prof. Carey K. Johnson for your kind guidance, support, and inspiration you gave me. I also make used of this opportunity to tell you that you are not only an inspirational mentor, but also one of the greatest human beings I have ever met during this journey. So Dr. Johnson, I really appreciate you for being there for me and being a role model for future generation.

Next, I want to thank my family for being an integral part of this path. Dear parents, this would not have been possible if you didn't raised me to point where I can take care of myself. My wife, Mekala has been there to support me taking care of everything at home to ensure smooth flow of life. Vijini and Themiya, thank you guys for continuously reminding me that there are as exciting things in the real life as in the sciences. It has been a great privilege to have coworkers like Jay Unruh, Abijith Mandal Shane Price, and Matt Devore during my graduate career at KU. Thank you very much folks for all the help you extended to me.

As I said before, this path has a long history full of extremely hard times. I am really grateful to the teaching of lord Buddha that gave me the faith and courage to gracefully tolerate most of the life threatening situations. I also take this opportunity thank the handful of people who were there for me in the times of misery. I also greatly appreciate all of my teachers who gave me the guidance for walking this path. Finally, the financial support from American Heart Association and petroleum Research Fund must be acknowledged.

Table of Contents

Chapter 1

Introduction to probing Ca^{2+}-signaling proteins

1.1 Calcium signaling

Calcium is considered as one of the most important second messengers within cells. Therefore, the proper regulation of the Ca^{2+} signals is critical to the temporal and spatial propagation of the responses within the cellular systems, which in turn control important cellular functions [1; 2; 3]. There are numerous regulatory pathways to control the intracellular Ca^{2+} concentrations such as the Na^{+} / Ca^{2+} exchangers [4] and several P-type ATPases which are actively involved in transporting Ca^{2+} ions across a membrane against a concentration gradient at the expense of ATP [5]. These ion exchangers and ATPases are integral parts of the cellular signaling system (see Figure 1.1).

Plasma membrane Ca^{2+}- ATPase (PMCA) is one of the most extensively studied P-type ATPase that helps maintain low intracellular Ca^{2+} concentration. This membrane protein containing 10 transmembrane domains and several intracellular loops was first discovered in 1961 [6]. PMCA possesses an ability to self-inhibit its enzyme activity by means of an autoinhibitory domain located near the C- terminus of the protein, which interacts with several regions of catalytic core of the enzyme [7; 8; 9]. The autoinihibition of the enzyme is relieved through binding of another calcium signaling protein, calmodulin [10]. When the C-terminus of PMCA including the autoinhibitory domain is removed by proteolytic cleavage, the enzyme becomes fully active without further increase in the activity upon addition of CaM [11]. The

addition of a CaM binding domain peptide to the truncated PMCA regains the original level of inhibition similar to the whole enzyme [7]. Thus the autoinhibitory domain of PMCA plays a crucial role in maintaining intracellular Ca^{2+} levels.

As seen in the Figure 1.2, the enzymatic cycle of PMCA has been categorized as a four-state system [12]. The E_1 state first exposes the calcium-binding site to the intracellular space (cytosol). Then ATP binds to the calcium bound E_1 state and ATP undergoes hydrolysis results in a phosphorylated state of enzyme (E_1-P). This E_1-P state is transformed into the E_2-P state through motions within the transmembrane helices, exposing the calcium-binding site of the enzyme to the intercellular space and decreasing the affinity of this site for Ca^{2+}. Then the enzyme returns to the E_2 state, which is supposed to be stabilized in the presence of little to no Ca^{2+}, through dephosphorylation of E_2-P state. Finally the E_2 state converts back to theE_1 state of PMCA poised to assume another cycle.

Calmodulin (CaM) is capable of binding and activating a wide variety of target proteins and peptides with varying structures and vast range of biological functions [13; 14; 15]. The biological processes that are regulated by CaM include, muscle contractions, neurotransmission, neuronal plasticity, cytosekletal assembly, gene transcription, and involving in the energy and the biosynthetic metabolism of the cell (reviewed in [16; 17]. Given the importance of calcium as a secondary messenger, the functions of CaM to trigger events that regulate the calcium levels in cells, are crucial for calcium homeostasis. Calmodulin mediates calcium signaling in eukaryotic cells by binding target proteins in response to Ca^{2+} levels of 0.1 to 1 μM.

The mechanism of Ca^{2+}signaling by calmodulin involves several steps, including Ca^{2+} binding, target binding, conformational changes, and activation [13; 14; 15; 17; 18]. One of the key challenges in understanding binding of a wide variety of targets to CaM with high affinity is its flexibility to adopt desired conformations as appropriate. A model for target binding by CaM has been formulated in which the molecular recognition is initially triggered by hydrophobic interactions [19; 20]. Interaction of CaM with its targets seems to enhance the Ca^{2+} affinities in both domains [21; 22; 23; 24].

1.2 Strategies for specific labeling of biomolecules with fluorescent tags

Labeling proteins and peptides with extrinsic fluorophores has many advantages. First of all, we can choose a fluorophore with improved photophysical properties to improve the sensitivity of the measurement. Another advantage is that fluorophores can be specifically attached to biomolecules wherever necessary. There are three major classes of fluorophores based on the reactivity towards biomolecules, including amine reactive probes, thiol reactive probes and probes with reactive groups other than thiol and amine reactive probes. This section will mainly focus on amine and thiol modification of proteins and peptides since these modifications are widely used in biochemical and biophysical research.

Amine reactive probes are often used to prepare bioconjugates for biochemical applications such as immunochemistry, fluorescence polarization assays, fluorescence *in situ* hybridization (FISH), and cell tracing, etc. The amine

modifications are frequently performed through three major reactive groups. These reactive groups include, isothiocyanates, active esters and carboxylic acids such as succinimidyl esters, carboxylic esters and tetrafluorophenyl (TFP) esters. However, succinimidyl esters are superior to isothiocyanates for amine modification because they form bonds as stable as peptide bonds. Therefore the bioconjugates prepared though succinimidyl esters last longer. Amine reactive probes can react with any deprotonated primary amines present in proteins and peptides and this behavior makes specific labeling of protein and peptide difficult. Nevertheless we can achieve a certain degree of selectivity towards the N-terminus by selecting the right pH, as the N-terminus amino group has a lower pKa (~7) than the ε-amino group of lysine residues (pKa ~ 9-10). Since the concentration of deprotonated amino groups from lysine residues under pH 8 is very low, kinetic factors favorably label the N-terminus of the protein and peptides around this pH. It is very advisable to avoid any buffer containing primary aliphatic amine such as Tris buffer for a better labeling efficiency [25].

Thiol reactive probes on the other hand are used to label biomolecules for biophysical studies of structures, functions, and interactions. Since the thiol reactive functional groups (such as cysteine residues) are typically rare in proteins and peptides, the selective labeling using thiol reactive probes at a desired site is possible. Iodoacetamide and maleimide are considered as major reactive groups to introduce thiol reactive probes into biomolecules. For a successful labeling using thiol reactive probes, the pH must be maintained below 8. This is due to two other competing

reactions that occur above pH 8: (a) thiol reactive probes tend to react with amine groups also above pH 8, and (b) hydrolysis of maleimide to meleic acid competes with the sulfhydryl group for maleimide above pH 8. The sulfhydryl groups present in proteins and peptides are prone to oxidation to form disulfide bonds [25]. Therefore these sulfhydryl groups need to be reduced before the introducing thiol reactive probes to ensure the reaction between maleimide and sulfhydryl groups. In order to perform the reducing reaction, we can use a reducing agent such as tris-(2-carboxyethy)phosphine (TCEP) [25; 26], which does not require separation of TCEP before performing the labeling reaction.

Some other approaches have also been reported to site specifically incorporate fluorophores into proteins and peptides. N-terminal labeling of streptavidin through formation of oxime linkages and AF 488 hydroxylamine has been performed [27]. Brustad et al have incorporated unnatural ketone amino acid into the protein for reactions with AF488-alkoxyamine [28]. Ting and coworkers have developed a method for site specific labeling of proteins using transglutaminase-catalyzed conjugation of small molecules [29; 30]. Site specific labeling of CaM has been accomplished through site directed mutagenesis to incorporate cysteine residues to protein [31]. There had been several attempts to specifically label PMCA with fluorescent dyes to study the enzyme. It has been reported specific labeling of only two cysteine residues out of 21 using the thiol reactive maleimide probe ThioGlo [32]. The specific labeling strategy to label the lysine 591 residue located close to the active site of PMCA has been reported by Penniston and coworkers [33].

1.3 Fluorescence Techniques

Fluorescence is a phenomenon that occurs when excited molecules in the excited electronic state radiatively relaxe back to the ground state. Figure 1.3 shows the fate of an excited molecule. Because of the intrinsic sensitivity, precision, and accuracy, fluorescence techniques have emerged as one of the most widely used approaches in biochemical and biophysical research. The advantages of fluorescence techniques are: the signal can be measured with high sensitivity and the fluorescence photons carry a wealth of information pertaining to protein structure, dynamics, and interactions. For this purpose we need to determine multiple parameters from fluorescence photons as follows: intensity, wavelength (λ), polarization (p), arrival time (t_a), time delay after excitation (t_d), and location (x,y on an imaging detector). These parameters can reveal a plethora of information about fluorescent dye such as the nature of its environment, its interaction with surrounding molecules, and its motions. These parameters provide the platform for all the florescence techniques that are currently available. A few examples can be listed as follows: (a) steady state fluorescence spectroscopy measures intensity and wavelength, (b) time-resolved fluorescence monitors time after excitation, (c) fluorescence correlation spectroscopy relies on the arrival time of photons, and (d) fluorescence based imaging is based on the location of the emitted photon.

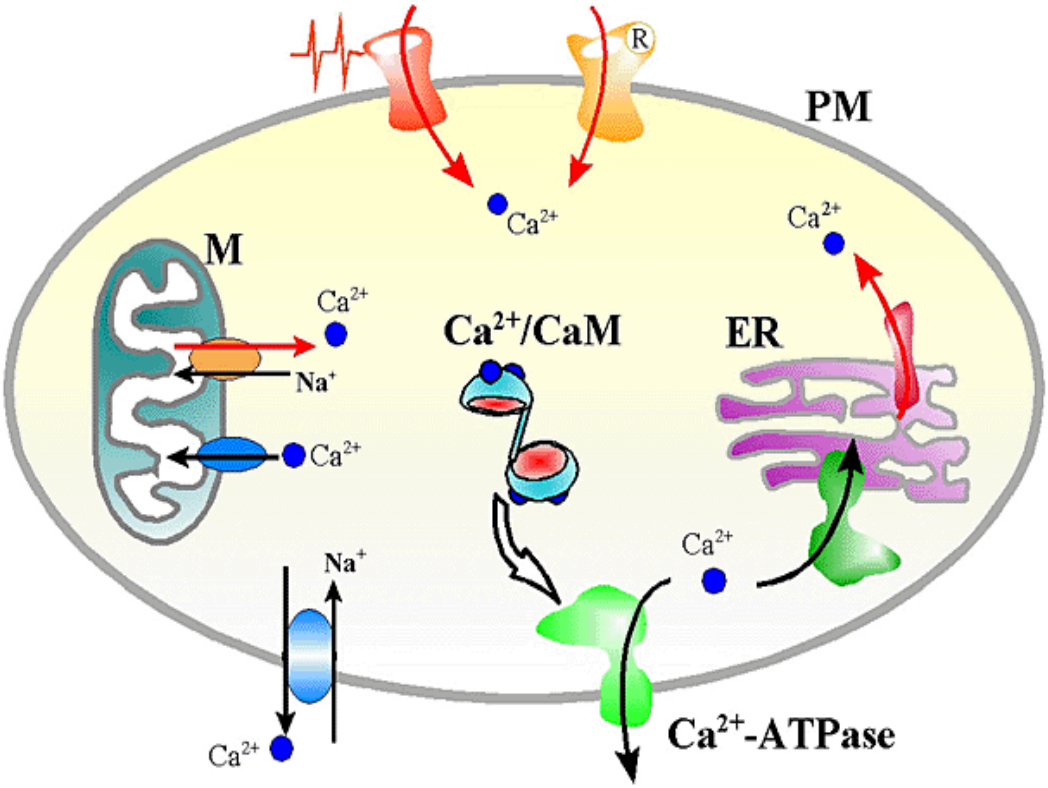

Figure 1.1 Calcium Transport Systems in the cell [34]. Ca-ATPase (green) in the plasma membrane (PM) and endoplasmic reticulum (ER): CaM enables phosphorylation of PMCA and phospholamban, which regulates the SERCA pump. CaM associates with voltage and ligand gated calcium release channels and functions to inhibit calcium release at high intracellular calcium concentrations.

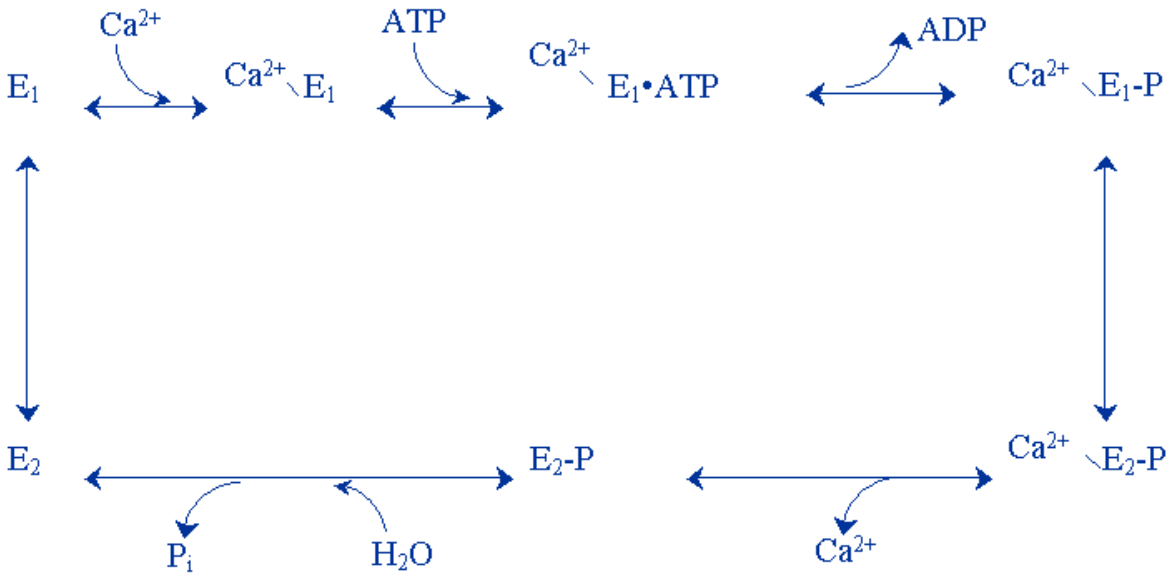

Figure 1.2 The proposed enzymatic cycle of plasma membrane Ca^{2+}-ATPase.

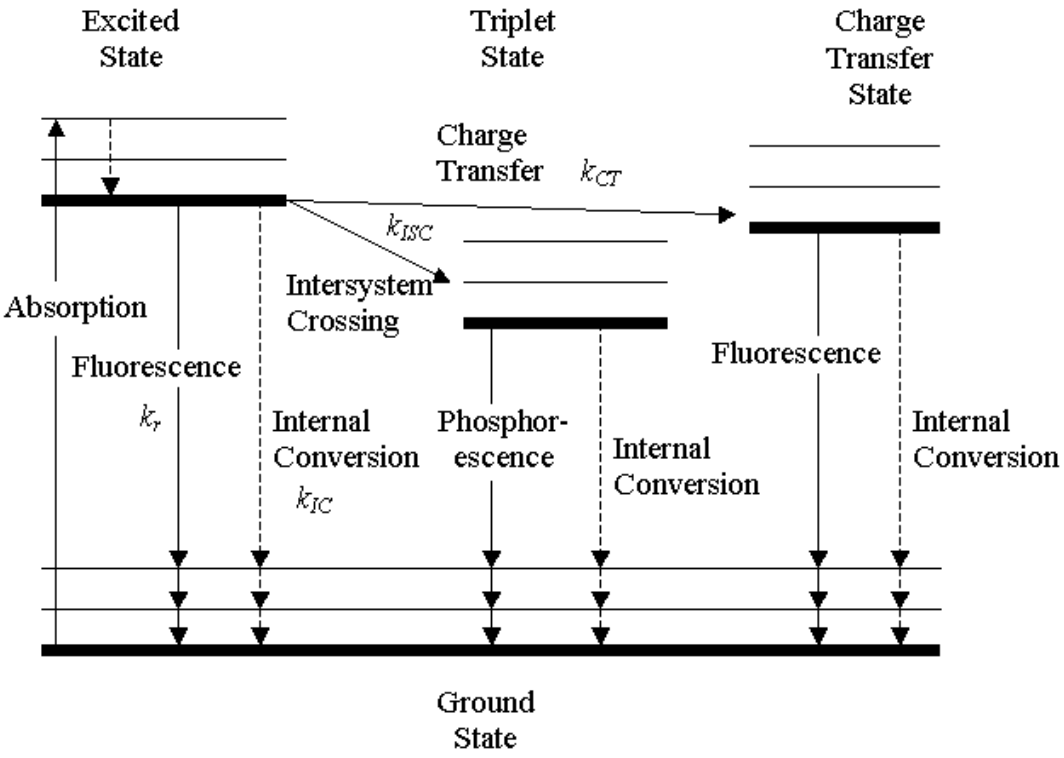

Figure 1.3 Jablolnski diagram showing different pathways of relaxing energy of excited molecules in the excited state

1.4 References

[1]N.L. Allbritton, and T. Meyer, Localized calcium spikes and propagating calcium waves. Cell Calcium 14 (1993) 691-697.

[2]M.J. Berridge, M.D. Bootman, and H.L. Roderick, Calcium signalling: Dynamics, homeostasis and remodelling. Nat. Rev. Mol. Cell Biol. 4 (2003) 517-529.

[3]E. Carafoli, Calcium signaling: A tale for all seasons. Proc. Natl. Acad. Sci. USA 99 (2002) 1115-1122.

[4]K.D. Philipson, Sodium-calcium exchange in plasma-membrane vesicles. Annu. Rev. Physiol. 47 (1985) 561-571.

[5]E. Carafoli, Biogenesis: Plasma membrane Ca^{2+}-ATPase: 15 years of work on the purified enzyme. Faseb. J. 8 (1994) 993-1002.

[6]E.T. Dunham, and I.M. Glyn, Adenosinetriphosphatase activity and the active movements of alkali metal ions. J. Physiol. 156 (1961) 274-293.

[7]A. Enyedi, T. Vorherr, P. James, D.J. McCormick, A.G. Filoteo, E. Carafoli, and J.T. Penniston, The calmodulin binding domain of the plasma-membrane Ca^{2+} pump interacts both with calmodulin and with another part of the pump. J. Biol. Chem. 264 (1989) 12313-12321.

[8]R. Falchetto, T. Vorherr, J. Brunner, and E. Carafoli, The plasma-membrane Ca^{2+} pump contains a site that interacts with its calmodulin-binding domain. J. Biol. Chem. 266 (1991) 2930-2936.

[9]R. Falchetto, T. Vorherr, and E. Carafoli, The calmodulin-binding site of the plasma-membrane Ca^{2+} pump interacts with the transduction domain of the enzyme. Protein Sci. 1 (1992) 1613-1621.

[10]H.W. Jarrett, and J.T. Penniston, Partial-purification of Ca^{2+}-Mg^{2+} ATPase activator from human erythrocytes - its similarity to activator of 3'-5'-cyclic nucleotide phosphodiesterase. Biochem. Biophys. Res. Commun. 77 (1977) 1210-1216.

[11]P. James, T. Vorherr, J. Krebs, A. Morelli, G. Castello, D.J. McCormick, J.T. Penniston, A. Deflora, and E. Carafoli, Modulation of erythrocyte Ca^{2+}-ATPase by selective calpain cleavage of the calmodulin-binding domain. J. Biol. Chem. 264 (1989) 8289-8296.

[12]H.P. Adamo, A.F. Rega, and P.J. Garrahan, The E_2-reversible-E_1 transition of the Ca^{2+}-ATPase from plasma-membranes studied by phosphorylation. J. Biol. Chem. 265 (1990) 3789-3792.

[13]A. Crivici, and M. Ikura, Molecular and structural basis of target recognition by calmodulin. Annu. Rev. Biophys. Biomol. Struct. 24 (1995) 85-116.

[14]P. James, T. Vorherr, and E. Carafoli, Calmodulin-binding domains - just 2-faced or multifaceted. Trends Biochem. Sci 20 (1995) 38-42.

[15]H.J. Vogel, Calmodulin: A versatile calcium mediator protein. Biochem. Cell Biol. 72 (1994) 357-376.

[16]L. Stantella, and E. Carafoli, Calcium signaling in the cell neucleus involves calmodulin. Faseb. J. 11 (1997) 1091-1109.

[17]L.J. Van Eldik, and D.M. Watterson, Calmodulin and signal transduction, Academic Press, New York, 1998.

[18]J. Trewhella, The solution structures of calmodulin and its complexes with synthetic peptides based on target enzyme binding domains. Cell Calcium 13 (1992) 377-390.

[19]M.R. Ehrhardt, J.L. Urbauer, and A.J. Wand, The energetics and dynamics of molecular recognition by calmodulin. Biochemistry 34 (1995) 2731-2738.

[20]P.J. Fisher, F.G. Prendergast, M.R. Ehrhardt, J.L. Urbauer, A.J. Wand, S.S. Sedarous, D.J. McCormick, and P.J. Buckley, Calmodulin interacts with amphiphilic peptides composed of all d-amino acids. Nature 368 (1994) 651-653.

[21]S.E. Brown, S.R. Martin, and P.M. Bayley, Kinetic control of the dissociation pathway of calmodulin-peptide complexes. J. Biol. Chem. 272 (1997) 3389-3397.

[22]J.D. Johnson, C. Snyder, M. Walsh, and M. Flynn, Effects of myosin light chain kinase and peptides on Ca^{2+} exchange with the n- and c-terminal Ca^{2+} binding sites of calmodulin. J. Biol. Chem. 271 (1996) 761-767.

[23]S. Mirzoeva, S. Weigand, T.J. Lukas, L. Shuvalova, W.F. Anderson, and D.M. Waterson, Analysis of the functional coupling between calmodulin's calcium binding and peptide recognition properties (vol 38, pg 3936, 1999). Biochemistry 38 (1999) 14117-14117.

[24]O.B. Peersen, T.S. Madsen, and J.J. Falke, Intermolecular tuning of calmodulin by target peptides and proteins: Differential effects on Ca^{2+} binding and implications for kinase activation. Protein Sci. 6 (1997) 794-807.

[25]R. Haugland, The handbook: A guide to fluorescent probes and labeling technologies., Molecular Probes, Eugene, OG, 2005.

[26]B. Sahaf, K. Heydari, L.A. Herzenberg, and L.A. Herzenberg, Lymphocyte surface thiol levels. Proc. Natl. Acad. Sci. USA 100 (2003) 4001-4005.

[27]K.L. Christman, R.M. Broyer, Z.P. Tolstyka, and H.D. Maynard, Site-specific protein immobilization through N-terminal oxime linkages. J. Mat. Chem. 17 (2007) 2021-2027.

[28]E.M. Brustad, E.A. Lemke, P.G. Schultz, and A.A. Deniz, A general and efficient method for the site-specific dual-labeling of proteins for single molecule fluorescence resonance energy transfer. J. Am. Chem. Soc. 130 (2008) 17664-+.

[29]I. Chen, M. Howarth, W.Y. Lin, and A.Y. Ting, Site-specific labeling of cell surface proteins with biophysical probes using biotin ligase. Nat. Methods 2 (2005) 99-104.

[30]C.W. Lin, and A.Y. Ting, Transglutaminase-catalyzed site-specific conjugation of small-molecule probes to proteins in vitro and on the surface of living cells. J. Am. Chem. Soc. 128 (2006) 4542-4543.

[31]M.W. Allen, R.J.B. Urbauer, and C.K. Johnson, Single-molecule assays of calmodulin target binding detected with a calmodulin energy-transfer construct. Anal. Chem. 76 (2004) 3630-3637.

[32]A. Zaidi, L. Barron, V.S. Sharov, C. Schoneich, E.K. Michaelis, and M.L. Michaelis, Oxidative inactivation of purified plasma membrane Ca^{2+}-ATPase by hydrogen peroxide and protection by calmodulin. Biochemistry 42 (2003) 12001-12010.

[33]A.G. Filoteo, J.P. Gorski, and J.T. Penniston, The ATP-binding site of the erythrocyte-membrane Ca^{2+} pump - amino-acid-sequence of the fluorescein isothiocyanate-reactive region. J. Biol. Chem. 262 (1987) 6526-6530.

[34]T.C. Squier, and D.J. Bigelow, Protein oxidation and age-dependent alterations in calcium homeostasis. Front. Biosci 5 (2000) 504-526.

Chapter 2

Studies of the Influence of Charge States of Fluorophores on Interactions with Calmodulin

2.1 Introduction

Modern highly sensitive analytical methods that are used to study the structure and dynamics of biomolecular interactions often rely on the fluorescent dye labels attached to biomolecules to generate fluorescence signals in the visible region of the spectrum. However, the interactions of the fluorescent dye molecules with the biomolecules to which they are attached may influence the measured fluorescence signal. Fluorescence polarization (FP) and fluorescence resonance energy transfer (FRET) have been deployed in sensitive detection of ligand binding or protein-protein interactions. It is crucial to understand the rotational mobility of the fluorophore on the time scale of the fluorescence lifetime for both FP and FRET methods. In FP methods, fluorescence depolarization is measured to extract the information about the dynamics of the system under study [1; 2; 3; 4; 5]. FRET is a technique based on the energy transfer efficiency between a donor dye and an acceptor dye [6; 7; 8]. For a reliable FRET signal high orientational mobility of the fluorescent dye is desired for averaging of the orientational factor (κ^2) [9]. On the other hand, FP methods require low orientational mobility of the fluorophore relative to the biomolecule to which it is attached, in order to detect a large change in rotational motion upon binding to a target.

Despite the crucial importance of dye-biomolecular interactions to interpret fluorescence polarization and FRET measurements, only a few studies can be found in the literature focusing on this topic. Srinivas and Bagchi (2001) have given a computational look into the effect of orientational motion of the fluorophores on the dynamics of the FRET in polymers [10]. Dietrich et al (2002) have discussed the importance of orientational averaging of dyes bound to DNA for unbiased determination of FRET distances [11]. Taekjip Ha (2001) has pointed out that if a dye labeled biomolecule yields a low anisotropy value the dye does not strongly interact with the host molecule and rotates relatively freely around it [12]. In order to determine the extent of dye-DNA interactions steady state anisotropy of dye labeled DNA molecules at ensemble level has been measured in solution by Rasnik et al (2004) [13]. Unruh et al (2005) have addressed the dye-DNA interactions in dye-labeled DNA aptamers using computational and experimental approaches [14; 15]. In a study to investigate DNA-protein interactions E. Rusinova and coworkers (2000) have considered three uncharged dyes at neutral pH to minimize the interactions of dye with biomolecules [16]. Hill and Royer have shown that the experimental anisotropy for dye labeled DNA is much lower than the calculated anisotropy for similar length oligonucleotides owing to local segmental motion of the dye [17]. Clegg et al in a classic study of DNA helical geometry have noted that rhodamine, which bear a net positive charge at neutral pH, tends to show strong interaction with negatively charged DNA resulting limited local motion of the dye [18].

Schroder et al have used a molecular dynamic simulation and experimental approach to investigate the dye-protein interactions to probe protein dynamics [19]. Orientational motion of single fluorescent labels in a peptide has been probed to extract the dynamic information at the single molecule level [20]. The use of a rigid tetracoordinate linkage of fluorescent probes 4', 5'-bis(1,2,3-dithioarssolan-2-yl) fluorescein (FlAsH) to label CaM mutated to possess four cysteine residues has been reported [21]. This rigid fluorescent conjugate has been employed in extracting fast intra-domain motion as well as overall rotation of CaM upon activation by calcium avoiding interference from the independent segmental motion of fluorophores. More vigorous theoretical treatments of the segmental motion of the dye molecules attached to macromolecules can be found in the literature [22; 23].

The applicability of dynamic quenching experiments in studying the solvent accessibility of fluorescence dyes conjugated to macromolecules paves the way to understand the physical behavior of dyes [24; 25]. To implement the dynamic quenching experiments, the lifetimes of the conjugated molecules are measured in the presence and absence of the quencher. When the dynamic quenching is present the ratio of the lifetimes in the absence and presence of the quencher follows a linear relationship with increasing quencher concentration. Schmitz and Schurr have put forward a model for the role of orientational constraints and rotational diffusion in bimolecular reaction kinetics [26]. An extensive investigation into the orientational constraints and rotational diffusion of reactive molecules using fluorescent quenching experiments on FITC labeled cobra α-toxins bound to the acetylcholine receptors

have been performed by Johnson and Yguerabide [27]. These studies have revealed that the immobilization of the dye molecules on the surface of the protein renders dye molecule less susceptible to quenching even without introducing additional steric shielding [25; 27; 28]. This information implies that the extent of quenching of fluorophores attached to macromolecules depends not only on the geometrical masking factors but also on the translational and rotational mobilities of fluorophores as well as orientational constraints [27]. Thus we can deploy dynamic quenching experiments to evaluate the extent of dye-protein interactions.

Time-resolve fluorescence has been widely used in the biochemical and biophysical research arena for studying fast domain motion of macromolecules as well as in investigation interactions of fluorescence dyes with conjugated molecules. In time-resolved fluorescence anisotropy experiments, fluorophores are excited by using a pulsed laser source, resulting in $\cos^2 \theta$ distribution of transition dipoles with respect to the electric filed vector after excitation. The excited dye molecules will initially have an anisotropic distribution of transition dipoles and with the time will decay back to isotropic distribution as a result of rotational motion of dyes. As the excited dye molecules undergo rotational diffusion the polarization of the emitted radiation is measured at a time *t* after the excitation [29]. The fluorescence anisotropy *r(t)* after that particular time period *t* is defined as

$$r(t) = [I_V(t) - I_H(t)] / [I_V(t) + 2I_H(t)] \qquad (2.1)$$

where $I_V(t)$and $I_H(t)$are the vertical and horizontal decays respectively, relative to the polarization of the excitation light source. The collected emission intensity in the vertical channel after time *t* can be written as follows:

$$3I_V(t) = I(t)[1 + 2r(t)] \qquad (2.2)$$

This form of expression assumes every decay component in *I(t)* experiences the same rotational dynamics described by *r(t)*. On the other hand, the emission intensity in the horizontal channel at time *t* is given by

$$3I_H(t) = I(t)[1 - r(t)] \qquad (2.3)$$

The time dependency of the decay is associated with the shape of the diffusing species as well as the interaction with the immediate environment. However, roughly globular diffusing species assume a single a single exponential decay as follows:

$$r(t) = r_0 e^{-t/\Phi} \qquad (2.4)$$

where Φ is the rotational correlation time, also written as τ_r, and r_0 is the initial anisotropy. The initial anisotropy is a function of both the geometry of the emission dipole relative to the absorption dipole and the distribution of excitation probability.

In the case where the fluorophore has been attached to a macromolecule, time-resolved anisotropy data can be fit as sum of exponentials, considering the global motion of the macromolecule as a long correlation time, Φ_{long}, and segmental probe motion due to the free rotation of the dye around the covalent bond between probe and macromolecule as a short correlation time, Φ_{short}. A heterogeneous model has also been proposed to account for the double exponential decay described by equation 2.5. In this heterogeneous model, the fluorophores attached to a biomolecule could

either be stuck on to the surface in a docking manner (long correlation time) or free to move around its linker arm (short correlation time). Anisotropy at time t for this system is given by

$$r(t) = r_0 [\alpha e^{-t/\Phi short} + (1-\alpha)e^{-t/\Phi long}] \qquad (2.5)$$

where α is a scaling factor with values ranging from 0 to 1.

In this study, we have conjugated a series of fluorophores having different electrostatic charges to CaM in order to characterize dye-protein interactions. Being a moderately acidic protein with an isoelectric point of 4.2, CaM offers many negatively charged amino acid residues near neutral pH (Figure 2.1). Here I focus on the effect of the electrostatic charges of dyes on their interactions with CaM. Table 2.1 lists selected fluorophores with their absorbance and emission maxima and electrostatic charges for this study. The structures of these dyes conjugated to CaM at the 34 site through a cysteine residue are depicted in Figure 2.2. During this investigation, I employed several fluorescence techniques including time-resolved and steady-state fluorescence anisotropy and dynamic quenching experiments.

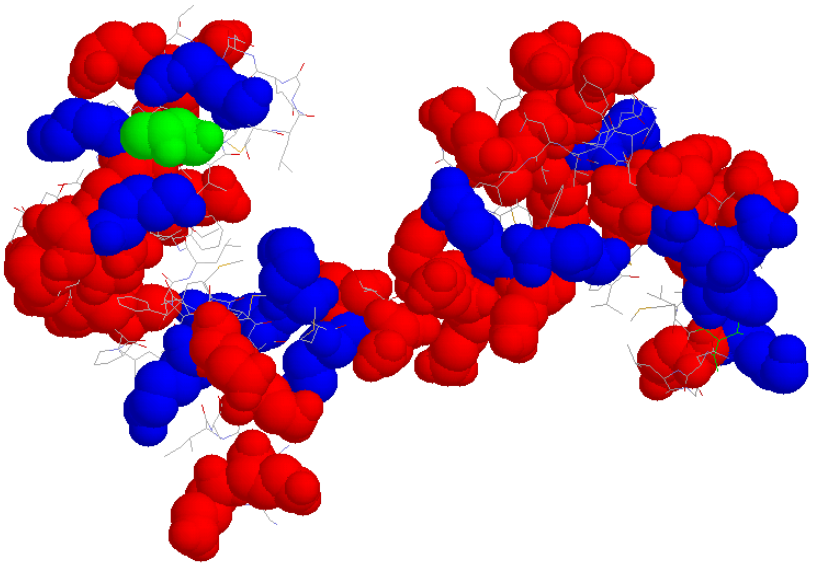

Figure 2.1. Structure of Ca^{2+}-CaM with color filled and space filled charged residues. Here negative (red), positive (blue), and T34 (green). (PDB file 1CLL). (Created by Jay Unruh)

Table 2. 1. Fluorescence dyes used in the study with their absorption/emission maxima and corresponding charges at neutral pH

Fluorophore	Absorption/Emission maxima (nm)	Charge at neutral pH
AlexaFluor 488	492/515	-1
Oregon Green 488	492/515	0
Atto 465	453/508	+1

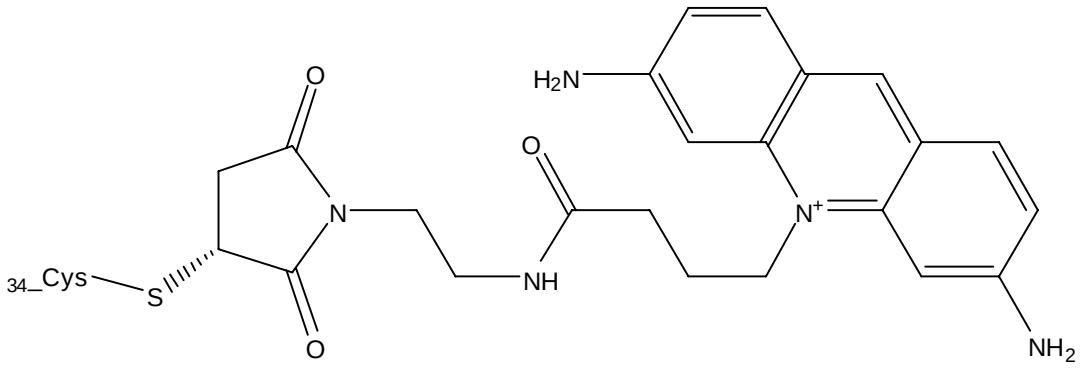

1A

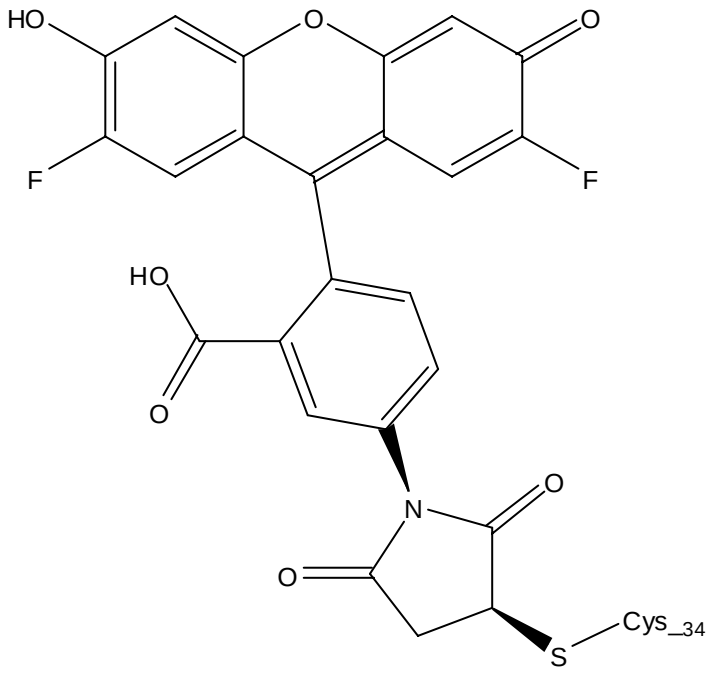

1B

Figure 2.2. The structures two representative maleimide derivatives of fluorescent dyes investigated in dye-protein interaction study. 1A is Atto465 and 1B is Oregon Green 488.

2.2 Materials and Methods

Growth and Purification of calmodulin: Phenyl sepharose CL-4B, and Sephadex G-25 resins were purchased from Amersham Biosciences (Amersham,). Fluorescence conjugations were carried out with maleimide derivatives of AlexaFluor 488, Oregon Green 488 (Molecular Probes Inc., Eugene, OR) and Atto465 (Atto-tec, Germany). All other reagents were purchased from Sigma-Aldrich (St. Louis, MO) and used as received.

Growth and purification of CaM-T34C was performed according to a protocol described previously as follows [30]. The glycerol stock containing *E. Coli* strains bearing expression vector for CaM-T34C mutant was grown in a Luria broth medium fortified with carbenicillin. During the growth procedure, 500 uL aliquot of glycerol stock was inoculated in 40 ml of growth media and the resulting solution was incubated while shaking at 250 rpm at 37 °C for 12 hours. The resulting culture was inoculated with 1 L of growth media and incubated at 37 °C while shaking at 250 rpm. An initial absorbance reading at 600 nm was measured before the incubation. The growth was monitored by measuring the extinction at 600 nm and subtracting the initial reading from it. When the corrected absorbance was ~ 0.7 the growth medium was induced with 2 mL of a 500 mM of sterile IPTG and further incubated for 3 hours. The completeness of the growth was ensured by taking a last absorbance reading of 1.2 –1.4. The cells were harvested by centrifugation in a SLA-3000 rotor at 6000 rpm at 4 °C for 15 minutes and resuspended in 50 mM MOPS (100 mM KCl, 1 mM EGTA, and 1mM DTT, pH 7.5). Cell lysis was achieved by incubating with 150

μg/mL of lysozyme at 37 °C for 30 minutes. Then the sample was sonicated and centrifuged in an SA-600 rotor at 12,000 rpm at 4 °C for 40 minutes. The supernatant was adjusted to a final calcium concentration of 5 mM and pH 7.5.

The supernatant was then loaded into a phenyl sepharose column (30 ml bed volume) equilibrated with 3-5 column volumes of buffer A (50 mM Tris-HCl, and 1 mM $CaCl_2$, pH 7.5). The flow rate was maintained at 1 mL/min. After the sample was fully loaded into the column bed, the column was washed with buffer A until absorbance at 280 nm came to a zero baseline and then with buffer B (50 mM Tris-HCl, 1 mM $CaCl_2$, and 500 mM NaCl, pH 7.5) ensuring the zero baseline absorbance at 280 nm. Finally CaM was eluted with buffer C (10 mM Tris-HCl, and 10 mM EDTA, pH 7.5). For further purification and solvent exchange the eluant was dialyzed three times against 4 L of HEPES buffer (10 mM HEPES, 0.1 M KCl, 1 mM $MgCl_2$, and 0.1 mM $CaCl_2$) at 4 °C using 8000 Da MWCO dialysis tubing. Protein concentration was determined by taking an absorbance reading at 280 nm with extinction coefficient of 5400 $M^{-1}cm^{-1}$for CaM. Then the ~ 1 mL aliquots of CaM stored in -80 °C until used in further experiments.

Fluorescent labeling of CaM-T34C: CaM was labeled with maleimide derivatives of AlexaFluor 488, Oregon green 488, and Atto 465 following the standard protocols from the manufacturer. Briefly, 2.7 mg (125 nmol) of CaM-T34C was incubated with 500 nmol of TCEP to reduce disulfide bonds between CaM due to the presence of a cysteine residue and then with 2 mmol of NaCl (1 mL of 2M NaCl) to open up the hydrophobic regions of CaM for 5 minutes. The resulting solution was

incubated with continuous stirring with 1 mg of dye to be used in the experiment at room temperature for 1 hour. To separate the unreacted free dye from the labeled protein, the reaction mixture was run through a size exclusion column packed with Sephadex G-25 resin followed by repeated dialysis against 4 L of a buffer consisting of 10 mM HEPES, 0.1 M KCl, 1 mM $MgCl_2$, and 0.1 mM $CaCl_2$. After dialysis, the resultant solution was centrifuged using a 10,000 molecular weight cutoff filter (Millipore) at a speed of 3200 rpm for 10 min to concentrate the labeled protein and further remove the free dye. The concentrations of all the CaM-fl conjugates were determined by measuring absorbance at 492 nm for AF488 and OG 488 and 453 nm for Atto 465 with their corresponding extinction coefficients at 492 nm (AF488 and OG488) and 453 nm (Atto465).

Time-resolved anisotropy measurements: Time-resolved anisotropy measurements were performed using time correlated single photon counting (TCSPC) as previously described [29; 31]. The excitation pulses were obtained from a mode-locked, cavity-dumped Mira Optima 900f Ti:sapphire pulsed laser pumped by a 10 W Verdi laser from Coherent Inc. (Santa Clara, CA). Two-MHz pulses were cavity dumped from the Ti:sapphire output by sending a radio-frequency signal for cavity dumping. Then the output from the Mira was frequency doubled to obtain the desired wavelength using a model 5-050 frequency-doubler made by Inrad Inc. (Northvale, NJ). The excitation power of 2 μW was maintained for the measurements using a neutral density filter wheel (Opto Sigma).

The sample temperature was held at 25 °C using a sample cell holder with stirrer and peltier temperature controller from Quantum Northwest (TLC-50 Spokane, WA). Vertically and horizontally polarized emission was simultaneously selected in a T-format configuration with Oriel 27320 polarizers (Oriel Corporation). The emission from both polarizations was then spectrally resolved using Sciencetech 9030 monochromators with bandpass of 8 nm (Sciencetech Inc.). Wavelength resolved emissions in vertical and horizontal channels were then detected using R-3809U-50 MCP-PMT modules (Hamamatsu, Tokyo, Japan). For the lifetime decays the polarizer of a given channel was set to the magic angle, 54.7°. A reference pulse for the arrival time determination was obtained from the fundamental output of Mira and a photodiode. PMT control, routing of the signal from different channels, and data acquisition were controlled by an SPC-630 PC board made by Becker and Hickl GmbH (Berlin, Germany). Instrumental response functions were collected at a wavelength 5 nm blue-shifted from each excitation wavelength using a colloidal solution of SDS micelles. To correct for the differential responses of two detectors due to polarization differences, the G factor was calculated by using a free fluorescein solution. Excitation and emission wavelengths for CaM-AF488 and CaM-OG488 were 475 nm and 515 nm respectively while those for CaM-Atto465 were 460 nm and 510 nm. For each dye conjugate a concentration of 320 nM was maintained during experiments. A standard high calcium buffer (10 mM HEPES, 0.1 M KCl, 1 mM $MgCl_2$, and 0.1 mM $CaCl_2$, pH 7.4) was used for all the experiments unless otherwise stated.

TCSPC data were analyzed with a program written in Microsoft Excel based on iterative reconvolution, which involved a convolution of instrumental response function with a model fitting function [29; 31]. The convolution can be described as follows:

$$C(t) = \int_0^t I(t) IRF(t-\tau) d\tau , \qquad (2.6)$$

where $I(t)$ is the model fitting function, and $IRF(t)$ is the instrument response function. Since the observed anisotropy decay does not reflect the actual anisotropy decay, especially at short time scales, the vertical and horizontal fluorescence intensity decays were fit simultaneously with this program (see Figure 2.3). This iterative fitting routine relies on the minimized χ^2 to obtain a good fit [32].

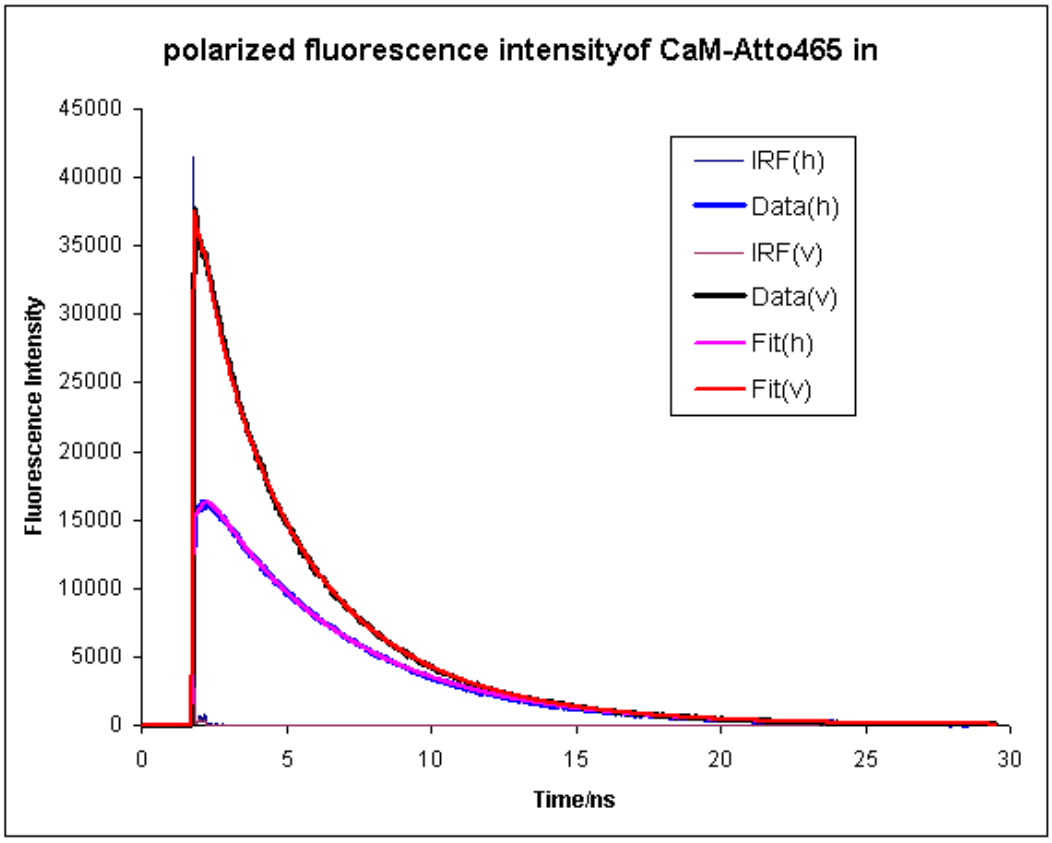

Figure 2.3 Fluorescence intensity decay profile in horizontal and vertical channels with polarized excitation for CaM-Atto465. The fluorescence decay in each channel is represented as follows: purple, blue, and pink lines are instrumental response function, data, and fit respectively for the horizontal channel; brown, black, and red lines are the instrumental response function, data, and fit for the vertical channel respectively.

Steady state anisotropy measurements: Steady-state fluorescence anisotropy experiments were performed at 25 °C using a Quantamaster fluorimeter (Photon Technology International Inc.). Excitation and emission polarization were selected with Glan Thompson polarizers with the medium aperture configuration (PTI Inc.). The fluorescence excitation for CaM-AF488 and CaM-OG488 was achieved with the 475 nm line from the xenon lamp and the emission wavelength of the PMT was set to 515 nm with 4 and 6 nm band pass for excitation and emission respectively. For CaM-Atto465 the only change was the excitation at 460 nm. Data collection was performed for all the experiments using Felix software from PTI Inc. The steady state anisotropy was calculated using following equation in Excel.

$$r = (I_{VV} - GI_{VH})/(I_{VV} + 2GI_{VH}) \quad (2.7)$$

$$G = I_{HV}/I_{HH} \quad (2.8)$$

where r is the steady state anisotropy; I is the intensity; V and H are the vertical and horizontal polarization respectively; and the first subscript represents the excitation polarization while the second subscript is for the emission polarization. G is a correction factor that accounts for the differential detection efficiencies in horizontally and vertically polarized emission.

Dynamic quenching experiments: Fluorescence quenching experiments were carried out by measuring the change in fluorescence lifetime (τ) as a function of KI concentration ranging from 0 to 100 mM. Fluorescence lifetimes were measured by TCSPC experiments as described in the time-resolved anisotropy section. Lifetime data were fit to a single-exponential decay since the change in χ^2 is minimal upon

adding a second component. The quenching constant, K_q, was calculated using the Stern-Volmer equation [33]:

$$\tau_0 / \tau = 1 + K_q [Q] \qquad (1.9)$$

where K_q is Stern-Volmer quenching constant, τ_0 is fluorescence lifetime in the absence of quencher, τ is fluorescence lifetime in the presence of quencher, and [Q] is the molar concentration of the quencher.

First the K_q for free fluorophores (AF488, OG488, and Atto465) were determined and then K_q for CaM with conjugated dyes were determined. In each case, the fluorophore concentration was maintained at 320 nM for both free and conjugated dyes by diluting stocks of which the concentration has previously been measured with absorbance readings as previously described in this chapter. All the experiments were carried out in a 1-cm path length quartz cuvette at 25 °C using a Cary100 UV/VIS spectrophotometer (Varian Inc.).

2.3 Results

A profound understanding of dye-protein interactions is crucial for unambiguous interpretation of FRET and time resolved anisotropy data as well as in developing sensitive fluorescence polarization based assays. To this end we investigated the interactions of three fluorescence dyes, Oregon green 488 (OG488), AF488, and Atto 465, with CaM to check for possible influence from the electrostatic charges on the dyes. This study was based on the fact that CaM possessed many negatively charged amino acid residues near neutral pH owing to its isoelectric point

of 4.2. The structures of these dye-protein conjugates are presented in Figure 2.2. Time-resolved anisotropy and corresponding lifetimes for these dye-protein conjugates are summarized in Table 2.2. CaM labeled with negatively charged AF488 (CaM-AF488) follows biexponential fluorescence anisotropy decay with two rotational correlation times (Figure 2.4). A long rotational correlation time of 5.6 ns and a short rotational correlation time of 200 ps possessing amplitudes of 0.49 and .51 respectively were observed for CaM-AF488. These results are consistent with previous time-resolved anisotropy measurements for CaM-AF488, which resulted in the same amplitudes for the long and short correlation time components [34]. In the case of CaM labeled with OG488 (CaM-OG488) where the fluorophore is electrically neutral, the time-resolved anisotropy also decayed biexponentially as in CaM-AF488 with similar amplitudes of corresponding correlation times. Both the long and short correlation times have amplitudes of 0.50.

However, when the positively charged Atto465 was attached to CaM (CaM-Atto465), the time-resolved anisotropy decay showed a marked difference in correlation time components and corresponding amplitudes in the biexponential anisotropy decay. The long correlation time had an amplitude of 0.71 while the short correlation time does only 0.29 providing strong evidences for the presence of the increased interaction of the dye with local environment of CaM restricting segmental motion of the conjugated dye. It is also clear from the lifetime measurements that nearly unchanged lifetimes of all the three conjugates are a sign of the absence of any quenching events due to the interaction of dyes with the protein surface. Therefore the

changes in time-resolved anisotropies are a clear measure of the extent of dye-protein interaction devoid of interference coming from quenching of fluorescence labels by the protein backbone. Therefore the domination of the slow rotational motion in CaM-Atto465 is an indication of strong coupling of dye motion to CaM.

Table 2.2. Rotational correlation times and the respective amplitudes for three fluorescence conjugates of CaM.

dye	**τ_f (ns)**	**θ_{fast} (± 0.2 ns)**	**Amplitude (±0.06)**	**θ_{slow} (ns) (± 2.2)**	**Amplitude (± 0.08)**
AF488	4.0	0.2	0.51	5.6	0.49
OG488	4.2	0.2	0.50	4.8	0.50
Atto465	4.6	0.7	0.29	7.9	0.71

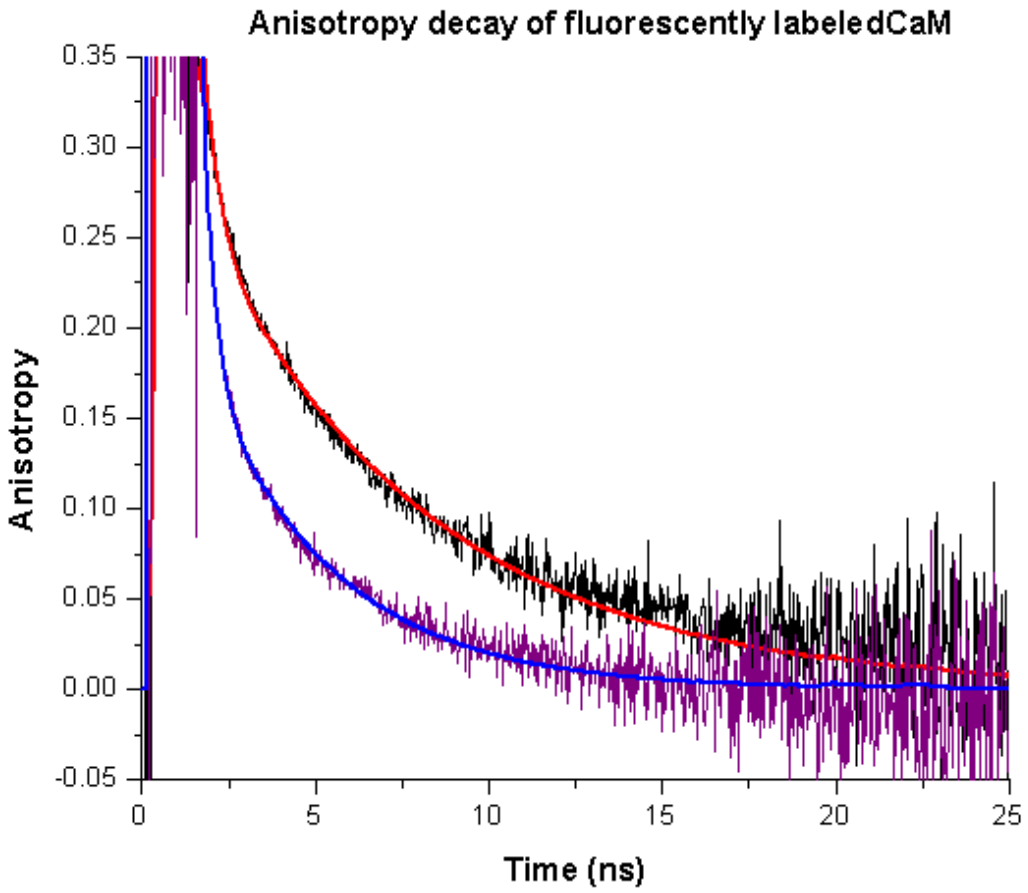

Figure 2.4. Anisotropy decays of fluorescent conjugates of CaM. The representation of each component is as follows. The black line: experimental anisotropy decay of CaM-Atto465, the red line: fit to the anisotropy decay of CaM-Atto465, purple: experimental anisotropy decay of CaM-AF488, and the blue line: fit to the anisotropy decay of CaM-AF488.

Steady state anisotropy: steady state anisotropy values also provide insight into the extent of segmental motion of conjugated dyes. The magnitude of the steady state anisotropy is governed by the relative amplitudes of long and short correlation times of the anisotropy decay and the fluorescence lifetime. Steady state anisotropy can be used in supporting the time-resolved findings as far as the lifetimes of the fluorophores remain comparable. Therefore the steady state anisotropy for each dye-protein conjugate was measured to assess the strength of interactions between the dye and CaM.

Steady state anisotropy data with the respective lifetimes for all the three dye-protein conjugates are listed in Table 2.3. CaM-AF488 and CaM-OG488 share the same steady state anisotropy value as a result of similar amplitudes for fast and slow component of the time-resolved anisotropy decay. CaM-Atto465 on the other hand yielded much higher steady state anisotropy than other two conjugates. This higher steady state anisotropy for CaM-Atto465 is consistent with its time-resolved anisotropy data since depolarization from the suppressed fast component is minimal in CaM-Atto465. The steady state anisotropy of CaM labeled with AF647 along with its lifetime is also listed in Table 2.3 to demonstrate the importance of the lifetime of the fluorophore in justifying time-resolved data using steady state anisotropy. Despite the strong negative charge (-2) of AF647 at neutral pH its conjugate form with CaM possesses a very steady state anisotropy (0.28) due to the short lifetime (2.2 ns) of AF647.

Table 2. 3 Steady state anisotropy of several fluorescence conjugates with the respective lifetimes.

Fluorophore	The charge state	Fluorescence lifetime (ns)	Steady state anisotropy
CaM-AF 488	-1	4.0	0.10
CaM-OG 488	0	4.2	0.10
CaM-Atto 465	+1	4.6	0.17
CaM-AF647	-2	2.2	0.28

Dynamic quenching Experiments: Orientational restriction of the fluorescent dyes conjugated to macromolecules is a very crucial parameter that can be extracted from fluorescence quenching experiments among other vital information. In order to assess the orientational restrictions of three fluorescent dyes conjugated to CaM under our interest, we performed a series of dynamic quenching experiments. The changes in fluorescence lifetime of each dye upon increasing fluorescence quencher concentration (KI) were used to determine the quenching constants for both free and conjugate form of each dye. Changes in fluorescence intensity decays for Atto465 and CaM-Atto465 are shown in the Figure 2.5 in the presence and absence of KI. It is obvious from the intensity decay curves that when the fluorophore is free in solution, there is a drastic change in fluorescence intensity decay curves as it is exposed to quencher. However, the extent to which the conjugated dye is quenched has been significantly reduced upon exposure to the quencher. The fluorescence lifetime of free Atto465 shows a shift from 4.9 ns to 1.0 ns while that of CaM-Atto465 shifts only from 4.4 ns to 2.6 ns for zero and 100 mM KI concentrations respectively.

The ratio of the fluorescence lifetime in the absence and presence of KI were plotted against KI concentration to construct Stern-Volmer plots and the gradients of the graphs yielded the quenching constant, K_q values for both free and conjugated dyes. In each case, the plot is a straight line that extrapolates to 1 at zero KI concentration, providing evidence for bimolecular reaction kinetics [26]. Stern-Volmer plots for free and conjugated form of all the dyes are presented in left and

right panels of Figures 1.6 respectively. Corresponding quenching constants determined from above graphs for all the species are listed in Table 1.4.

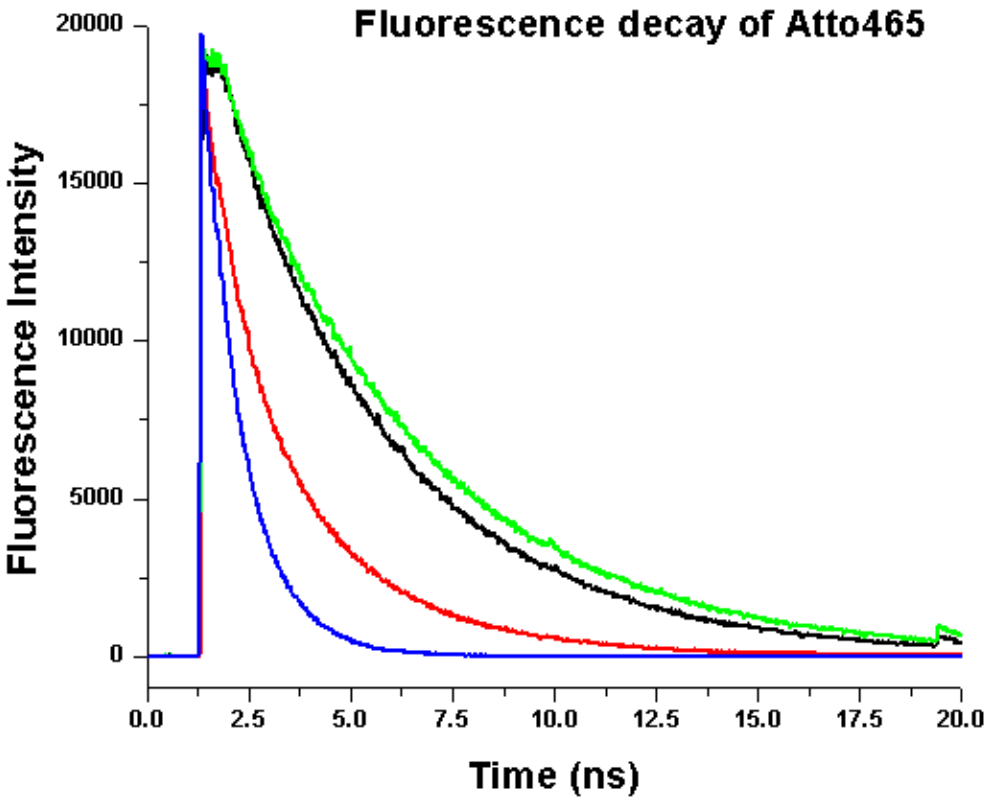

Figure 2.5 Fluorescence intensity decays for free Atto465 and CaM-Atto465 in the presence and absence of KI. Black line: CaM-Atto465 without KI, red line: CaM-Atto465 with KI, green line: free Atto465 without KI, and, blue line: Atto465 with KI.

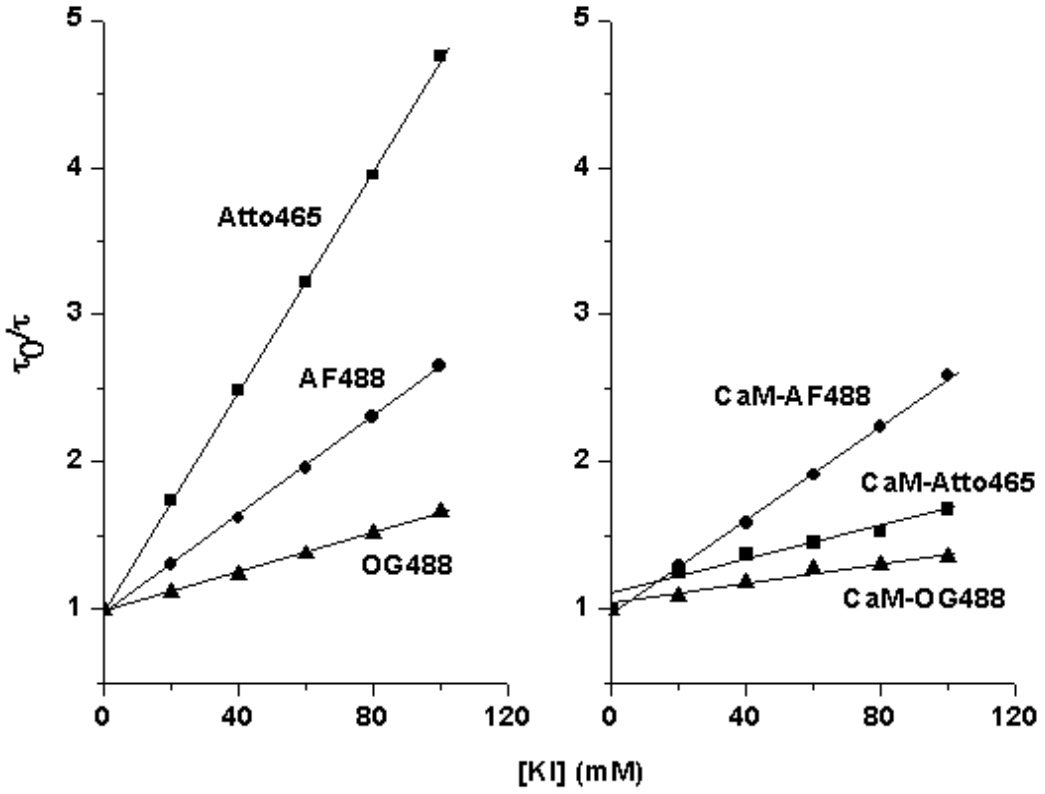

Figure 2. 6. Stern-Volmer plots for three fluorescence probes from KI (left panel). Circles: AF488, squares: Atto465, and triangles: OG488. Stern-Volmer plots for three fluorescence conjugates of CaM upon quenching by KI (right panel). Circles: CaM-AF488, squares: CaM-Atto465, and triangles: CaM-OG488.

Table 2.4 Change in K_q values of fluorescence dyes upon conjugations to CaM.

Fluorophore	Kq of Free dye (M^{-1})	Kq of Conjugated dye (M^{-1})
OG488	6.7 ± 0.1	3.6 ± 0.3
AF488	16.6 ± 0.2	15.8 ± 0.2
Atto465	37.3 ± 0.3	6.2 ± 0.7

There is no significant change in K_q for AF488 upon conjugation to CaM indicating that the attached dye is as susceptible to quenching as the free dye in solution. Therefore AF488 attached to CaM seems to show more rotational freedom and less orientational restriction as a result of poor interaction with CaM surface. In the case of OG488, K_q decreased by approximately a factor of two upon attachment to CaM indicating less accessibility of the quencher to dye. As expected, free Atto465 exhibited the highest Kq value ($37.3M^{-1}$) of all fluorophores studied owing to its net positive charge causing strong electrostatic interactions between dye and I^- ions. Very interestingly, the K_q value of CaM-Atto465 turns out to be drastically diminished to 6.2 M^{-1}.

2.4 Discussion

The photophysical behavior of fluorescent dyes conjugated to macromolecules has influences on three major research areas: (1) In spFRET studies, coupling of the dye motion to the domain motion of biomolecules interferes with interpretation of FRET results as this requires orientational averaging of dipoles of the dyes in the time scale of the measurements [9; 12; 35]; (2) In contrast to FRET, for time-resolved anisotropy, data on protein dynamics necessitates strong coupling of conjugated dyes to the macromolecule, which in tern results in restricted free segmental motion of dyes to resolve fast domain motions of biomolecules [21]; (3) fluorescence polarization based assays depend on the changes in fluorescence anisotropy upon binding of a larger molecule to small fluorescence conjugate. The sensitivity of the

assay is governed by the interactions of fluorophore with biomolecules since depolarization caused by free segmental motion of dyes results in a limited change in anisotropy making target binding less sensitive. For instance, the change in steady state anisotropy of a TR-aptamer (dye has a strong coupling to the aptamer) has been reported to be four-fold higher than that of a fluorescein-aptamer (dominant segmental motion of the dye) upon binding IgE [3; 36; 37]. These are the motivations for a thorough investigation of the effect of dye-protein-protein interactions to provide insight into photophysical behavior of fluorescent bioconjugates. The vital information that can be extracted from these studies eventually will help to develop molecular dynamic simulations to predict the nature of interaction of a particular dye with a given biomolecule [19; 38; 39]. Such sort of advance knowledge of a given system will help better plan experiments saving time and resources as well as enhance the sensitivity of the experimental approach.

The working hypothesis for this study was based on the fact that CaM offers many negatively charged residues at neutral pH, as is obvious from the Figure 2.1 showing charged residues distribution of CaM. Therefore CaM may have differential interactions with fluorescent dyes with different electrostatic charges on them. Time-resolved anisotropy, steady state anisotropy, and dynamic quenching studies on AF488, OG488, and Atto465 conjugates indicated that the extent to which dyes interact with CaM is significantly influenced by the electrostatic charge on each fluorophore. Positively charged Atto465 has shown convincing evidence for strong interaction with available negatively charged residues neighboring the labeling site.

This strong coupling of the dye to the protein makes it an ideal candidate for the study of fast protein dynamics by time-resolved anisotropy as well as for the development of fluorescence polarization based assays for target binding. However, the strong interaction of Atto465 with CaM is detrimental for FRET based studies due to the slow orientational motion of dipoles of dyes. Having 50% of the rotational correlation time amplitude for both slow and fast component of the anisotropy decay, AF488 and OG488 have similar interactions with CaM. Similar behaviors of these negatively charged and neutral dyes needs to be further tested with more dyes with strong negative charges and molecular dynamic simulations of related experimental findings.

Time–Resolved anisotropy: Fluorescence anisotropy decay was calculated by fitting data in vertical and horizontal channels. Interpretation of the decay behavior of vertical and horizontal channels can be accomplished by assuming single exponential decay kinetics for the fluorescence and rotational decays. For a single exponential decay, equation 2.2 and 2.3 take the form [28; 29; 31]:

$$3I_V(t) = A\exp^{-t/\tau} + 2Ar_0\exp^{-t(1/\tau + 1/\Phi)} \qquad (2.10)$$

$$3I_H(t) = A\exp^{-t/\tau} - Ar_0\exp^{-t(1/\tau + 1/\Phi)} \qquad (2.11)$$

These equations show that the polarized decays are simply biexponential decays. The first term is the fluorescence decay and the second component decays at a rate of the sum of fluorescence and rotational decay rates. In the vertical decay, we are adding these two components, and the decay due to rotation is always faster than the fluorescence decay. Therefore, at short times, the vertical decay will be faster than the fluorescence decay, and a long times the vertical decay will converge with the

fluorescence decay. In the horizontal decay, the rotational component is subtracted; therefore there will be a rising component initially, and at long times the decay will converge to the fluorescence decay.

As seen in the Table 2.2 the corresponding amplitudes of the fast rotational correlation times provide insight into the independent probe motion of each dye-protein conjugate. Given the importance of understanding the photophysical behavior of conjugated dyes in various fluorescence techniques, we will focus this discussion onto the probe's segmental motion. Consider the negatively charged AF488 and the neutral OG488, where both share the same amplitudes of 50 % for the fast correlation time component. This enhanced segmental motion of AF488 and OG488 can be understood by assuming repulsive forces exerted by negatively charged residues on AF488. The presence of both long and short correlation times suggests that the interaction between CaM and AF488 seems to be governed by electrostatic repulsions as well as by some other factors like hydrophobic interactions to keep segmental motion from completely taking over the correlation time component. Suppose the interaction between CaM and AF488 is purely electrostatic. There could have been only a single correlation time as reflected by faster probe since the electrostatic repulsion between CaM and AF488 will always keep the dye free. This argument can be reinforced by the findings by Unruh et al for a fluorescein-aptamer. They reported only a single correlation time of 590 ps for temperature range of 15 to 75^0C. Lack of a long correlation time component provides evidence for an uncoupled dye motion

from the global motion due to repulsion of negatively charged fluorescein and aptamer backbone [14].

By comparison with the rotational correlation time amplitudes of CaM-Atto465, the influence of the electrostatic charge of the dye on interactions with protein can be assessed. The faster rotational correlation time component of CaM-Atto465 possesses an amplitude of only 30%. The diminished amplitude of the shorter component can be accounted by attributing this to a lower population with free dye. The stronger coupling of the dye to CaM is a result of an enhanced electrostatic attraction between positively charged Atto465 with neighboring negatively charged residues.

Existence of these fast and slow components in a dye-protein (dye-macromolecule) conjugate could manifest itself in two ways: First, the slow and fast component of the anisotropy decay could indicate two different species of the dye conjugates in solution as in Figure 2.7. One species has a little or no interaction (see species A in Figure 2.7) with the protein displaying a large amount of local rotational freedom for segmental motion of the dye independent of rotation of protein molecules to which it is attached. The second species (B in Figure 2.7) in which the dye sticks to the protein domains in a docking configuration. This form of interaction of the dye will result in slow rotational amplitude reflecting the percentage of dye conjugate in this form. Secondly, the rotation of the dye could be restricted, in which case the amplitude of the fast rotational component indicates the extent (or angular distribution) of the rotational motion of the dye. This behavior of the dye is often

described by the wobbling-in-a-cone model, in which the rotational dipole of the dye is assumed to rotate freely within a certain "cone" (A in Figure 2.8). During its confined free rotation within the cone when dye passes by the edge of the cone, the extent of depolarization of emission corresponds to the amplitude of the fast rotational decay component. Overall rotation of the protein is responsible for the rest of depolarization of anisotropy decay [38; 39]. In this model anisotropy can be approximated by

$$t_{(t)} = r_0[(1-A_\infty)\, e^{-t/\Phi} + A_\infty] \qquad (2.12)$$

where $r_0 = 0.4\ P_2(\cos\ \lambda)$, and λ is defined as the angle between absorption and emission dipole moment fixed in the coordinate frame of the dye. A_∞ is a measure of degree of motional restriction and related to the semi cone-angle θ_{max} (B in Figure 1.9).

$$A_\infty = [\tfrac{1}{2}\ (1 + \cos\ \theta_{max})\ \cos\ \theta_{max}]^2 \qquad (2.13)$$

This expression shows that the smaller the cone angle the larger the A_∞. Obviously when the interaction of the dye and protein is stronger the cone angle will be smaller since the rotation is confined to a smaller cone.

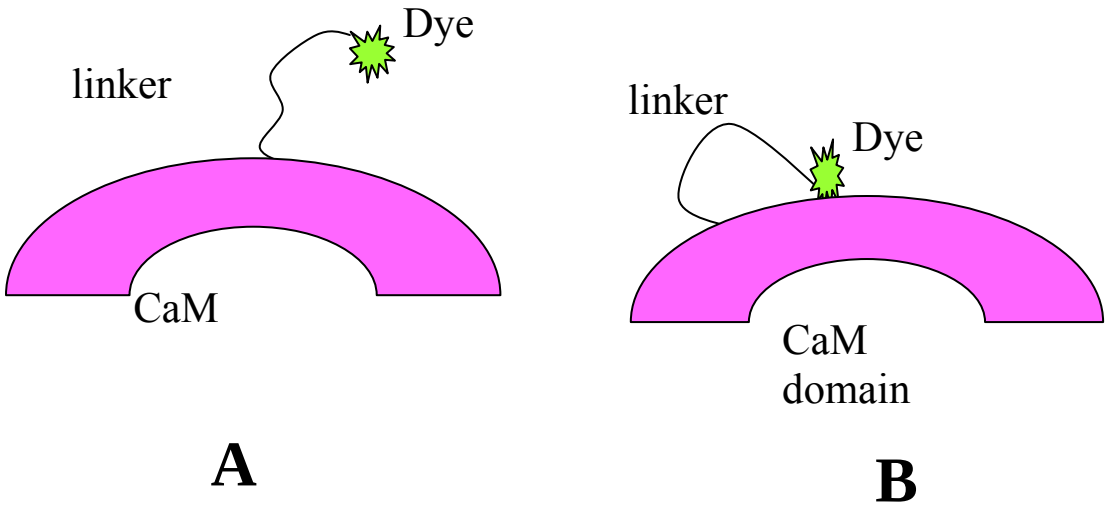

Figure 2.7 Model for dye-protein interaction assuming presence of two species in solution.

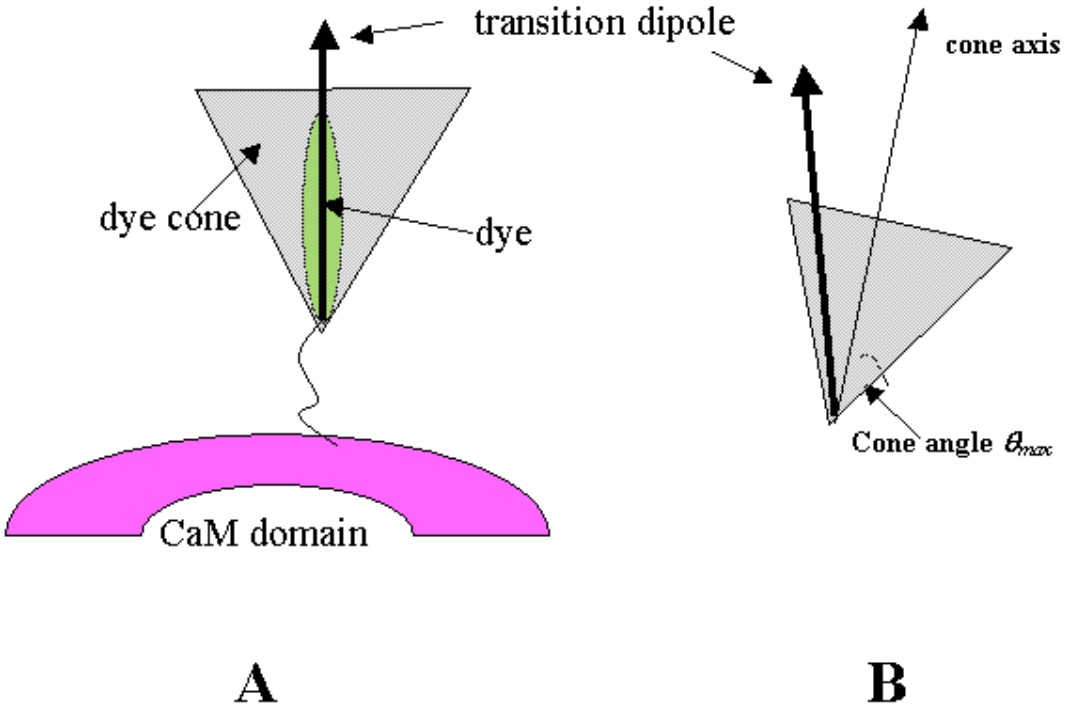

Figure 2.8 Wobbling-in-a-cone model for dye-protein conjugates. The transition dipole moment is assumed to have a confined diffusion inside a cone with the semicone angle θ_{max}.

Steady state Anisotropy: According to the Perrin equation (eq. 2.14), the steady state anisotropy of a given fluorophore depends on the lifetime of the fluorophore and the size of the fluorophore or the size of the molecule, which it is attached to.

$$r = r_0\left(\frac{1}{1+\tau/\phi}\right) \qquad (2.14)$$

According to the equation 2.14, for a given biomolecule labeled with different fluorophores with comparable lifetimes, the steady state anisotropy should be the same for each dye conjugate. The steady state anisotropy we obtained for CaM labeled with three fluorophores with comparable lifetimes are listed in the Table 2.3. The steady state anisotropy of AF488 and OG488-labeled CaM (0.10) was significantly smaller than that of Atto465 labeled CaM. Since all the three fluorophores have identical lifetimes, the CaM-conjugates should have the same anisotropy values. Thus the diminished anisotropy of AF488 and OG488 can be attributed to the presence of significant amplitude of segmental dye motion leading to depolarization of the emission. This further bolsters the claim made by using time-resolved anisotropy measurements. As expected Atto465-labeled CaM possesses a larger steady state anisotropy than other conjugates because the restricted motion of the dye minimizes depolarization coming from the segmental motion. We have also listed the anisotropy of a strongly negatively charged (-2) AF647 labeled CaM (Table 2.3) just to show the effect of lifetime has on the steady state anisotropy. Although AF647 is strongly negatively charged, its CaM conjugate has a very highest

anisotropy (0.28) among listed conjugates. This large anisotropy is a result of shorter lifetime of AF647 (2.2 ns) than other dyes (4-4.5 ns).

Dynamic Quenching Experiments: By comparing K_q values for CaM-dye conjugates under study, it is possible to evaluate the extent to which each dye interacts with CaM. The factor of six in K_q of Atto465 upon conjugation to CaM can be attributed to vastly reduced quencher accessibility to the fluorophore due to restricted segmental motion of the conjugated dye molecules. If K_q changes by a factor of greater than two for a given biomolecule, this change comes from the orientational restriction of fluorophores without introducing additional steric hindrance [25; 27]. Fluorescence lifetimes of free and conjugated dyes can be fit to a single lifetime without a significant change in χ^2 when trying to fit to two lifetime components. Furthermore the linearity of Stern-Volmer curves obtained for both free and conjugate form of dyes shows that fluorophores are equally accessible to the quencher in each conjugate with differential exposure depending on the fluorophore. These results indicate that only a single class of fluorophore is present in each conjugate. If two class of fluorophores were present, the plots would have deviated from the linearity towards the X axis [28]. This findings along with time resolved fluorescence anisotropy data therefore prefers the motion in-a-cone-model to interpret the nature of the interaction of dyes with CaM.

2.5 Conclusion

The strong correlation among the experimental results for time-resolved and steady state anisotropy as well as dynamic quenching experiments for three fluorophores provides solid evidence for differential interactions with CaM depending on the charge of the dye. The positively charged Atto465 interacts strongly with the negatively charged residues of CaM. However, results obtained for negatively charged AF488 and neutral OG488 indicated identical interaction behavior yet different from Atto465. Therefore more experiments need to be done with more strongly negative charged dyes such as fluorescein and AF647, to assess the influence of negative charge on the extent of dye interaction with CaM. The experimental results for the CaM conjugates require further verification by performing molecular dynamic (MD) simulations to unambiguously interpret these interactions. A thorough understating of the nature of dye-protein interaction and prediction though MD simulations will provide ample of information to better design FRET and anisotropy measurements based experiments.

2.6 References

[1]W.B. Dandilker, and V.A. De Saussre, Fluorescence polarization in immunochemistry. Immunochemistry 7 (1970) 799-828.

[2]D.M. Jameson, and W.H. Sawyer, Fluorescence anisotropy applied to biomolecular interactions. Methods Enzymol. 246 (1995) 283-300.

[3]M.U. Kumke, G. Li, L.B. McGown, G.T. Walker, and C.P. Linn, Hybridization of fluorescein-labeled DNA oligomers detected by fluorescence anisotropy with protein-binding enhancement. Anal. Chem. 67 (1995) 3945-3951.

[4]V. Letilly, and C.A. Royer, Fluorescence anisotropy assays implicate protein-protein interactions in regulating trp repressor DNA-binding. Biochemistry 32 (1993) 7753-7758.

[5]C.A. Royer, T. Ropp, and S.F. Scarlata, Solution studies of the interactions between the histone core proteins and DNA using fluorescence spectroscopy. Biophys. J. 43 (1992) 197-211.

[6]P.R. Selvin, Fluorescence resonance energy transfer. Methods Enzymol. 246 (1995) 300-334.

[7]B.W. Van der Meer, G. Cocker, and S.Y. Chen, Resonance energy transfer: Theory and data, VCH, New York, 1994.

[8]P. Wu, and L. Brand, Resonance energy transfer: Methods and applications. Anal. Biochem. 218 (1994) 1-13.

[9]B.W. Van der Meer, Kappa-squared: From nuisance to new sense. Rev. Mol. Biotech. 82 (2002) 181-196.

[10]G. Srinivas, and B. Bagchi, Effect of orientational motion of mobile chromophores on the dynamics of forster energy transfer in polymers. J. Phys. Chem. B 105 (2001) 9370-9374.

[11]A. Dietrich, V. Buschmann, C. Muller, and M. Sauer, Fluorescence resonance energy transfer (fret) and competeing processes in donor-acceptor substituted DNA strands: A comparative study of ensemble and single-molecule data. Rev. Mol. Biotech. 82 (2002) 211-231.

[12]T. Ha, Single-molecule fluorescence resonance energy transfer. Methods 25 (2001) 78-86.

[13]I. Rasnik, S. Myong, W. Cheng, T.M. Lohman, and T. Ha, DNA-binding orientation and domain conformation of the *E-coli* rep helicase monomer bound to a partial duplex junction: Single-molecule studies of fluorescently labeled enzymes. J. Mol. Biol. 336 (2004) 395-408.

[14]J.R. Unruh, G. Gokulrangan, G.H. Lushington, C.K. Johnson, and G.S. Wilson, Orientational dynamics and dye-DNA interactions in a dye-labeled DNA aptamer. Biophys. J. 88 (2005) 3455-3465.

[15]J.R. Unruh, G. Gokulrangan, G.S. Wilson, and C.K. Johnson, Fluorescence properties of fluorescein, tetramethylrhodamine and Texas red linked to a DNA aptamer. Photochem. Photobiol. 81 (2005) 682-690.

[16]E. Rusinova, V. Tretyachenko-Ladokhina, O.E. Vele, D.F. Senear, and J.B.A. Ross, Alexa and Oregon green dyes as fluorescence anisotropy probes for

measuring protein-protein and protein-nucleic acid interactions. Anal. Chem. 308 (2002) 18-25.

[17]J.J. Hill, and C.A. Royer, Fluorescence approaches to study of protein-nucleic acid complexation, Fluorescence spectroscopy, Academic Press Inc, San Diego, 1997, pp. 390-416.

[18]R.M. Clegg, A.I.H. Murchie, A. Zechel, and D.M.J. Lilley, Observing the helical geometry of double-stranded DNA in solution by fluorescence resonance energy-transfer. Proc. Natl. Acad. Sci. U.S.A. 90 (1993) 2994-2998.

[19]G.F. Schroder, U. Alexiev, and H. Grubmuller, Simulation of fluorescence anisotropy experiments: Probing protein dynamics. Biophys. J. 89 (2005) 3757-3770.

[20]T. Tokimoto, T.R.C. Bethea, M. Zhou, I. Ghosh, and M.J. Wirth, Probing orientations of single fluorescent labels on a peptide reversibly binding to the human delta-opioid receptor. Appl. Spectrosc. 61 (2007) 130-137.

[21]B.W. Chen, M.U. Mayer, L.M. Markillie, D.L. Stenoien, and T.C. Squier, Dynamic motion of helix a in the amino-terminal domain of calmodulin is stabilized upon calcium activation. Biochemistry 44 (2005) 905-914.

[22]D. Wallach, Effects of internal rotation on angular correlation function. J.Chem. Phys. 47 (1967) 5258-5268

[23]G. Lapari, and A. Szabo, Effects of vibrational motion on fluorescence depolarization and nuclear magnetic resonance relaxation in macromolecules and membranes Biophys. J. 30 (1980) 489-506.

[24]M.M. Fonseca, H.M. Scofano, P.C. Carvalho-Alves, H. Barrabin, and J.A. Mignaco, Conformational changes of the nucleotide site of the plasma membrane Ca^{2+}-ATPase probed by fluorescence quenching. Biochemistry 41 (2002) 7483-7489.

[25]D.A. Johnson, J. Yguerabide, and P. Taylor, Effect of rotational diffusion on fluorescence quenching by iodide - assessment of solute assessability to nepsilon-fluorescein isothiocyanate-lysine-23-cobra alpha-toxin bound to the acetylcholine-receptor. Biophys. J. 45 (1984) A380-A380.

[26]K.S. Schimitz, and J.M. Schurr, The role of orientational constraints and rotational diffusion in bimolecular solution kinetics. J. Phys.Chem. 76 (1972) 534-541.

[27]D.A. Johnson, and J. Yguerabide, Solute accessibility to n-epsilon-fluorescein isothiocyanate-lysine-23 cobra alpha-toxin bound to the acetylcholine-receptor - a consideration of the effect of rotational diffusion and orientation constraints on fluorescence quenching. Biophys. J. 48 (1985) 949-955.

[28]J.R. Lakowicz, Advanced topics in fluorescence quenching Principles of fluorescence spectroscopy, Kluwer acedemics/ Plenum publishers, New York, 1999.

[29]J.R. Unruh, Development of fluorescence spectroscopy tools for the measurments of biomolecular dynamics and heterogeneity, Chemistry, University of Kansas, Lawrence, 2006.

[30]M.W. Allen, R.J.B. Urbauer, A. Zaidi, T.D. Williams, J.L. Urbauer, and C.K. Johnson, Fluorescence labeling, purification, and immobilization of a double cysteine mutant calmodulin fusion protein for single-molecule experiments. Anal. Biochem. 325 (2004) 273-284.

[31]D.V. O'Connor, and D. Phillips, Time-correlated single photon counting, Academic Press, London, 1984.

[32]D.P. Shoemaker, and C.W. Garland, Experiments in physical chemistry, McGraw-Hill Book Company, New York, 1967.

[33]M.R. Eftink, Fluorescence quenching: Theory and applications. in: J.R. Lakowicz, (Ed.), Principles of fluorescence, Plenum Publishing, New York, 1983.

[34]B.D. Slaughter, J.R. Unruh, M.W. Allen, R.J.B. Urbauer, and C.K. Johnson, Conformational substates of calmodulin revealed by single-pair fluorescence resonance energy transfer: Influence of solution conditions and oxidative modification. Biochemistry 44 (2005) 3694-3707.

[35]E. Haas, E. Katchalskikatzir, and I.Z. Steinberg, Effect of orientation of donor and acceptor on probability of energy-transfer involving electronic-transitions of mixed polarization. Biochemistry 17 (1978) 5064-5070.

[36]G. Gokulrangan, J.R. Unruh, D.F. Holub, B. Ingram, C.K. Johnson, and G.S. Wilson, DNA aptamer-based bioanalysis of IgE by fluorescence anisotropy. Anal. Chem. 77 (2005) 1963-1970.

[37]M.U. Kumke, L.C. Shu, L.B. McGown, G.T. Walker, J.B. Pitner, and C.P. Linn, Temperature end quenching studies of fluorescence polarization detection of DNA hybridization. Anal. Chem. 69 (1997) 500-506.

[38]K. Kinosita, A. Ikegami, and S. Kawato, On the wobbling-in-cone analysis of fluorescence anisotropy decay. Biophys. J. 37 (1982) 461-464.

[39]K. Kinosita, S. Kawato, and A. Ikegami, Theory of fluorescence polarization decay in membranes. Biophys. J. 20 (1977) 289-305.

Chapter 3

Fluorescence polarization assay for calmodulin binding to plasma membrane Ca^{2+}-ATPase

3.1 Introduction

Fluorescence polarization (FP) occurs when fluorescent molecules are excited by linearly polarized light, resulting in polarized emission from the excited molecules. The extent of FP of a molecule depends on the relative values of the fluorescence lifetime and the rotational correlation time, which is proportional to the molecular volume of the molecule when the temperature and viscosity of the medium are kept constant [1]. Small fluorescent tracers rotate rapidly resulting in a low FP. Upon binding to a larger molecule the tumbling rate of the fluorescent tracer slows down, generating a higher FP.

The ratiometric nature of the FP measurement cancels out intensity differences due to variability in concentration, making FP a reliable measure for assay development. Therefore FP assays are extensively used for detecting interactions of biomolecules. This powerful and sensitive detection method has been a robust tool in studying protein-DNA and protein-protein interactions [2; 3; 4; 5; 6; 7; 8], in human and animal clinical diagnostics [9; 10; 11; 12; 13], in detecting toxins in agricultural products [14], and in high-throughput screening [15; 16; 17] . Due to the fact that FP is a rapid, sensitive, simple and homogeneous technique that does not require a separation step, the method can readily be adapted to high-throughput screening applications. FP assays have been extensively used to screen small molecule libraries

to select compounds having desired binding properties to target biomolecules [18]. Recently, FP was used to detect binding of fluorescently labeled CaM to calcineurin [19].

Sensitive methods are needed to detect and characterize the interactions among CaM and its targets. CaM binds four Ca^{2+} ions in response to elevation in intracellular Ca^{2+} levels [20; 21]. Ca^{2+} pumping by PMCA has been proposed to occur via a mechanism characteristic of P-type ATPases in which ATP binding and subsequent autophosphorylation of a conserved aspartate residue on the enzyme are coupled with conformational changes that alter the Ca^{2+} binding affinity and the intracellular and extracellular access to Ca^{2+} binding sites [22; 23]. Binding of CaM to PMCA leads to dissociation of an autoinhibitory domain of PMCA from close proximity to the active site of the enzyme, removing the self-inhibition of the enzyme and thereby stimulating the PMCA activity several fold [24]. PMCA has also been shown to play a role in mediating the loss of Ca^{2+} homeostasis in cells under oxidative stress [25; 26], and an inhibition of CaM-stimulated activity has been observed upon oxidative modification of PMCA [27].

Previously, the CaM-PMCA binding affinity has been measured only indirectly by detection of enzyme activity [28; 29]. In this paper, we report an FP measurement of the binding affinity of CaM and PMCA in a simple and direct manner. The dissociation constant (K_d) of the CaM-PMCA complex that we derived using this method is consistent with previous measurements [28]. For oxidatively modified PMCA the dissociation constant measured by the FP assay was also nearly

the same, indicating that loss of CaM-induced activity is not the result of a decreased CaM binding affinity. This finding adds to our understanding of the mechanism underlying the loss of activity of oxidized PMCA. The measurements also revealed the concentration-dependent onset of oligomerization of PMCA. We also studied the Ca^{2+} dependence of CaM-PMCA interaction, which reveals cooperativity in Ca^{2+} binding to CaM in the presence of PMCA. The affinity of CaM for Ca^{2+} was enhanced by the presence of PMCA, but not as much as might be expected based on the differences in affinities of CaM for PMCA in the presence and absence of Ca^{2+}.

Precise control of free Ca^{2+} concentrations in the low nanomolar range is challenging given the complexity of biological samples, especially those containing metal ion chelating agents as an integral part of the sample. Tsien and co workers have developed a method to control Ca^{2+} in biological samples by using a calcium buffer consisting of high concentrations of Ca^{2+} ions and EGTA [30]. Measuring the free Ca^{2+} concentrations with great accuracy under a biological environment is also crucial in studying the effect of Ca^{2+} on biological events. Ca^{2+}-sensitive dyes have been used to measure free Ca^{2+} by means of changes in the absorbance or luminescence characteristics of dyes upon binding to Ca^{2+} [30; 31; 32]. Fura-2 has been used to measure Ca^{2+} in ratiometric approaches where the effect of uneven dye concentrations and photobleaching are cancelled put by the ratiometric measurements.

3.2 Materils and Methods

Anisotropy measurements. Fluorescence anisotropy experiments were performed at 25^0C using a standard Quantamaster fluorimeter (Photon Technology International Inc.). Excitation and emission polarization were selected with Glan-Thompson polarizers with the medium aperture configuration of the fluorimeter. Fluorescence excitation by a xenon lamp at 488 nm and emission at 520 nm were selected with 4 and 6-nm bandpass filters for excitation and emission, respectively. The steady-state anisotropy *r* was calculated with the equations 2.7 and 2.8 (See chapter 2):

Sample preparation. The T34C-CaM mutant was prepared by replacing a threonine residue at position 34 with a cysteine as previously described [33]. T34C-CaM was labeled with Oregon green 488 maleimide (Molecular Probes, Eugene, OR) following the standard protocols from the manufacturer. To separate unreacted free dye from the labeled protein, the reaction mixture was passed through a size exclusion column packed with Sephadex G-25 resin (Amersham Biosciences) followed by repeated dialysis against 4 L of a buffer consisting of 10 mM HEPES, 0.1 M KCl, 1 mM $MgCl_2$, and 0.1 mM $CaCl_2$. After dialysis, the resultant solution was centrifuged with a 10,000 molecular weight cut off filter (Millipore) at a speed of 3200 rpm for 10 min to concentrate the labeled protein and further remove the free dye.

PMCA was purified from freshly drawn human blood by affinity chromatography on a CaM-sepharose column as described previously by Osborn and

coworkers [34], and stored at −80 °C. The concentration of the purified PMCA was determined with the Follin-Ciocalteu reagent [35] and found to be 167 nM. The activity of the purified PMCA was tested as previously described [27]. To generate oxidatively modified PMCA, 200 μL of 167-nM purified PMCA was exposed to 100 μM H_2O_2 for 10 minutes at 37 °C as described previously [27]. The reaction was quenched by the addition of two units of catalase, and the vial was incubated at 23 °Cto allow the remaining H_2O_2 to decompose.

Determination of K_d of PMCA. A 1.00-mL sample of 3.2-nM CaM fluorescently labeled with Oregon Green 488 (CaM-OG488) was titrated by addition of 10-μL aliquots of 167-nM PMCA. The final concentrations of CaM-OG488 and PMCA were determined by taking into account the dilutions upon addition of each PMCA aliquot. The assay buffer contained 10 mM HEPES (pH 7.4), 0.1 M KCl, 1 mM $MgCl_2$, and 0.1 mM $CaCl_2$ resulting in a 10-μM free Ca^{2+}concentration. Before measuring the anisotropy of the CaM-PMCA mixture, CaM-OG488 and PMCA were mixed well and allowed to incubate for 10 min after addition of each aliquot of PMCA. The anisotropy of CaM-OG488 was determined after addition of each PMCA aliquot.

Ca^{2+} Dependence of CaM binding to PMCA. The Ca^{2+} ion dependence of the interaction of CaM with PMCA was determined in a series of solutions ranging from a few nanomolar to a few micromolar Ca^{2+}. The buffers containing 10 mM CaEGTA (10 mM HEPES, 100 mM KCl, 10 mM EGTA, 1.35 mM $MgCl_2$ and 10 mM $CaCl_2$) and 0 mM CaEGTA (10 mM HEPES, 100 mM KCl, 10 mM EGTA, and

1.35 mM $MgCl_2$) were mixed in varying proportions to achieve the desired Ca^{2+} concentration. Equal amounts of CaM-OG488 and PMCA were added to both high Ca^{2+} and zero Ca^{2+} buffers before mixing and the final concentrations were 3 nM CaM-OG488 and 10 nM PMCA. Ca^{2+} concentrations were determined with the Ca^{2+} indicator dyes fura-2 and 2,2'-dibromobapta (Molecular Probes) in the ranges 50 nM to 1 μM and 1 μM to 10 μM, respectively [36]. Calibration standard buffers (Molecular Probes) were mixed according to the procedure recommended by the manufacturer to calibrate the indicator dyes. Briefly, the procedure was as follows: 10 μL of 120 μM fura-2 was dissolved in 2 mL of 0-mM Ca^{2+}-EGTA and 30 μL of 120-μM fura-2 was dissolved in 6 mL of 10-mM Ca^{2+}-EGTA. These solutions were mixed in varying proportions to obtain a series with varying free Ca^{2+} concentration. The free Ca^{2+} concentration upon subsequent dilutions was determined from:

$$[Ca^{2+}]_{Free} = K_d^{EGTA} \cdot \frac{[\mathrm{CaEGTA}]}{[\mathrm{K_2EGTA}]} \qquad (3.1)$$

For high Ca^{2+} concentrations, the absorbance at 262 nm in the presence of 2,2'-dibromobapta was monitored with a Cary 100 spectrophotometer (Varian Inc.) for each dilution. For lower concentrations, (<1 μM) the data collected with the dilution series for fura-2 was used to generate the calibration curve from:

$$[Ca^{2+}]_{Free} = K_d \frac{[R - R_{\min}]}{[R_{\max} - R_{\min}]} \cdot [F^{380}{}_{\max}/F^{380}{}_{\min}] \qquad (3.2)$$

where R is the ratio of emission intensities at 510 nm upon excitation at 340 nm and 380 nm; R_{min} is the ratio at zero free Ca^{2+} and R_{max} is the ratio at saturating free Ca^{2+} ; $F^{380}{}_{\max}$ and $F^{380}{}_{\min}$ are the fluorescence intensities at 380 nm excitation for zero free

Ca^{2+} and saturating free Ca^{2+} respectively. The K_d of fura-2 and 2, 2'- dibromobapta derived from the calibration plots were used in the determination of free Ca^{2+} in test samples along with other measured experimental parameters as described above.

3.3 Results

CaM-PMCA dissociation constant. To determine the dissociation constant of the CaM-PMCA complex, CaM-OG488 was titrated against PMCA in a quartz cuvette. The steady state anisotropy of CaM-OG488 increased as it bound to the larger PMCA (see Figure 3.1). The emission intensity of the solution remained nearly constant during the entire course of titration.

In order to achieve the desired sensitivity, the labeled protein concentration was kept low enough to minimize the anisotropy contribution from free labeled protein but high enough to generate adequate fluorescence intensity. We used an optimum initial CaM-OG488 concentration of 3.2 nM (lower than the K_d of PMCA) in the titration to achieve the desired sensitivity. The steady-state anisotropy of CaM-OG488 in the absence of PMCA was 0.11. For low concentrations of PMCA, the anisotropy changes for CaM-OG488 appeared to follow a bimolecular binding curve, approaching saturation at PMCA concentrations of 10 to 15 nM. However, as the PMCA concentration was increased further, large increases in anisotropy were observed (inset in Figure 3.1). As a result, it was not possible to record a binding curve to full saturation. The onset of these anisotropy increases occurred around the enzyme concentration where oligomerization of PMCA has been previously reported

(12 to 18 nM) [37]. This suggests that increases in anisotropy at concentrations above 16 to 20 nM may be attributed to PMCA oligomerization. It is therefore necessary to base the determination of the dissociation constant on anisotropy data for PMCA concentrations less than 10 nM, i.e., conditions where it is monomeric.

The changes in anisotropy and the concentrations of proteins were fit by nonlinear least square regression to the equation:

$$\Delta r = \frac{\Delta r_{\max}}{2C_t}\left\{\left(C_t + P_t + K_d\right) - \sqrt{\left(C_t + P_t + K_d\right)^2 - 4P_tC_t}\right\} \qquad (3.3)$$

where Δr is the change in anisotropy relative to the anisotropy of free CaM-OG488, K_d is the dissociation constant of the CaM-PMCA complex, C_t is the total CaM concentration, and P_t is the total PMCA concentration. The K_d for CaM-PMCA binding was 5.8 ± 0.5 nM (averaged over five data sets; the uncertainty is the standard error). The value for K_d determined from these measurements is consistent with the previously measured K_d values of PMCA obtained by kinetic activity measurements [28](37). For oxidatively modified PMCA (Figure 3.2), the K_d was nearly the same (9.8 ± 2.0 nM based on one measurement, with uncertainty determined by the F statistic applied to the χ^2 curve as a function of PMCA concentration). Modeling suggested that the K_d for binding to PMCA monomers may be on the order of 40% lower (see Supplementary Material of Liyanage et al [38]. However, without more detailed knowledge of the composition and concentration dependence of PMCA oligomers, it is only possible to estimate the contribution of oligomers to the binding curve. Therefore, we have based the reported dissociation

constants on PMCA concentrations below 10 nM. Even so, this assay provides a direct and rapid way to determine the affinity of CaM-target binding without relying on indirect kinetic methods. The assay was further tested with two other fluorophores. CaM labeled with Alexa Fluor 488 and Atto 465 yielded comparable binding constants for PMCA (results not shown).

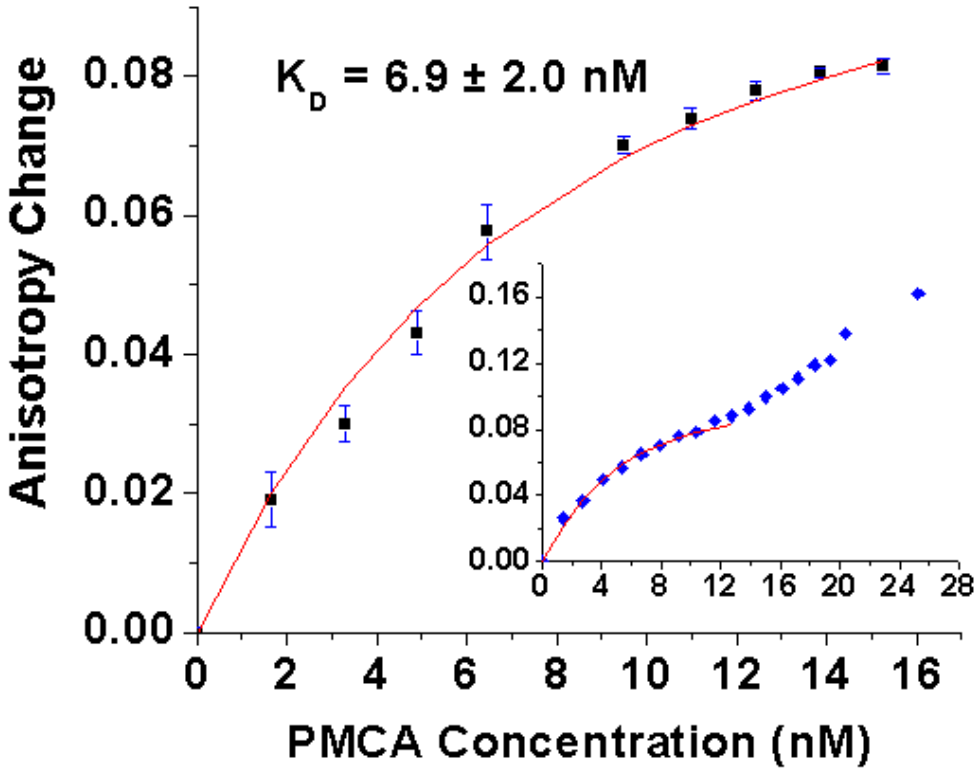

Figure 3.1 Binding of native PMCA to CaM-OG488 at 10 μM Ca^{2+} as monitored by the changes in anisotropy during the titration. The initial anisotropy was 0.11. The data were fit to eq. 3.5. The solid lines show fits with $K_d = 6.9^{+2.1}_{-1.6}$ nM (errors evaluated from the error surface with the F statistic corresponding to one standard deviation). The mean and standard error from five measurements of the K_d for binding of native PMCA to CaM-OG488 were 5.8 ± 0.5 nM. The inset shows the drastic change in anisotropy as the concentration of PMCA was increased above 14 nM.

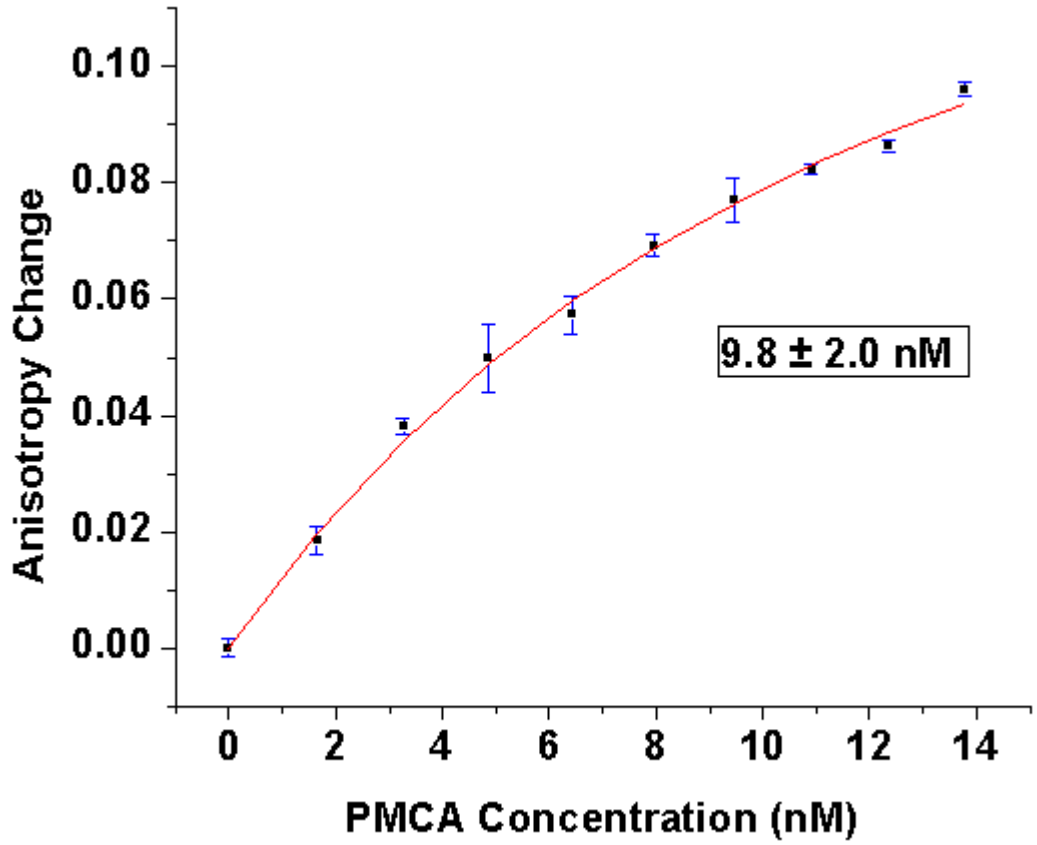

Figure 3.2 Binding of oxidatively modified PMCA to CaM-OG488 at 10 μM Ca^{2+} as monitored by the changes in anisotropy during the titration. The initial anisotropy was 0.11. The data were fit to eq. 3.5. The solid lines show fits with K_d = 9.8 ± 2.0 nM (errors evaluated from the error surface with the F statistic corresponding to one standard deviation).

Ca^{2+} dependence of CaM binding to PMCA. In order to measure the concentrations of free Ca^{2+}, the shifts in the fluorescence excitation spectra of Fura-2 were monitored as the Ca^{2+} concentrations changes. Figure 3.3 shows the recorded excitation spectra of Fura-2 at various Ca^{2+} concentrations. The calibration plot was constructed with the ratio of the excitation intensity at 380 nm and 340 nm with corresponding concentrations of Ca^{2+} is shown in Figure 3.4

CaM binds to PMCA at elevated levels of Ca^{2+}. Understanding the Ca^{2+} dependence of CaM binding to PMCA is crucial to understanding the regulation of PMCA. To investigate the Ca^{2+} dependence, we carried out anisotropy measurements of CaM in the presence of PMCA in solutions with varying molarities of Ca^{2+}. The results are shown in Figure 3.5. In order to fix the Ca^{2+} concentration in the presence of EDTA and Ca^{2+} contained in the PMCA preparation, we prepared a systematic series of Ca^{2+} buffers containing EGTA and Ca^{2+} as described in Experimental Methods. The increase in the anisotropy as the Ca^{2+} concentration increased shows the Ca^{2+} dependence of CaM target binding.

The changes in anisotropy values of CaM-OG488 and PMCA complex upon changing Ca^{2+} concentration were fit to the Hill equation (eq. 3.4) to facilitate comparison of the empirical Hill coefficient with results from other labs:

$$\Delta r = \Delta r_{\max} \cdot \frac{\left[Ca^{2+}\right]^n}{\left(K_d^{eff}\right)^n + \left[Ca^{2+}\right]^n} \quad . \qquad (3.4)$$

In eq 6, n is the Hill coefficient and K_d^{eff} is the effective macroscopic dissociation constant for Ca^{2+} ions. The solid line in Figure 3.5 shows the fit to this equation. The

data followed a simple Hill plot (n = 1.6 ± 0.2 and K_d^{eff} = 1.01 ± 0.1 μM) demonstrating cooperative binding of Ca^{2+} to CaM upon target binding. The binding curves were also fit to a two-state binding model:

$$\Delta r = \Delta r_{\max} \cdot \frac{K_1\left[Ca^{2+}\right] + 2K_1K_2\left[Ca^{2+}\right]^2}{2\left(1 + K_1\left[Ca^{2+}\right] + K_1K_2\left[Ca^{2+}\right]^2\right)} \quad , \qquad (3.5)$$

where K_1 is the macroscopic equilibrium constant for binding the first Ca^{2+} ion and K_2 is the macroscopic equilibrium constant for binding the second. A fit to eq. 3.5 yielded values of $K_1 = 4.1 \times 10^5 \pm 0.3 \times 10^5$ M^{-1} and $K_2 = 2.4 \times 10^6 \pm 0.7 \times 10^6$ M^{-1}.

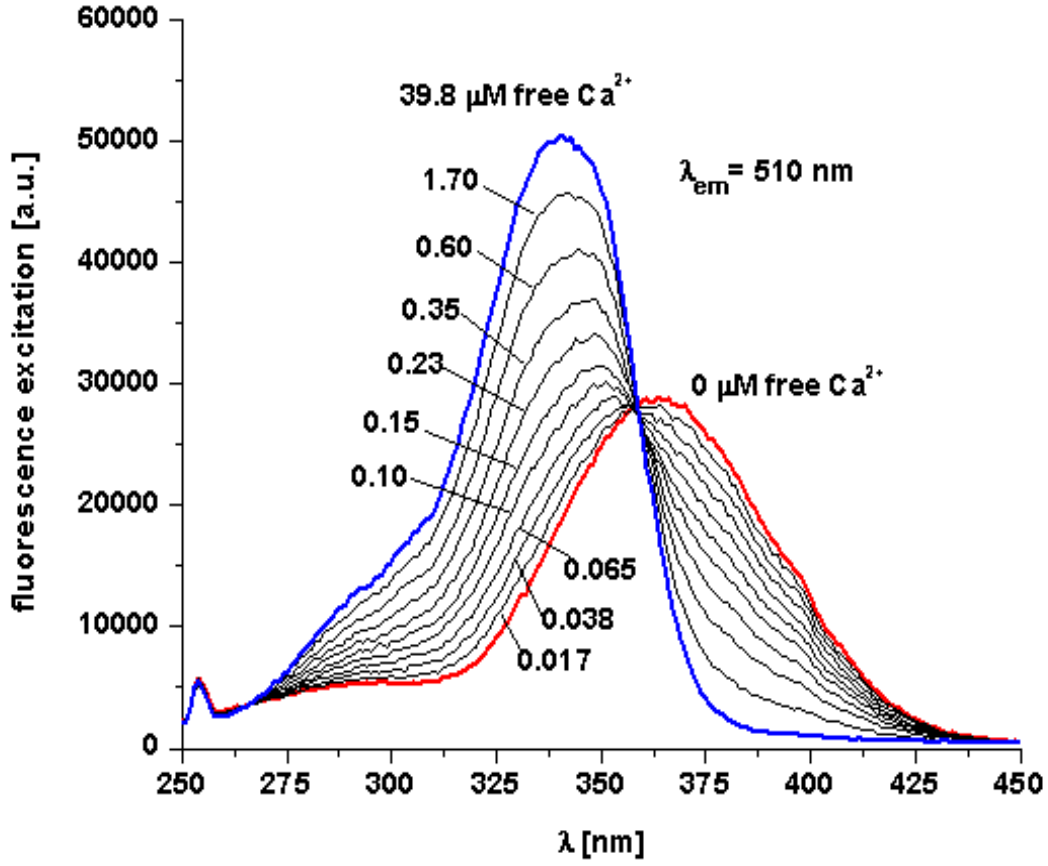

Figure 3.3 The shifts in fluorescence excitation spectra of Fura-2 upon increasing Ca^{2+} concentration from 0 39 μM. The excitation spectra of Fura-2 at two extremes are shown with red for 0 Ca^{2+} and blue for 39 μM Ca^{2+}.

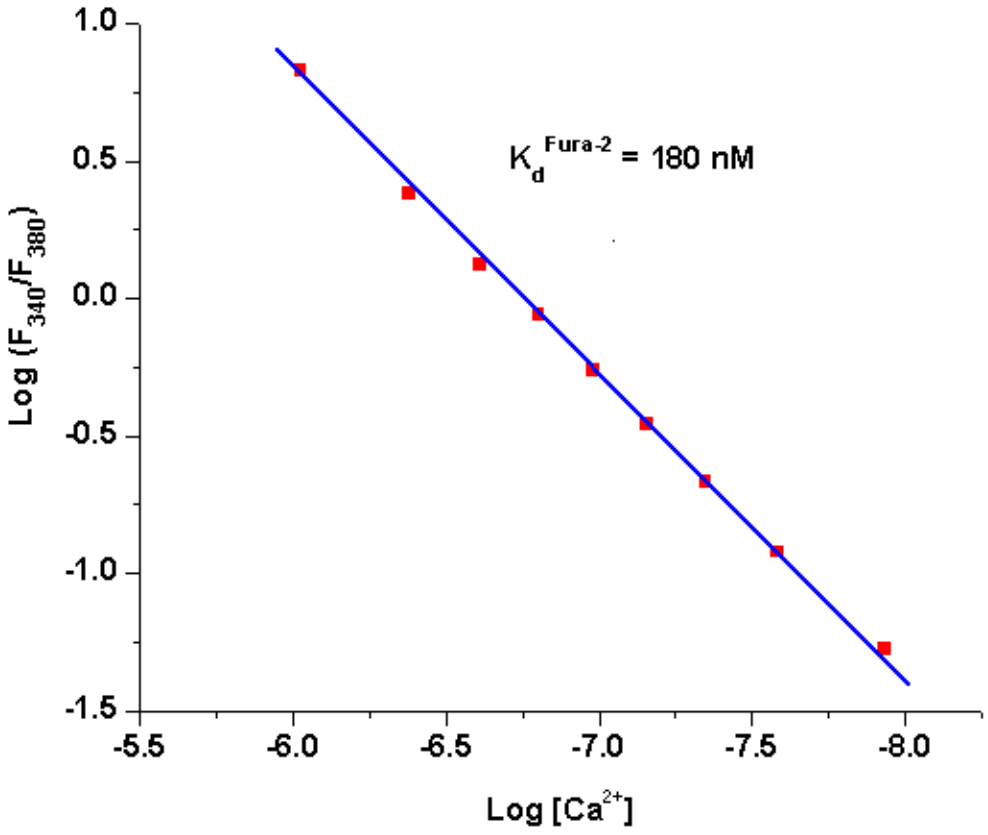

Figure 3.4 The calibration plot constructed with calcium standards to derive the calcium dissociation constant of Fura-2 at pH 7.2.

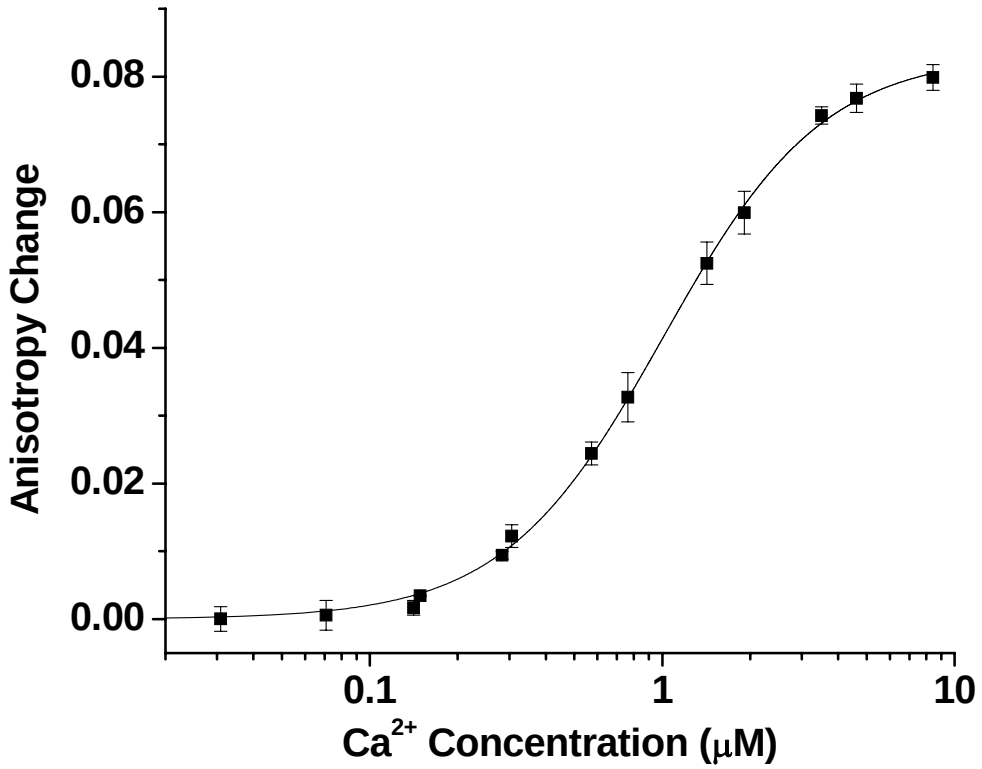

Figure 3.5. Ca^{2+} dependence of the anisotropy changes upon CaM-OG488 binding to PMCA. The solid line shows a fit to the Hill equation (eq. 3.4) with n = 1.6. The macroscopic dissociation constant, K_d^{eff}, and Hill coefficient, n, determined from the fit are listed in Table 3.1.

Table 3.1 Ca^{2+} binding constants for CaM in presence of PMCA.[a]

n [b]	K_d^{eff} [c] (μM)	K_1 [d] (μM^{-1})	K_2 [d] (μM^{-1})
1.6 ± 0.2	1.01 ± 0.10	0.4 ± 0.3	2.4 +0.7/–0.1

[a]Uncertainties were estimated from the F statistic corresponding to one standard generation applied to the χ^2 surface generated with all other fitting parameters free to vary.

[b]Hill coefficient from fit of binding Ca^{2+} binding data to eq 3.4

[c]Effective dissociation constant from fit of Ca^{2+} binding data to eq 3.5

[d]Ca^{2+} macroscopic binding constants for the first (K_1) and second (K_2) Ca^{2+} ions to the two high-affinity Ca^{2+} binding sites

3.4 Discussion

FP measurement. The ratiometric nature of steady-state anisotropy measurements makes them a robust and sensitive method for assays, as the technique is insensitive to slight differences in the loading of labeled protein. In applications where V and H polarizations can be measured simultaneously, intensity fluctuations also cancel out. The inherent sensitivity of FP measurements upon binding a small tracer to a bigger target comes from the dependence of the rotational correlation time on the volume of the molecule. As has been pointed out previously [39], it is important to optimize the balance between the rotational correlation times measured (in this case those of CaM-OG488 and PMCA-CaM-OG488) and the fluorescence lifetime of the fluorophore. Oregon Green 488 is a useful dye for such measurements owing to its photochemical and photophysical stability [39].

The sensitivity of the FP assay is strongly influenced by dye-protein interaction. If the dye molecule itself undergoes free rotation independent of the rotation of the protein (CaM), the fluorescence emission depolarizes rapidly even though a complex has formed. In this case the change in fluorescence polarization upon binding to a bigger molecule is not significant. Therefore a sensitive FP assay requires that the fluorescent dye stick to the protein used as the reporter in the FP assay so that its fluorescence depolarization reports the rotational correlation time of the reporter protein. The interaction of OG488 with CaM was confirmed by time-resolved fluorescent anisotropy measurements, which showed that 50% of the anisotropy decay of OG488 occurs with the rotational motion of CaM. As described

in chapter 2, the other 50% occurs by segmental motion of the dye. A large anisotropy decay fraction due to protein rotation is consistent with the sensitivity of CaM-OG488 anisotropy to binding to PMCA.

The anisotropy increases upon binding of CaM to PMCA are substantial. From an initial value of 0.11, the anisotropy increased by 0.08 to 0.12. According to the Perrin equation, the maximum anisotropy change Δr_{max} associated with the change in volume can be written as:

$$\Delta r_{\max} = \Delta\left[r_0\left(1+ \tau/\phi\right)^{-1}\right] \qquad (3.6)$$

where τ is the fluorescence lifetime (4.1 ns) and ϕ is the rotational correlation time of the tracer (CaM-OG488) upon forming the complex. The anisotropy r_0 is the maximum steady-state anisotropy in the absence of rotational diffusion, i.e. the anisotropy value *after* segmental motion of the dye but *before* reorientation of CaM. From the time-resolved anisotropy decay of CaM-OG488 (data not shown), r_0 has a value of ca. 0.17 to 0.19 for CaM-OG488. Based on these considerations, the expected maximum anisotropy upon binding of CaM is 0.06 to 0.08. The measured anisotropy changes are in fact larger: the maximum anisotropy change from the fit in Figure 3.1 to a binding equilibrium is 0.12. The anisotropy change must therefore result from factors other than the change in hydrodynamic volume. This suggests decreased segmental motion of the dye upon CaM binding to PMCA. Although independent segmental motion of the dye was lower in OG488 than in some other dyes we tested, it was not completely eliminated. Thus, it appears that the maximum

anisotropy r_0 increases upon CaM binding to PMCA, enhancing the sensitivity of the FP measurement.

Dissociation constant for PMCA-CaM-OG488. Previous measurements of the K_d of CaM binding to PMCA have yielded values of 4.2 nM to 7.6 nM [28; 29], in good agreement with the value of 5.8 ± 0.5 nM reported here. The previous measurements, however, relied on assays of enzyme activity to determine CaM on and off rates from which the K_d of CaM-PMCA could be calculated. This technique is based on the ATP turnover rate of PMCA in the presence of CaM and the assumption that ATP turnover directly tracks CaM binding to PMCA. Therefore, in addition to the quickness of FP measurements, a further advantage of FP measurements is that they directly measure the CaM binding to PMCA. This direct, simple and homogeneous assay therefore opens the way to study PMCA under different environments or to investigate the differences of PMCA in different tissues.

The dissociation constant for oxidatively modified PMCA (9.8 ± 2.0 nM) was not significantly different from the value for native PMCA. This result is consistent with the finding that the activation constant for CaM stimulation of PMCA activity was only modestly altered by oxidative modification of PMCA (0.8×10^{-8} M for native PMCA vs. 1.9×10^{-8} M for H_2O_2-treated PMCA) [27]. This finding suggests that the loss in CaM-stimulated activity of PMCA upon treatment with H_2O_2 is not a result of a reduced affinity for CaM, but is rather a consequence of altered coupling between CaM binding and enzyme activation, as suggested previously .

PMCA oligomerization. Another feature in the titration of CaM-OG488 with PMCA is the further increase in the anisotropy change for PMCA concentrations above 15-20 nM (see Figure 3.1 inset). It has long been known that PMCA oligomerizes at concentrations above 10 to 20 nM [37]. Another study of the oligomerization of PMCA yielded a value of 140 ± 50 nM for the dissociation constant for oligomeric PMCA [40]. Our results are consistent with an onset of oligomerization between 15 and 20 nM under our experimental conditions.

Considerations similar to those discussed above for the magnitude of the anisotropy change must also apply to the anisotropy changes that occur upon oligomerization. The observed anisotropy increases by 0.05 with an increase in PMCA concentration from 12 to 20 nM (Figure 3.1 inset), an anisotropy increase that is larger than could be accounted for by an increase in volume alone. For CaM-OG488 bound to the PMCA monomer, the ratio τ/ϕ is already a small number (less than ca. 0.07). Thus, the volume change upon oligomerization can change the anisotropy by only a few percent. The larger anisotropy increases detected for PMCA concentrations above 12 nM are therefore likely a result of further decreases in the freedom of segmental motion of the dye. It is possible that as the size of oligomers increases, such interactions progressively decrease the segmental motion of OG488, resulting in continued anisotropy increases. This result shows that the FP assay can also be used to study conditions that affect PMCA aggregation.

Because such a process depends on the details of interactions of OG488 as oligomers form, and these details are not known, it is not possible to model the

anisotropy increase except in an approximate manner. Therefore, we report a value for the dissociation constant of PMCA-CaM-OG488 based on PMCA concentrations less than 10 nM, where oligomerization appears to be negligible. An approximate treatment including a model for oligomerization is discussed in Supplemental Information of Liyanage et al [38] to show that this approach does not significantly undermine the determination of the dissociation constant.

Ca^{2+} dependence of PMCA binding. The binding of CaM to PMCA is regulated by Ca^{2+}. Figure 3.5 shows the response of the anisotropy of CaM-OG488 to Ca^{2+} in the presence of PMCA. CaM is known to bind to PMCA upon Ca^{2+} binding to the two C-terminal Ca^{2+} binding sites of CaM [41]. As a result, we expect that the anisotropy change is sensitive to Ca^{2+} binding to the two C-terminal binding sites, but is probably not sensitive to binding to the two N-terminal Ca^{2+} binding sites. The Ca^{2+} binding curves were therefore fit to a two-site binding model (eq 3.5). However, the Ca^{2+} affinity of CaM in the presence of PMCA is not as high as that reported for CaM in the presence of peptides representing the CaM binding domain of PMCA [42; 43], indicating an altered coupling between Ca^{2+} binding and target binding in the peptide alone compared to the full enzyme.

As has been noted previously [43; 44; 45; 46; 47], the effect of Ca^{2+} binding by CaM on its affinity for targets such as PMCA has a thermodynamic corollary. The greatly enhanced affinity of CaM for PMCA by binding of Ca^{2+} to CaM requires that the affinity of CaM for Ca^{2+} is increased in the presence of PMCA. The Ca^{2+} dependence of CaM-PMCA binding (Figure 3.5) confirms this result. The enhanced

Ca^{2+} affinity is manifested by an increased affinity for Ca^{2+} in the presence of PMCA (see Table 3.1) compared to CaM in the absence of PMCA. The value for K_d^{eff} reported here can be compared to a value of 2.0 ± 0.1 μM reported for a Hill fit for the high-affinity pair of Ca^{2+} binding sites in CaM . Alternatively, the product of the binding constants K_1 and K_2 in equation 7 (~1.0 μM^{-2}, see Table 3.1), i.e. the equilibrium constant for binding two Ca^{2+} ions, can be compared with values of ~0.3-0.4 μM^{-2} determined previously for CaM under similar conditions but in the absence of target [44; 48; 49].

It is intriguing to consider the apparent three-fold increase in the equilibrium constant K_1K_2 for binding two Ca^{2+} ions to CaM in the presence of PMCA compared to CaM in the absence of target. The simplest model (consisting of the states apoCaM, $(Ca^{2+})_2$-CaM, $(Ca^{2+})_2$-CaM-PMCA, and apoCaM-PMCA), would predict only a three-fold corresponding decrease in the affinity of apoCaM for PMCA compared to CaM with two Ca^{2+} ions bound. However, the affinity of apoCaM for PMCA is clearly much more than a factor of three lower than the affinity of CaM for PMCA in the presence of Ca^{2+}. Indeed, we were unable to detect *any* binding of CaM-OG488 with PMCA in the absence of Ca^{2+} for PMCA concentrations up to 30 nM. This suggests either that such a simple model does not adequately represent the binding mechanism, or that the anisotropy change detected in our measurements involves binding of Ca^{2+} to both the N-terminal and C-terminal Ca^{2+} binding sites of CaM, rather than to the two high-affinity Ca^{2+} sites alone.

3.5 Conclusion

FP provides a rapid method for screening CaM interactions with target enzymes. We applied this method to measure the K_d for PMCA-CaM complexes in a simple, direct manner, rather than indirectly via activity measurements. The results presented here demonstrate FP measurements with CaM-OG488 as a method with high sensitivity, capable of measuring dissociation constants for CaM targets in the nanomolar range. The sensitivity of the assay results from the high brightness of Oregon green and from interactions between the dye and protein that limit independent segmental motion of the dye. We have measured the K_d of CaM for PMCA and the affinities for the Ca^{2+} binding processes that drive the formation of CaM-PMCA complexes. The method presented here can be readily adapted to a high-throughput screening format and could be used to rapidly screen for CaM-binding proteins or for changes in CaM binding affinity.

3.6 References

[1]F. Perrin, The polarisation of flourescence light. Average life of molecules in their excited state. J. Phys. Radium 7 (1926).

[2]W.J. Checovich, R.E. Bolger, and T. Burke, Fluorescence polarization - a new tool for cell and molecular-biology. Nature 375 (1995) 254-256.

[3]W.B. Dandilker, and V.A. De Saussure, Fluorescence polarization in immunochemistry. Immunochemistry 7 (1970) 799-828.

[4]T. Heyduk, Y.X. Ma, H. Tang, and R.H. Ebright, Fluorescence anisotropy: Rapid, quantitative assay for protein-DNA and protein-protein interaction, RNA polymerase and associated factors, pt b, 1996, pp. 492-503.

[5]J.J. Hill, and C.A. Royer, Fluorescence approaches to study of protein-nucleic acid complexation, Fluorescence spectroscopy, 1997, pp. 390-416.

[6]D.M. Jameson, and W.H. Sawyer, Fluorescence anisotropy applied to biomolecular interactions, Biochemical spectroscopy, 1995, pp. 283-300.

[7]P.Y. Kwok, Snp genotyping with fluorescence polarization detection. Hum. Mutat. 19 (2002) 315-323.

[8]C.A. Royer, T. Ropp, and S.F. Scarlata, Solution studies of the interactions between the histone core proteins and DNA using fluorescence spectroscopy. Biophys. Chem. 43 (1992) 197-211.

[9]N.J. Gibson, H.L. Gillard, D. Whitcombe, R.M. Ferrie, C.R. Newton, and S. Little, A homogeneous method for genotyping with fluorescence polarization. Clin. Chem. 43 (1997) 1336-1341.

[10]M.E. Jolley, and M.S. Nasir, The use of fluorescence polarization assays for the detection of infectious diseases. Comb. Chem. High Throughput Screen. 6 (2003) 235-244.

[11]M. Lin, E.A. Sugden, M.E. Jolley, and K. Stilwell, Modification of the mycobacterium bovis extracellular protein MPB70 with fluorescein for rapid detection of specific serum antibodies by fluorescence polarization. Clin. Diagn. Lab. Immunol. 3 (1996) 438-443.

[12]K. Nielsen, M. Lin, D. Gall, and M. Jolley, Fluorescence polarization immunoassay: Detection of antibody to *Brucella abortus*. Methods-a Companion to Methods in Enzymology 22 (2000) 71-76.

[13]S.B. Tencza, K.R. Islam, V. Kalia, M.S. Nasir, M.E. Jolley, and R.C. Montelaro, Development of a fluorescence polarization-based diagnostic assay for equine infectious anemia virus. J. Clin. Microbiol. 38 (2000) 1854-1859.

[14]M.S. Nasir, and M.E. Jolley, Development of a fluorescence polarization assay for the determination of aflatoxins in grains. J. Agric. Food Chem. 50 (2002) 3116-3121.

[15]T.J. Burke, K.R. Loniello, J.A. Beebe, and K.M. Ervin, Development and application of fluorescence polarization assays in drug discovery. Comb. Chem. High Throughput Screen. 6 (2003) 183-194.

[16]E. Matayoshi, and K. Swift, Applications of fcs to protein-ligand interactions: Comparison with fluorescence polarzation. in: F.P. Scaefer, J.P. Toennies, and

W. Zinth, (Eds.), Fluorescence correlation spectroscopy, Springer, Berlin, Germany, 2001, pp. 85-98.

[17]M.S. Nasir, and M.E. Jolley, Fluorescence polarization: An analytical tool for immunoassay and drug discovery. Comb. Chem. High Throughput Screen. 2 (1999) 177-190.

[18]D.M. Jameson, and J.C. Croney, Fluorescence polarization: Past, present and future. Comb. Chem. High Throughput Screen. 6 (2003) 167-176.

[19]N.J. Carruthers, and P.M. Stemmer, Methionine oxidation in the calmodulin-binding domain of calcineurin disrupts calmodulin binding and calcineurin activation. Biochemistry 47 (2008) 3085-3095.

[20]A. Crivici, and M. Ikura, Molecular and structural basis of target recognition by calmodulin. Annu. Rev. Biophys. Biomol. Struct. 24 (1995) 85-116.

[21]H. Kuboniwa, N. Tjandra, S. Grzesiek, H. Ren, C.B. Klee, and A. Bax, Solution structure of calcium-free calmodulin. Nat. Struct. Biol. 2 (1995) 768-776.

[22]L. de Meis, and A.L. Vianna Energy interconversion by the Ca^{2+}-dependent ATPase of the sarcoplasmic-reticulum. Annu. Rev. Biochem. 48 (1979) 275 - 292.

[23]J. Rossi, P.J. Garrahan, and A.F. Rega, The activation of phosphatase-activity of the Ca^{2+}-ATPase from human red-cell membranes by calmodulin, ATP and partial proteolysis. Biochim. Biophys. Acta 858 (1986) 21-30.

[24]A. Enyedi, T. Vorherr, P. James, D.J. McCormick, A.G. Filoteo, E. Carafoli, and J.T. Penniston, The calmodulin binding domain of the plasma-membrane ca^{2+}

pump interacts both with calmodulin and with another part of the pump. J. Biol. Chem. 264 (1989) 12313-12321.

[25]M.L. Michaelis, D.J. Bigelow, C. Schoneich, T.D. Williams, L. Ramonda, D. Yin, A.F.R. Huhmer, Y. Yao, J. Gao, and T.C. Squier, Decreased plasma membrane calcium transport activity in aging brain. Life Sci. 59 (1996) 405-412.

[26]T.C. Squier, and D.J. Bigelow, Protein oxidation and age-dependent alterations in calcium homeostasis. Front. Biosci 5 (2000) 504-526.

[27]A. Zaidi, L. Barron, V.S. Sharov, C. Schoneich, E.K. Michaelis, and M.L. Michaelis, Oxidative inactivation of purified plasma membrane Ca^{2+}-ATPase by hydrogen peroxide and protection by calmodulin. Biochemistry 42 (2003) 12001-12010.

[28]A.J. Caride, N.L. Elwess, A.K. Verma, A.G. Filoteo, A. Enyedi, Z. Bajzer, and J.T. Penniston, The rate of activation by calmodulin of isoform 4 of the plasma membrane Ca^{2+} pump is slow and is changed by alternative splicing. J. Biol. Chem. 274 (1999) 35227-35232.

[29]E. Graf, and J.T. Penniston, Equimolar interaction between calmodulin and the Ca^{2+} -ATPase from human-erythrocyte membranes. Arch. Biochem. Biophys. 210 (1981) 257-262.

[30]G. Grynkiewicz, M. Poeni, and R.Y. Tsien, A new generation of Ca^{2+} indicators with greatly improved fluorescence properties J. Biol. Chem. 260 (1985) 3440-3450.

[31]A. Takahashi, P. Camacho, J.D. Lechleiter, and B. Herman, Measurement of intracellular clacium. Physiological Rev. 79 (1999) 1089.

[32]R.Y. Tsien, New calcium indicators and buffers with high selectivity against magnesium and protons: Design, sysnthesis, and properties of prtotype structures. Biochemistry 19 (1980) 2396-2404.

[33]M.W. Allen, R.J.B. Urbauer, A. Zaidi, T.D. Williams, J.L. Urbauer, and C.K. Johnson, Fluorescence labeling, purification, and immobilization of a double cysteine mutant calmodulin fusion protein for single-molecule experiments. Anal. Biochem. 325 (2004) 273-284.

[34]K.D. Osborn, A. Zaidi, R.J.B. Urbauer, M.L. Michaelis, and C.K. Johnson, Single-molecule characterization of the dynamics of calmodulin bound to oxidatively modified plasma-membrane Ca^{2+}-ATPase. Biochemistry 44 (2005) 11074-11081.

[35]G.L. Peterson, Simplification of protein assay method of Lowry et al - which is more generally applicable. Anal. Biochem. 83 (1977) 346-356.

[36]Calcium calibration buffer kits.

[37]D. Kosk-kosicka, T. Bzdega, and A. Wawrzynow, Fluorescence energy-transfer studies of purified erythrocyte Ca^{2+} -ATPase - Ca^{2+}-regulated activation by oligomerization. *J. Biol. Chem.* 264 (1989) 19495-19499.

[38]M.R. Liyanage, A. Zaidi, and C.K. Johnson, Fluorescence polarization assay for calmodulin binding to plasma membrane Ca^{2+}-ATPase: Dependence on enzyme and Ca^{2+} concentrations. Anal. Biochem. 385 (2009) 1-6.

[39]E. Rusinova, V. Tretyachenko-Ladokhina, O.E. Vele, D.F. Senear, and J.B.A. Ross, Alexa and Oregon green dyes as fluorescence anisotropy probes for measuring protein-protein and protein-nucleic acid interactions. Anal. Chem. 308 (2002) 18-25.

[40]V. Levi, J. Ross, P.R. Castello, and F.L.G. Flecha, Structural significance of the plasma membrane calcium pump oligomerization. Biophys. J. 82 (2002) 437-446.

[41]H.Y. Sun, and T.C. Squier, Ordered and cooperative binding of opposing globular domains of calmodulin to the plasma membrane Ca^{2+}-ATPase. J. Biol. Chem. 275 (2000) 1731-1738.

[42]O.B. Peersen, T.S. Madsen, and J.J. Falke, Intermolecular tuning of calmodulin by target peptides and proteins: Differential effects on Ca2+ binding and implications for kinase activation. Protein Sci. 6 (1997) 794-807.

[43]M. Yazawa, T. Vorherr, P. James, E. Carafoli, and K. Yagi, Binding of calcium by calmodulin - influence of the calmodulin binding domain of the plasma-membrane calcium-pump. Biochemistry 31 (1992) 3171-3176.

[44]P.M. Bayley, W.A. Findlay, and S.R. Martin, Target recognition by calmodulin: Dissecting the kinetics and affinity of interaction using short peptide sequences. Protein Sci. 5 (1996) 1215-1228.

[45]Y. Maulet, and J.A. Cox, Structural-changes in melittin and calmodulin upon complex-formation and their modulation by calcium. Biochemistry 22 (1983) 5680-5686.

[46]B.B. Olwin, and D.R. Storm, Calcium-binding to complexes of calmodulin and calmodulin binding-proteins. Biochemistry 24 (1985) 8081-8086.

[47]P.M. Stemmer, and C.B. Klee, Dual calcium-ion regulation of calcineurin by calmodulin and calcineurin-b. Biochemistry 33 (1994) 6859-6866.

[48]S. Linse, A. Helmersson, and S. Forsen, Calcium-binding to calmodulin and its globular domains. J. Biol. Chem. 266 (1991) 8050-8054.

[49]B.R. Sorensen, and M.A. Shea, Interactions between domains of apo calmodulin alter calcium binding and stability. Biochemistry 37 (1998) 4244-4253.

Chapter 4

Fluorescence Anisotropy Based Competitive Binding Assay for CaM Target Binding

4.1 Introduction

Calmodulin (CaM), functioning as a major intracellular calcium receptor, is responsible for triggering and regulation of diverse range of cellular functions. These functions are controlled by CaM by binding to a vast array of targets including phosphatases, kinases, receptors, channels, and pumps [1; 2; 3]. Determination of the binding affinities of these targets to CaM is crucial to understand the CaM-target interactions. It has been a common practice to use model peptides to obtain information about protein-protein interactions. Binding of model peptides to CaM in a calcium-dependent manner has been reported in the literature [4; 5; 6; 7; 8; 9]. Blumenthal et al have reported that the peptide binding domain of myosin light chain kinase (MLCK) binding to CaM has an indistinguishable affinity from native MLCK [10]. Kinetic analysis of CaM-binding regions of plasma membrane Ca^{2+}-ATPase (PMCA) isoform 4b has been performed using several peptides including C28W [11]. Chemically synthesized CaM-binding domain peptides have paved the way to studying interactions of CaM with target peptides by replacing amino acids within the peptide sequence [12].

Numerous biochemical and biophysical approaches have been deployed in studying CaM-target peptide interactions. In order to determine the K_d values of several CaM binding regions of PMCA, Penheiter and coworkers have measured the

decrease in PMCA activity upon competition by binding of peptides [11]. A peptide array of four hundred and twenty five different peptides have been screened for CaM binding making use of ^{35}S labeled CaM [13]. Melencik and Anderson have studied binding of mastoparans with CaM by monitoring the changes in fluorescence spectrum and fluorescence anisotropy of tryptophan residues in the peptides [7; 14; 15]. Binding of simple peptides, hormones and neurotransmitters by CaM have been investigated using fluorescence enhancement of dansyl labeled CaM [7; 16]. In another study, the decrease in steady state fluorescence of pyrene maleimide labeled CaM upon peptide binding has been used to determine the affinity of the interactions [17]. Blumenthal has labeled MLCK (M13) peptide with acrylodan maleimide at the C-terminus cysteine residue of the peptide and measured the change in fluorescence intensity and the anisotropy upon binding to CaM [12].

Fluorescence anisotropy assays are very attractive for studying protein-ligand interactions because they are homogeneous, highly sensitive, and derivatization with only a single fluorophore is required. On the other hand, fluorescence anisotropy assays can be implemented in high throughput assay screening formats [18]. We have recently developed an fluorescence anisotropy based binding assay for CaM binding to PMCA with direct labeling of CaM with Oregon Green 488 [19]. However, developing a fluorescence anisotropy based assay for every CaM target in this manner is challenging due to the complex nature of the interactions of CaM with a vast range of targets and the sensitivity of the assay may be limited since CaM is already a large molecule. Further some targets tend to quench the fluorescence of the fluorophore

attached to CaM upon binding; for example eNOS quenches the fluorescence of CaM labeled with a wide range of fluorophores such as AF488, OG488, Texas Red, AF594, and AF647 (see Figure 4.1).

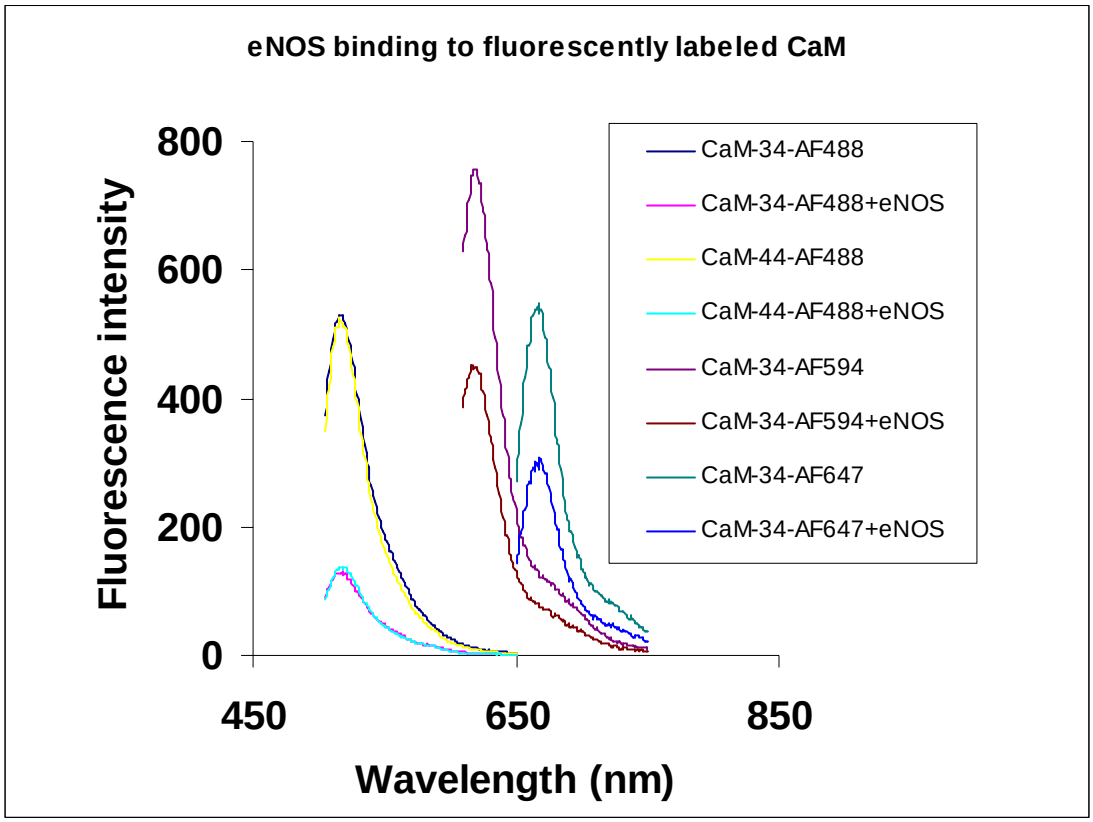

Figure 4.1 Quenching of fluorescence of fluorescently labeled CaM with different dyes upon binding to eNOS. The fluorescence spectra were collected in standard high Ca^{2+} HEPES buffer at pH 7.4 and 25 °C.

Furthermore, the characterization of most of the CaM-target interactions have been performed using CaM binding domain peptides of target proteins [17].

Under the above circumstances, determination of affinities of CaM-target complexes needs to be performed using competitive binding assays involving a fluorescently labeled peptide. The conceptual basis for the competitive binding assay is illustrated in Figure 4.2. In this assay, binding of small peptides to CaM can be detected as a change in fluorescence anisotropy upon competitive displacement of the tracer peptide. Since the methods for labeling peptides are well established, derivatization of the tracer peptide is not a challenging task [20; 21]. In this study we chose the CaM binding domain of MLCK as the tracer since it has been well characterized in terms of CaM binding and fluorescent labeling [22].

In the development of sensitive assays for interactions of proteins or peptides with their targets especially in the nanomolar range in terms of protein or peptide concentrations, the losses of protein/peptide from the solution affect the sensitivity, precision, and accuracy of the assay. The loss of the analytes from the solution is a direct result of adsorption onto a variety of surfaces that they come into contact with, such as pipettes, glassware, and cuvettes or microwells, during sample handing and measurements [23; 24; 25; 26]. For instance, there have been reports about errors in experimental results of circular dichroism experiments due to adsorption of five proteins out of six investigated onto the surface of the uncoated cell [27]. There are two predominant surfaces we need to pay thorough attention to in an assay development since most of the sample handing accessories are made up of glass and

plastic [25]. The factors influencing the degree of protein or peptide adsorption can considered as temperature, ionic strength, pH, surface chemistry, and protein or peptide conformations [28].

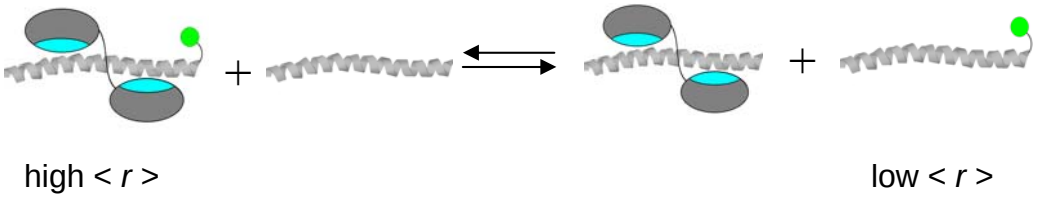

Figure 4.2 Schematic of FP competition assay. CaM bound to fluorescently labeled MLCK peptide (left) will display high FP. Release of MLCK peptide upon binding another peptide will result in low FP (right).

The mechanism underlying the adsorption of proteins or peptides is a negative free energy resulting from the exchange of solution interactions for surface interactions of molecules. The processes behind this change in energetics could come from charge-charge, and hydrophobic interactions. However, lesser mechanisms including charge-dipole, dipole-dipole, and Van der Waals interactions may also contribute [29; 30].

Adsorption phenomena and preventive measures for protein or peptide adsorption onto surfaces are well characterized [23; 24; 25; 26]. Bovine serum albumin (BSA) has favorable adsorption properties to glass and plastics above pH 2.5 [25; 31]. Thus BSA has been widely used in solutions with analyte proteins/peptides to minimize analyte adsorption to surfaces [25; 31]. In the single-molecule detection community using optical methods, coating of glass slides and coverslips with BSA has been customarily used to eliminate adsorption of species of interest on to the surfaces [32; 33].

The use of surfactants in preventing protein or peptide adsorption has also rendered a remarkable improvement in elimination of analyte losses from the solution [25; 34; 35; 36; 37]. Duncan et al have investigated the influence of cationic, anionic, and non-ionic surfactants on adsorption of proteins or peptides onto glass and polypropylene surfaces and reported that the non-ionic surfactant was most effective in eliminating protein or peptide adsorption. Furthermore the extent of the hydrophobicity has been a crucial factor in reducing adsorption [25]. In an attempt to develop an assay for analyzing some specific proteins of a single cell using microchip based CE separation, which require a substantial reduction in surface adsorption,

Huang et al have used a non-ionic surfactant, n-dodecyl-β-D-maltoside (DDM), as a dynamic coating agent in the CE run buffer [38; 39]. Modulating the pH and the ionic strength of the solution as appropriate to individual analyte can reduce the adsorption onto surfaces [39].

4.2 Material and Methods

Calmodulin was purchased from Sigma-Aldrich (St. Louis, MO) and used as received without further purification. The CaM binding domain of myosin light chain kinase (MLCK) was custom synthesized from Sigma Genosys. The twenty amino acid peptide sequence was selected and a cysteine residue was incorporated into the C-terminal of the peptide so that the peptide has the amino acid sequence KRRWKKAFIAVSAAARFKKC. This peptide was fluorescently labeled in a site-specific manner using a method described by Blumenthal as described below. For the labeling reaction, 0.5 mg of MLCK peptide was dissolved in 750 uL of 10 mM PBS. Then this peptide solution was incubated with 10 fold molar excess of TCEP while stirring for 10 min. To prepare the desired dye solution, 1 mg of Atto465 malemide (Atto-tec, Germany) was dissolved in a mixture of DMSO and PBS buffer (1:6) so that this solution has 10-fold molar excess of fluorophore with respect to the peptide concentration. Then the dye solution was added drop-wise to the peptide solution, and the mixture was incubated for 2 hours while being stirred in the dark. The entire reaction mixture was covered with aluminum foil to keep it away from room light.

Separation and characterization of labeled Peptide For the size exclusion separation, a 50 cm long Econo column (BioRad) was packed with Sephadex G-25 (Amersham Biosciences) according to the manufacturer's protocol. Then the column was equilibrated with 10 mM HEPES buffer by running more than 5 column volumes through the column. The reaction mixture containing labeled peptide and free dye was loaded into the column and the first band eluting out of the column was collected as the labeled peptide. The purity of the labeled peptide was checked by reverse-phase HPLC. The reverse-phase separation was carried out on a Vydac C-18 protein and peptide separation column with the following specifications. The column with dimensions of 250 x 4.6 mm was composed of 5 μm diameter particles with a 300 Å average pore size. The composition of the aqueous mobile phase A was 95 % water (v/v), 5 % acetonitrile (v/v), and 0.1 % TFA (v/v). The composition of the organic mobile phase B was 95 % acetonitrile (v/v), 5 % water (v/v), and 0.1 % TFA (v/v). The labeled peptide was eluted by a linear solvent gradient from 2 min to 22 min from 5 to 55 % of B with a flow rate of 1 mL/min. Absorbance from Atto465 and peptide backbone was monitored at 453 nm and 220 nm respectively during elution. The labeling efficiency of the peptide was determined using the absorbance at 453 nm and the extinction coefficient of Atto465 at 453 nm (75,000 M^{-1} cm^{-1}) to calculate the concentration of M13-Atto465 peptide. The concentration of peptide was confirmed by micro BCA assay.

Determination of concentrations of the protein and peptides. The Micro BCA protein assay kit was purchased from Pierce Biotechnology (Rockford, IL). The

standard BSA solution provided with the assay kit was diluted using a high Ca^{2+} buffer (10 mM HEPES, 0.1 M KCl, 1 mM $MgCl_2$, and 1 mM $CaCl_2$, pH 7.4). The resulting solution was subsequently diluted according to the manufacturer's instructions to prepare a series of BSA standards with concentrations ranging from 200 μg/ml to 0.5 μg/ml and high Ca^{2+} buffer alone used as the blank. The working reagent for the micro BCA assay was prepared by mixing 25 parts of micro BCA reagent MA and 24 parts of reagent MB with 1 part of reagent MC. Then 150 μl of each standard was pipetted into a microwell plate in three replicates. The above step was repeated for three different concentrations of calmodulin and M13 labeled with Atto465, C28W, and CKII peptides. Three different free Atto465 solutions with similar concentration to M13-Atto465 was also pipetted to see if the absorbance from Atto465 interferes with the assay performance. A solution of 150 μl of the working reagent was then spiked into each well and the plate was mixed thoroughly on a plate shaker for 30 seconds. Then the plate was coved with an aluminum foil and incubated for 2 hours at 37 ^{o}C. After incubation the assay plate was allowed to cool to room temperature and absorbance at 562 nm was measured on a SpectraMax M5 plate reader (Molecular Device). The average absorbance reading of blank standard replicates was subtracted from all other individual standard and sample replicates. A calibration curve was constructed by plotting the corrected absorbance readings at 562 nm of each BSA standard against its concentration in μg/ml. The concentrations of all unknown samples were determined using this calibration plot.

The influence of the bovine serum albumin (BSA), polylysine, n-dodecyl-β-D- maltoside (DDM) (a non-ionic surfactant), and ionic strength on the adsorption of peptide onto surfaces was studied as follows. The adsorption losses of M13-Atto465 were monitored as changes in fluorescence intensity at 510 nm as a function of time. Fluorescence intensities were measured using a PTI fluorimeter (PTI technologies). The excitation and emission wavelength were set to 453 nm and 510 nm respectively. The fluorescence intensity of each solution was recorded as the average intensity of a 10 second long fluorescence intensity trajectory. The average value for 10 second long fluorescence intensity collection was obtained using Felix software that is available to use with PTI data. Both the excitation and emission monochromater slit widths were set to 4 nm. The fluorescence intensity of each solution was measured at intervals of 15 minutes for one hour and the solution was mixed well before and after every measurement to ensure a homogeneous distribution of M13. A final concentration of 5 nM of M13-Atto465 was maintained during each experiment. For the study of buffer modifying agents, 50 μg/ml of BSA, 0.01 % (w/v) of polylysine and DDM concentrations were maintained. The influence of ionic strength was investigated by a salt concentration of 500 mM with a spike of NaCl. A 5 nM solution of Atto465 free in solution was also included in the experiment in order to ensure there is no substantial reduction in the fluorescence intensity due to photobleaching of the fluorescence dye and the reduction in fluorescence intensity is solely coming from the peptide adsorption. After selecting the desired adsorption preventive agents, their responses to quartz and plastic cuvettes (polypropylene) were investigated using the

above approach. For this fluorescence intensity at 510 nm was collected for 50 μg /ml BSA, and 0.01 % DDM in both quartz and plastic cuvettes.

The successful implementation of BSA and DDM in eliminating adsorption of M13-465 onto surfaces was the key motivation for us to consider these two candidates for further studies. The steady state anisotropy of M13-Atto465 was measured to evaluate the feasibility of using BSA or DDM for the assay development. The steady state anisotropy of 5 nM Atto465 labeled MLCK peptide was measured using a PTI fluorimeter and two polarizers in the excitation and emission paths. The excitation wavelength was selected to 453 nm while the emission wavelength was set to 508 nm. The excitation and emission monochromater slit widths were set to 6 and 12 nm respectively. Anisotropy measurements were repeated five times to obtain an average fluroescenence anisotropy for each case.

Determination of K_d of M13-Atto465. Determining the dissociation constant of the M13-Atto465 and CaM complex is crucial for development of a competitive binding assay for the target binding to CaM. The steady-state anisotropy measurements were performed on a SpectraMax fluorescence plate reader (Molecular Device, CA). Flat bottom, non-binding surface, black polystyrene 96 well assay plates (Corning Inc. Corning, NY) were used for all the measurements. The fluorescence anisotropy was monitored using the top reading configuration of the fluorescence plate reader. Excitation and emission wavelengths were set to 453 nm and 510 nm respectively. The 495 nm emission cutoff filter was selected for the spatial resolution of the emitted light. High PMT sensitivity settings and 100 readings/well were chosen for

all the measurements. The temperature of the plate chamber was set to 25^{o}C. To construct the binding isotherm for the M13-Atto465, a final concentration of 9 nM was maintained in each well. Then desired volumes of 100 nM stock of CaM were added to each well in order to titrate M13-Atto465. The concentration range of CaM ranged from 0 to 25 nM in the final 200 μl volume of assay reagents. Each CaM concentration was replicated three times. The standard high Ca^{2+} HEPES buffer (10 mM HEPES, 0.1 M KCl, 1 mM $MgCl_2$, and 100 μM $CaCl_2$, pH 7.4) was used for all the measurements in the presence of 0.01 % DDM. The assay plate was mixed well on a shaker and incubated 15 minutes at 25 ^{o}C before taking anisotropy readings. The same experiment was performed at different DDM concentrations (0.005%, 0.01%, and 0.02%) to assess the influence of the presence of DDM on CaM-M13-Atto465 interactions. Based on the results of DDM concentration dependence, 0.01 % of DDM was chosen for further experiments. The experimental anisotropy data and concentrations of peptide and CaM were fit to the eq.4.1 using non-linear least square fitting routine using reduced χ^2 as the goodness of fit, written in Excel to obtain the K_d of CaM-M13-Atto465 complex. The error associated with K_T was evaluated by using the support plane error analysis algorithm.

$$\Delta r = \frac{\Delta r_{\max}}{2Ct}\left\{\left(C_t + P_t + K_T\right) - \sqrt{\left(C_t + P_t + K_T\right)^2 - \left(4P_tC_t\right)}\right\} \qquad (4.1)$$

In eq. 4.1, Δr is the change in anisotropy relative to anisotropy of free M13-Atto465; K_T is the dissociation constant of M13-Atto465-CaM complex; C_t is the total M13-Atto465 concentration and P_t is the total CaM concentration.

For the competitive binding assay, a final concentration of 9 nM in the final assay buffer was selected for both CaM and M13-Atto465 using the saturation curve for the CaM binding to M13-Atto465. Each well in the assay plate was filled with the assay reagent composed of 9 nM CaM, 9 nM M13-Atto465 in high Ca^{2+} buffer in the presence of 0.01% DDM. The competitive displacement of the M13-Atto465 from CaM was performed by adding varying concentrations of each peptide/protein. To construct the competitive binding curve for the analyte, nine different concentrations were generated. The highest concentrations of the competitor peptide/protein were 2 μM, 3 μM, 250 nM, and 200 nM for CKII, C28W (peptides), eNOS and calcineurin respectively. The potential of the fluorescence anisotropy assay to be implemented in a high-throughput format was tested by determining the Z′ factor, which reflects the viability of the assay for screening by incorporating the precision of an assay [40]. Z′ was calculated by using following equation.

$$Z' = 1 - \frac{(3SD_f + 3SD_b)}{(\mu_b - \mu_f)} \qquad (4.2)$$

where, μ_b and μ_f are the mean anisotropy from several microwells for saturated tracer with its target and free tracer respectively while SD_f and SD_b are standard deviations of free and bound form of tracer respectively.

4.3 Data analysis

The derivation of an equation that fits all the values of the binding curve to calculate the K_d of a competitive ligand to replace the tracer is necessary since this has not been reported before. Suppose that *C, T, CT, P*, and *CP* represent the equilibrium concentrations of target protein (CaM), tracer (M13-Atto465), protein-tracer complex, competitive ligand, and protein-competitive ligand complex respectively, and C_{tot}, P_{tot}, and T_{tot} represent the total concentrations of protein, ligand and the tracer respectively. This derivation assumes that both ligand and the tracer compete for the same binding site of the protein and the stoichiometry of ligand and tracer binding to protein is 1:1. The equilibrium represented in the Figure 4.2 for the competitive replacement of the tracer by the competitive ligand can be broken down into two equilibria for the purpose of mathematical derivation of the final equation.

When the system is at equilibrium,

$$K_T = \frac{(C_{tot} - CT - CP)(T_{tot} - CT)}{CT} \tag{4.3}$$

$$K_D = \frac{(C_{tot} - CT - CP)(P_{tot} - CP)}{CP} \tag{4.4}$$

Now CP takes a quadratic form:

$$CP = \frac{\left(K_T CT - C_{tot}T_{tot} + C_{tot}CT + CTT_{tot} - CT^2\right)}{\left(-T_{tot} + CT\right)} \tag{4.5}$$

Solution for CP is;

$$CP = C_{tot} - CT - \frac{K_T CT}{T_{tot} - CT} \tag{4.6}$$

Substituting CP in equation 4.4;

$$K_D = \frac{\left[C_{tot} - CT - \left(C_{tot} - CT - \frac{K_T CT}{T_{tot} - CT}\right)\right]\left[P_{tot} - \left(C_{tot} - CT - \frac{K_T CT}{T_{tot} - CT}\right)\right]}{C_{tot} - CT - \frac{K_T CT}{T_{tot} - CT}} \tag{4.7}$$

Equation 4.7 can be written as;

$$K_D = \frac{K_T CT\left[\left(P_{tot} - C_{tot} + CT\right)\left(T_{tot} - CT\right) + K_T CT\right]}{\left(C_{tot} - CT\right)\left(T_{tot} - CT\right)^2 - K_T CT\left(T_{tot} - CT\right)} \tag{4.8}$$

At a given concentration of ligand, the fraction of tracer displaced by ligand (x) is given by

$$CT = \left(1 - x\right)CT_0 \tag{4.9}$$

where CT_0 is the concentration of the protein-ligand complex at zero ligand concentration. Substituting solution for CT from equation 4.8 gives;

$$\left(1 - x\right)CT_0 = \frac{C_{tot} K_D\left[T_{tot} - \left(1 - x\right)CT_0\right]}{\left[T_{tot} - \left(1 - x\right)CT_0\right]K_D + K_T K_D + K_T P} \tag{4.10}$$

from equation 4.6:

$$P = P_{tot} - C_{tot} + \left(1 - x\right)CT_0 + \frac{K_T\left(1 - x\right)CT_0}{T_{tot} - \left(1 - x\right)CT_0} \tag{4.11}$$

Substituting 4.11 in 4.10 gives;

$$\left(1 - x\right)CT_0 = \frac{C_{tot} K_D\left[T_{tot} - \left(1 - x\right)CT_0\right]}{\left[T_{tot} - \left(1 - x\right)CT_0\right]K_D + K_T K_D + K_T\left(P_{tot} - C_{tot} + \left(1 - x\right)CT_0 + \frac{K_T\left(1 - x\right)CT_0}{T_{tot} - \left(1 - x\right)CT_0}\right)}$$

(4.12)

In order to calculate K_d, x can be experimentally determined as follows;

$$x = \frac{r - r_T}{r_b - r_T} \tag{4.13}$$

where r is the steady-state anisotropy at a given ligand concentration, r_T is steady-state anisotropy of free tracer, r_b is the anisotropy of the tracer bound to protein in the absence of the ligand. The experimentally determined anisotropy values can be used find x and other known parameters will be used to derive dissociation constants for competing ligands by fitting data to eq. 4.12 using minimized χ^2 as the criterion for the goodness of the fit. Therefore this equation allows us to fit all the point of the ligand binding curve without depending on a single point based on the 50 % inhibition as previously reported.

4.4 Results

For development of sensitive assays for CaM-target binding interactions, we performed some peptide adsorption studies and preventive measures for adsorption. This is necessary because changing concentrations of peptide interferes with both the sensitivity of the signal and the accuracy of the affinity parameters. In this study we monitored changes on fluorescence intensity as a function of time in order to measure the peptide adsorption onto surfaces. Figure 4.3 shows changes in fluorescence intensity at 453 nm with time for a few dynamic surface modifiers in the bulk solution. Since the fluorescence intensity is directly proportional to the amount of fluorescent species in the solution, the decrease in fluorescence intensity is

proportional to the loss of peptide from the solution due to adsorption. There is a sharp decrease in the fluorescence intensity in the absence of surface modifiers as well as the case of polylysine. The similar behavior of polylysine and the absence of modifiers is evidently an indication of dramatic loss of the peptide from the solution due to adsorption. BSA and DDM on the other hand show only a slight change in fluorescence intensity over the time period of one hour. Since this slight change in fluorescence intensity for BSA and DDM is comparable with the decrease in fluorescence intensity of free Atto465, it can be a direct result from photobleaching of the fluorescent tag on M13 due to exposure to the light. By comparing fluorescence intensity changes of for BSA and DDM with the instance where there is no modifier in the solution, we can infer that both BSA and DDM cause a little or no peptide loss from the solution by eliminating adsorption onto the surfaces.

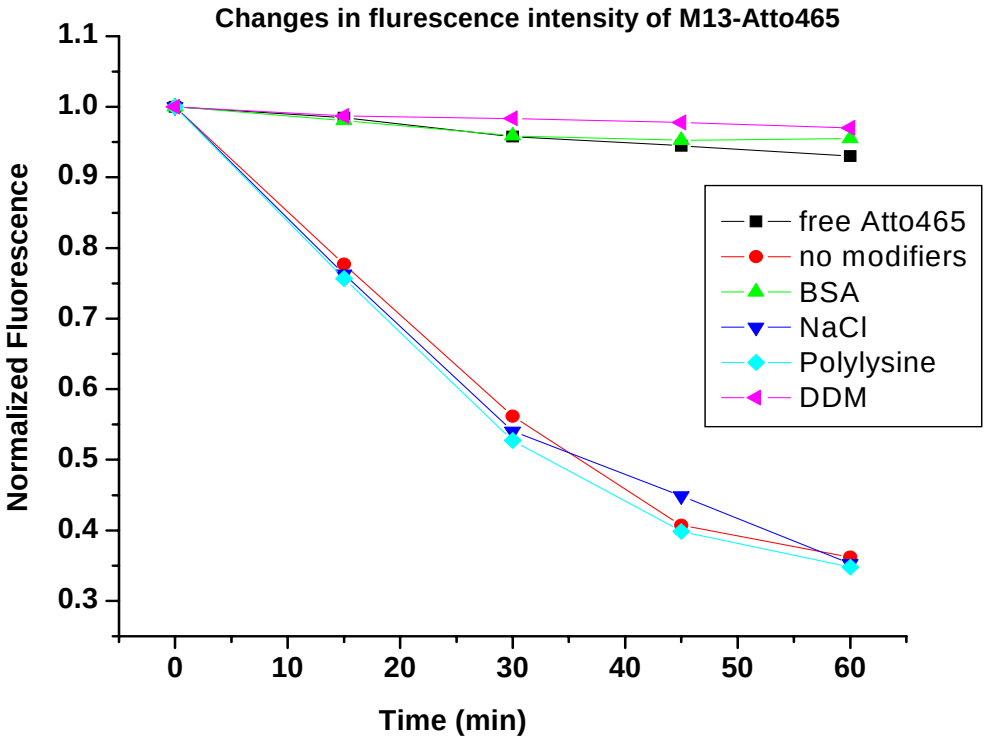

Figure 4.3 Influence of the presence of surface modifying agents on the change in fluorescence intensity of 5 nM M13-Atto465. Fluorescence intensities were measured in standard high Ca^{2+} HEPES buffer at pH 7.4 and 25 °C in a polystyrene cuvette. The fluorescence intensity at each time interval is an average of 10 second time trace collected at 510 nm by exciting at 453 nm.

For the study of the influence of BSA and DDM on peptide adsorption onto glass and plastic surfaces, we carried out fluorescence intensity measurements as described above in quartz and polystyrene cuvettes. Fluorescence intensity changes of M13-Atto465 with time are shown in Figure 4.4. The presence of BSA in solution has caused only a slight change in fluorescence intensity in both the quartz and polystyrene indicating a minimal amount of peptide adsorption onto surfaces. DDM also showed only a minute change in fluorescence intensity over time in polystyrene cuvettes providing evidence for preventing peptide adsorption. However, there is a significant change in fluorescence intensity of M13-Atto465 in the presence of DDM in quartz quvettes. Thus use of DDM for keeping peptide from adsorbing onto the surfaces only works if the experiment is conducted on a plastic surface using non-glass sample-handing equipment.

Proper evaluation of the influence of the buffer modifiers have on the fluorescence anisotropy measurements of M13-Atto465, is essential because the accuracy in the initial anisotropy measurements governs the accuracy of the assay. To accomplish this requirement I measured the steady state fluorescence anisotropy of M13-Atto465 in the presence of BSA and DDM individually. Table 4.1 lists the fluorescence anisotropy values for M13-Atto465 for the presence of both modifiers and absence of modifier in the solution. Fluorescence anisotropy of M13-Atto465 in the presence of DDM is the same as in the absence of DDM making it a promising surface modifying agent to be used in the assay development.

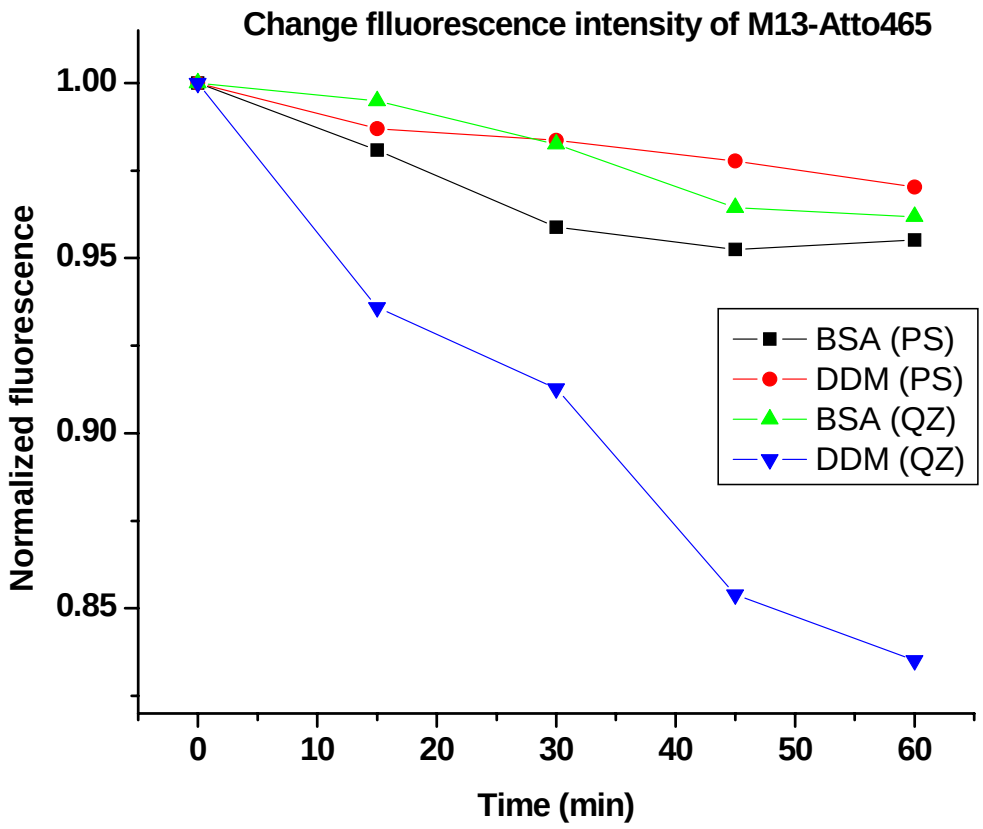

Figure 4.4 Influence of the presence of surface modifying agents on the change in fluorescence intensity of 5 nM M13-Atto465 in quartz and polystyrene cuvettes. Fluorescence intensities were measured in standard high Ca^{2+} HEPES buffer at pH 7.4 and 25 °C. The fluorescence intensity at each time interval is an average of 10 second time trace collected at 510 nm by exciting at 453 nm.

Table 4.1 Steady state anisotropy of M13-Atto465 in the presence of some surface modifying agents used for eliminating protein or peptide adsorption

Species Present	Anisotropy
No modifier	0.043 ± 0.006
BSA	0.100± 0.008
DDM	0.046 ± 0.006
CaM	0.152 ± 0.002

[a] Anisotropy values presented here are an average of five replicate measurements and the uncertainties were estimated from the standard deviation of the five replicate readings.

Despite its remarkable potential to be used in preventing peptide adsorption, BSA yields an unacceptably high initial anisotropy for M13-Atto465. This initial anisotropy of M13-Atto465 in the presence of BSA is comparable to that of M13-Atto465 bond to CaM (see Table 4.1). After meticulous searches for an appropriate surface modifying agent for the use in the assay development, we subsequently selected DDM as the buffer modifier. The experiments carried out with fluorescently labeled CaM in the presence of DDM showed that DDM is also capable of preventing CaM adsorption onto the surfaces

According to the final equation (equation 4.13), the dissociation constant of the fluorescently labeled tracer (K_T) should be predetermined so that it can be substituted in the final equation during data fitting to calculate the K_D values of the competitive ligands. We have to titrate M13-Atto465 with CaM while measuring the anisotropy changes in order to obtain the K_T for M13-Atto465 interaction with CaM. The binding curve for CaM binding to M13-Atto465 is shown in the Figure 4.5. The K_T values for different DDM concentrations were obtained by fitting the CaM binding data to eq. 4.1. Since DDM is an integral part of the assay development to eliminate proteins and peptide adsorption in this assay, an evaluation of the influence of DDM on M13-CaM interactions was performed by measuring the dissociation constants of M13-Atto465 binding to CaM (K_T) in the presence of varying concentrations of DDM. The K_T values listed in Table 4.2 for 0 and 0.005 % DDM show very close K_T values, although a little higher than those for 0.01 % and 0.02 % DDM concentrations. The K_T value (101 ± 70 pM) determined at 0.01 % DDM

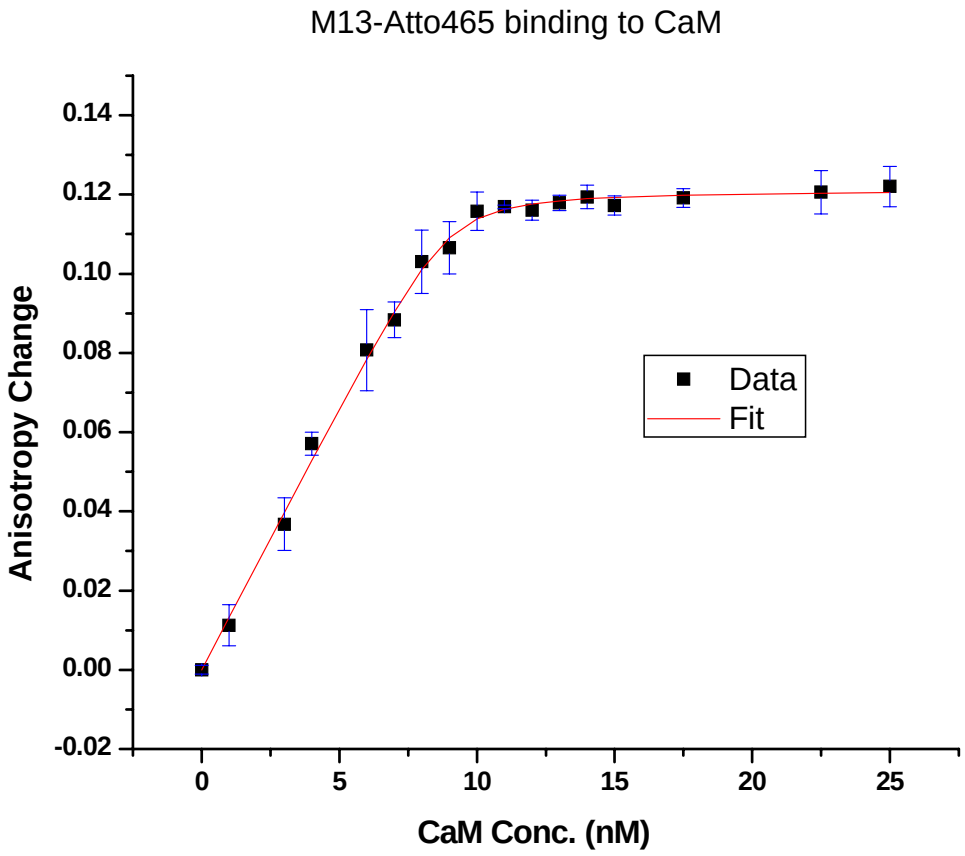

Figure 4.5 The binding isotherm of M13-CaM interaction constructed by plotting changes in fluorescence anisotropy of M13-Atto465 upon titrating with CaM at pH 7 and 25 °C. The red curve is the fitting for data to the eq. 4.1. The fitting yielded a dissociation constant (K_T) of 101 ± 70 pM for M13-Atto465 binding to CaM.

concentration is consistent with a previously measured value for M13-CaM complex using a method relying on the fluorescence intensity changes upon CaM binding to M13 with an unnatural amino acid (85 pM, see Table 4.2) [41]. Therefore the results obtained from this approach measuring fluorescence anisotropy in the presence of DDM are promising and can be used in the competitive assay to obtained K_d values of competitive ligands.

It is worth checking the potential of using this assay to be implemented in a high-throughput screening format since this investigation is performed using a 96-well assay plate. The evaluation of the assay can be done by measuring a parameter called Z' factor using the eq. 4.2, which assesses the performance of high throughput screening assays. Table 4.3 lists parameters required for obtaining Z' and calculated the Z' for CaM-M13, C28W, eNOS. In the 96-well assay plates, Z' factor for competitive binding is greater than 0.8. A Z' of greater than 0.5 is typically considered as acceptable for high throughput screening [40].

Fluorescence anisotropy based competitive assays are elegantly designed to measure the dissociation constants of the competing ligands without having to label all the targets. When a given analyte protein has many targets that compete for the same binding site, one of those target ligand can be fluorescently labeled and used as a tracer to obtain the K_d values of other competing ligands. In this investigation, we present a way to determine K_d values of many CaM binding target by using fluorescently labeled M13 as a tracer peptide. Figure 4.6 shows the fluorescence

Table 4.2 K_d values obtained as a function of DDM concentration

% of DDM present	Dissociation constant (± 0.07 nM)
0	0.30
0.005	0.24
0.01	0.10
0.02	0.13
Loving and Imperiali (2008)	0.085 (± 0.025) nM

Table. 4.3 Z' factors for three different biomolecules investigated in this study

Species	Z'
M13	0.85
C28W	0.86
eNOS	0.96

anisotropy changes of M13-Atto465 bound to CaM upon competitive displacement by C28W (upper left panel), CKII (lower left panel), mastoparan (lower right panel), and eNOS (upper right panel). There is a marked decrease in anisotropy of the tracer in the cases where C28W and eNOS were used as the competitive ligands. However, the anisotropy of the tracer bound to CaM remains constant for CKII and Mastoparan under the concentrations we used for them. Competitive binding curves for these peptides were fit to eq. 4.13 to obtain K_d. values for the competing ligands. These dissociation constants for C28W and eNOS were determined to be $K_d = 8.6^{+2.4}_{-1.5} nM$ and $K_d = 3.2^{+3.0}_{-1.7} nM$ respectively

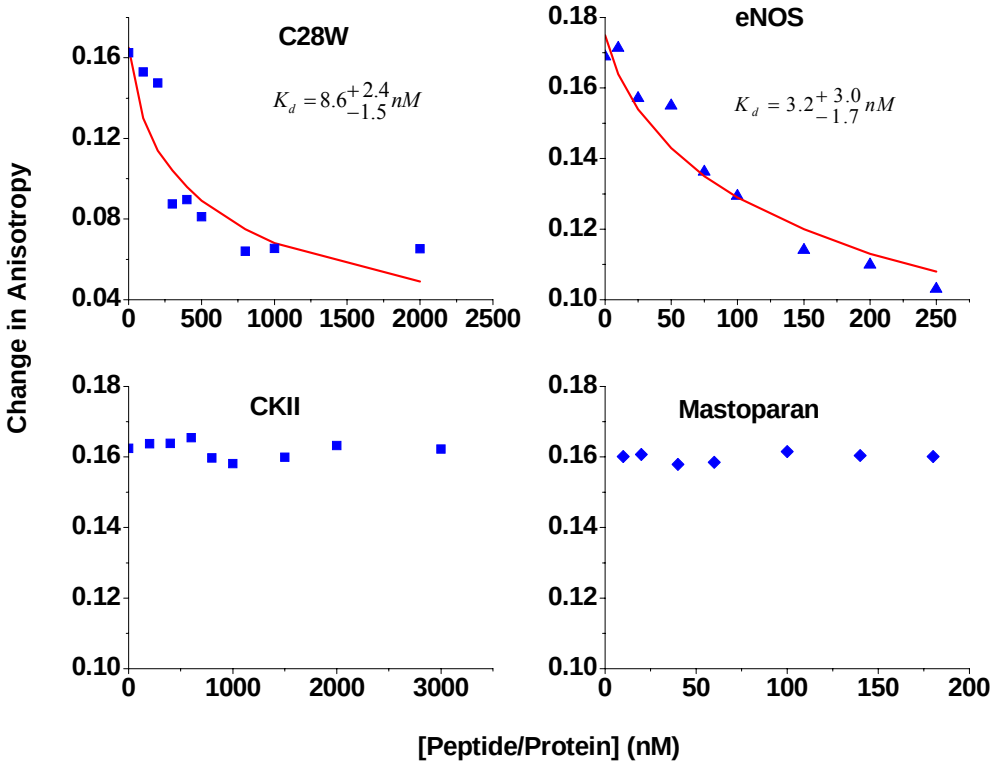

Figure 4.6 The change in fluorescence anisotropy of M13-Atto65 bound to CaM upon competitive ligands binding to CaM. The dissociation constants of $K_d = 8.6^{+2.4}_{-1.5} nM$ and $K_d = 3.2^{+3.0}_{-1.7} nM$ were obtained for C28W and eNOS respectively by fitting data to eq. 4.13 in upper left and upper right panels respectively. The fitting routine was not performed on CKII and matoparan since there is no obvious change in anisotropy.

4.5 Discussion

Determination of the binding affinities of CaM of its targets is crucial for understanding the nature of target activation upon elevated calcium levels. We have previously developed an assay based on the fluorescence anisotropy for CaM binding to plasma membrane Ca^{2+}-ATPase (PMCA) using fluorescently labeled CaM [19]. Even though this fluorescence anisotropy based binding assay is a straightforward and simple way of determining affinities of CaM binding to its targets, implementation of this assay poses some practical difficulties even though they can be taken into account with a proper data analysis. For example, protein (PMCA) aggregation, and quenching of the fluorescent tags on CaM upon binding to eNOS (Figure 4.1) can interfere with the assay performance. These limitations led us to develop a more general approach for CaM-target interactions based on the competitive displacement of a fluorescently labeled trace by other ligands. Since the fluorescence label is on a small peptide and this peptide becomes free upon target binding, this approach is immune to said limitations.

We chose M13 peptide as the tracer in this assay development as it binds to CaM with a high affinity and it has been well characterized for fluorescence labeling and CaM binding. Incorporation of the cysteine residue in the C-terminus helps keep the fluorescent label away from the residues involved in the binding interactions. It has been reported that the binding affinity of C-terminal labeled M13 is about three orders of magnitude higher than the N-terminal labeled peptide, because the label on the N-terminus is too close to the tryptophan residue which plays a major role in

binding interaction with CaM [12]. However, these differential affinities of M13 to CaM depending on the labeling site could be advantageous for assay developments since we can modulate the binding affinities of M13 to CaM. This will enable us to track the binding of wide range of CaM targets, from high affinity targets to targets with low affinities for CaM. In this study we specifically labeled the C-terminus of M13 since our interest is in high affinity targets. Considering these facts M13 can be highly regarded as a prime candidate for CaM-target binding assay development.

Fluorescence anisotropy based assays are simple and homogeneous, making fluorescence anisotropy assays easy to implement in high throughput screening formats for the assay automation. For this reason we performed the assay on a 96-well assay plate on fluorescence plate reader to evaluate the quality of the assay for the high throughput-screening format. The Z' determined for peptide and protein used in this study displayed an excellent sample-to-sample and day-to day-reproducibility as reflected by Z' factors greater than 0.8 (Table 4.3).

Previous measurements of the K_d values of competitive ligands have been performed by using Cheng-Prusoff equation [42; 43]. However, Nikolovska-Coleska et al [42] have pointed out that this equation is not valid for fluorescence anisotropy based competitive assays since the exact concentration of free inhibitor is not known at 50 % inhibition. They have developed an equation to get rid of this issue but this equation also only takes into account three data points of the competitive assay curve. In this study we present an equation that takes into account all the points in the anisotropy assay curve upon displacement of the tracer by competitive ligands. Since

this approach weighs all the data points, the uncertainty of the calculated dissociation constant should be lower than the previous approaches.

The accurate protein, tracer and ligand concentrations in the assay mixture are key to a sensitive assay development. When we perform biological assay under the nanomolar range of analyte concentrations, precise control of the species is really challenging. Despite the fact that state-of- the-art technology bioassays are capable of measuring concentrations down to low nanomolar level, keeping proteins and peptides in the solution is not always a very simple task. Non-specific adsorption of proteins and peptides onto the surfaces of sample handling devices and containers that they are contained in is the biggest issue associated with protein and peptide losses from solutions during an assay development.

One may think that it is possible to adopt solution conditions that are already developed for protein and peptide adsorption for a particular assay development. While this kind of adaptation may work for limited number of assays, it's not always the case. There are some assays that require proper optimization of the buffer modifiers since the presence of buffer modifier may interfere with the measurement being made. Thus we need to perform a thorough study into the buffer modifier to make sure that its performance does not interfere with the measurement being made while helping keep the analyte from adsorbing onto the surfaces. Our selection of buffer modifiers was based on the long-standing interest in BSA and some other surfactants as dynamic surface coating agents for preventing protein and peptide adsorption. According to the fluorescence intensity changes with time, BSA and

DDM are promising for being deployed in this assay development. It is obvious from the comparison between the presence of polylysine and the absence of any surfactant that polylysine does not provide a conducive environment for eliminating peptide adsorption. We initially selected polylysine assuming that its richness in positively charged lysine may out-compete M13 from the surface interactions due to strong interaction of highly positively charged polylysine with negative charged glass surface.

Being a non-ionic surfactant, DDM showed great potential as a good surface modifying agent for being used in the assay development. It is a well established fact that the hydrophobic portion of non-ionic surfactants has a great influence on eliminating protein/peptide adsorption. The sharp change in the fluorescence intensity in the presence of the polylysine and the absence of a modifier in the solution are well correlated and can be attributed to the peptide adsorption onto the surface since the contribution from photobleaching of the fluorescence dye is minimal. This can be confirmed by comparing the changes in fluorescence intensity of free Atto465, which is only ~5 % of the initial fluorescence intensity. The presence of polylysine or no modifier on the other hand results in changes of fluorescence intensity of M13-Atto465 down to ~70 % of the initial fluorescence intensity. This information provides strong evidence for only a slight decrease in fluorescence intensity coming from the photobleaching of fluorophore. This change in the fluorescence intensity of free dye is strongly correlated with the decrease in fluorescence intensity of BSA and DDM, where there is less or no peptide loss due to peptide adsorption.

In the study of peptide adsorption onto glass and polystyrene BSA was proven to work equally well for both materials even though DDM worked only for polystyrene. This behavior of DDM is not surprising, as it has been deployed for the preventions of protein adsorption onto the hydrophobic surfaces such as PDMS [38]. This finding however, is not a setback as far as the assay development is concerned because our intention is to implement the assay on a 96-well assay plate. Most of the assay plates are made up of polystyrene and we had better luck with DDM on polystyrene.

The feasibility of using DDM or BSA in the assay buffer was studied by measuring the initial fluorescence anisotropy of M13-Atto465 in the presence of BSA or DDM. The purpose of this experiment is to make sure the initial anisotropy of the tracer peptide remains the same in the presence and absence of modifiers. According to Table 4.1, BSA has an adverse effect on the initial anisotropy of the tracer as indicated by the unacceptably high initial anisotropy of the tracer. This anisotropy is very close to the anisotropy of CaM bound tracer making the assay is insensitive to CaM binding if performed in the presence of BSA. This high anisotropy could be a result of either non-specific adsorption of tracer peptide onto freely moving BSA molecules or scatter coming from the solution due to high BSA concentration. It is very reasonable to expect that non-specific adsorption is the most probable phenomenon since BSA is capable of accommodating many proteins and peptides for non-specific adsorption. In contrast, the presence of DDM did not change the initial

anisotropy of the tracer, making DDM a successful candidate for being used in the assay development.

According to Table 4.2, the differences of K_T may reflect a slight difference in the measured affinities of CaM for the M13-Atto465 at different DDM concentrations. However, the uncertainty of peptide and protein concentrations may cause the difference in K_T of 0 and 0.005 % DDM concentrations. The K_T values determined at 0.01 % and 0.02 % seem to be very promising because those values are consistent with the previously measured K_T of M13-CaM complex using a completely different approach. Due to the intact affinity of CaM-M13 interaction in the presence of 0.01 % DDM, and the fact that the given DDM concentration is capable of eliminating proteins and peptides adsorption, we selected 0.01 % DDM to be used in the assay buffer.

Figure 4.6 shows the change in fluorescence anisotropy of M13-Atto465 bound to CaM upon replacement by competitive ligands. The decrease in anisotropy in upper panel can be explained by using the model presented in Figure 4.2. As seen in the model the tracer bound to CaM is bigger than the tracer alone. Initially the tracer is saturated with CaM so that all the tracer molecules stay bound to CaM leading to a maximum initial anisotropy. As the competing ligands replace the tracer, tracer molecules become free in solution and the anisotropy gradually decreases due to the fraction of smaller tracer becomes larger. Eventually when the tracer bound to CaM is entirely replaced by competing ligand, the anisotropy decreased to a value equal to that of free tracer. When the competing ligands fail to replace the tracer

bound to CaM, the initial anisotropy stays constant as depicted in the lower panels of Figure 4.6.

C28W and eNOS have competitively replaced M13-Atto465 bound to CaM as can be seen in the upper left and right panels of Figure 4.6 respectively. The dissociation constants of 8.6 nM derived for C28W by means of competition experiment is consistent with the previously measured values (5-10 nM) using other approaches [11]. This value is also similar to the dissociation constant (~7 nM) we obtained using whole protein (PMCA) using direct binding of fluorescently labeled CaM to PMCA [19]. The whole protein (eNOS) we used in this study is also capable of competitively replacing M13-Atto465 from CaM as seen in the upper right panel of Figure 4.6. The dissociation constant derived for eNOS in this study is also consistent with previously determined values using both whole protein and CaM binding domain peptide of eNOS (2-4 nM) [44; 45]. Therefore these results provide strong evidence for the accuracy of the results obtained from the competitive binding assay. However, the absence of competition between M13 peptide and CKII and mastoparan leaves us some unanswered questions. It could be that the dissociation constants of CKII and mastoparan are well beyond the range that can be assessed using this tracer, which has a very high affinity for CaM.

4.6 Conclusion

Use of DDM as a surface modifying agent to mitigate protein and peptide adsorption on to the surfaces worked extremely well for CaM and M13-Atto465.

Developing a competitive binding assay for CaM-target interactions seems to overcome limitations such as fluorescence quenching and ligand oligomerization associated with direct binding of CaM to its targets. The CaM binding domain peptide of MLCK (M13) can be used to determine the dissociation constants of high affinity binding targets of CaM. The dissociation constants obtained for C28W and the whole protein eNOS were consistent with previously reported values demonstrating the accuracy of the assay. CKII and mastoparan were not able to competitively replace the tracer bound to CaM. This issue needs to be addressed by using more concentrated ligand solutions.

4.7 References

[1]R. Chattopadhyaya, W.E. Meador, A.R. Means, and F.A. Quiocho, Calmodulin structure refined at 1.7 angstrom resolution. J. Mol. Biol. 228 (1992) 1177-1192.

[2]A. Crivici, and M. Ikura, Molecular and structural basis of target recognition by calmodulin. Annu. Rev. Biophys. Biomol. Struct. 24 (1995) 85-116.

[3]J. Trewhella, The solution structures of calmodulin and its complexes with synthetic peptides based on target enzyme binding domains. Cell Calcium 13 (1992) 377-390.

[4]M. Comte, Y. Maulet, and J.A. Cox, Ca^{2+}-dependent high-affinity complex-formation between calmodulin and melittin. Biochem. J. 209 (1983) 269-272.

[5]D.P. Giedroc, D. Puett, N. Ling, and J.V. Staros, Demonstration by covalent cross-linking of a specific interaction between beta-endorphin and calmodulin. J. Biol. Chem. 258 (1983) 16-19.

[6]D.A. Malencik, and S.R. Anderson, Binding of hormones and neuropeptides by calmodulin. Biochemistry 22 (1983) 1995-2001.

[7]D.A. Malencik, and S.R. Anderson, Binding of simple peptides, hormones, and neurotransmitters by calmodulin. Biochemistry 21 (1982) 3480-3486.

[8]R.A. Newman, and M.A. Shea, Energetics and interfaces of domain-specific binding of calmodulin to peptides. Biophys. J. 88 (2005) 85A-85A.

[9]B.R. Sorensen, and M.A. Shea, Domain-specific regulation of calcineurin by calmodulin, Biophys. J., 2004, pp. 454A-454A.

[10]D.K. Blumenthal, K. Takio, A.M. Edelman, H. Charbonneau, K. Titani, K.A. Walsh, and E.G. Krebs, Identification of the calmodulin-binding domain of skeletal-muscle myosin light chain kinase. Proc. Natl. Acad. Sci. U.S.A. 82 (1985) 3187-3191.

[11]A.R. Penheiter, A.G. Filoteo, J.T. Penniston, and A.J. Caride, Kinetic analysis of the calmodulin-binding region of the plasma membrane calcium pump isoform 4b. Biochemistry 44 (2005) 2009-2020.

[12]D.K. Blumenthal, Development and characterization of fluorescently-labeled myosin light chain kinase calmodulin-binding domain peptides. Mol. Cell. Biochem 127-128 (1993) 45-50.

[13]C. Hultschig, H.J. Hecht, and R. Frank, Systematic delineation of a calmodulin peptide interaction. J. Mol. Biol. 343 (2004) 559-568.

[14]D.A. Malencik, and S.R. Anderson, High-affinity binding of the mastoparans by calmodulin. Biochem. Biophys. Res. Commun. 114 (1983) 50-56.

[15]D.A. Malencik, and S.R. Anderson, Association of melittin with the isolated myosin light-chains. Biochemistry 27 (1988) 1941-1949.

[16]J. Anagli, F. Hofmann, M. Quadroni, T. Vorherr, and E. Carafoli, The calmodulin-binding domain of the inducible (macrophage) nitric-oxide synthase. Eur. J. Biochem. 233 (1995) 701-708.

[17]Y.H. Yao, and T.C. Squier, Variable conformation and dynamics of calmodulin complexed with peptides derived from the autoinhibitory domains of target proteins. Biochemistry 35 (1996) 6815-6827.

[18]M.E. Jolley, and M.S. Nasir, The use of fluorescence polarization assays for the detection of infectious diseases. Comb. Chem. High Throughput Screen. 6 (2003) 235-244.

[19]M.R. Liyanage, A. Zaidi, and C.K. Johnson, Fluorescence polarization assay for calmodulin binding to plasma membrane Ca^{2+}-ATPase: Dependence on enzyme and Ca^{2+} concentrations. Anal. Biochem. 385 (2009) 1-6.

[20]R.P. Haugland, Hand book of fluorescent probes and research products, Molecular Probes Inc., Eugene, Oregon, 2002.

[21]J.Y. Tang, E. Mei, C. Green, J. Kaplan, W.F. DeGrado, A.B. Smith, and R.M. Hochstrasser, Probing structural dynamics of individual calmodulin : Peptide complexes in hydrogels by single-molecule confocal microscopy. J. Phys. Chem. B 108 (2004) 15910-15918.

[22]T.J. Lukas, W.H. Burgess, F.G. Prendergast, W. Lau, and D.M. Watterson, Calmodulin binding domains - characterization of a phosphorylation and calmodulin binding-site from myosin light chain kinase. Biochemistry 25 (1986) 1458-1464.

[23]C.J. Burke, B.L. Steadman, D.B. Volkin, P.K. Tsai, M.W. Bruner, and C.R. Middaugh, The adsorption of proteins to pharmaceutical container surfaces. Int. J. Pharm. 86 (1992) 89-93.

[24]M. Duncan, M. Gilbert, J. Lee, and M. Warchol, Development and comparison of experimental assays to study protein peptide adsorption onto surfaces. J. Colloid Interface Sci. 165 (1994) 341-345.

[25]M.R. Duncan, J.M. Lee, and M.P. Warchol, Influence of surfactants upon protein peptide adsorption to glass and polypropylene. Int. J. Pharm. 120 (1995) 179-188.

[26]A. Kondo, and K. Higashitani, Adsorption of model proteins with wide variation in molecular-properties on colloidal particles. J. Colloid Interface Sci. 150 (1992) 344-351.

[27]C.S. Wu, and G.C. Chen, Adsorption of proteins onto glass surfaces and its effect on the intensity of circular-dichroism spectra. Anal. Biochem. 177 (1989) 178-182.

[28]H. Grohganz, M. Rischer, and M. Brandl, Adsorption of the decapeptide cetrorelix depends both on the composition of dissolution medium and the type of solid surface. Eur. J. Pharm. Sci. 21 (2004) 191-196.

[29]J.D. Andrade, and V. Hlady, Protein adsorption and materials biocompatibility - a tutorial review and suggested hypotheses. Advances in Polymer Science 79 (1986) 1-63.

[30]W. Norde, Adsorption of proteins from solution at the solid-liquid interface. Adv. Colloid. Interface Sci. 25 (1986) 267-340.

[31]A.V. Elgersma, R.L.J. Zsom, W. Norde, and J. Lyklema, The adsorption of bovine serum-albumin on positively and negatively charged polystyrene lattices. J. Colloid Interface Sci. 138 (1990) 145-156.

[32]T. Ha, T. Enderle, D.F. Ogletree, D.S. Chemla, P.R. Selvin, and S. Weiss, Probing the interaction between two single molecules: Fluorescence resonance

energy transfer between a single donor and a single acceptor. Proc. Natl. Acad. Sci. U.S.A. 93 (1996) 6264-6268.

[33]X.W. Zhuang, L.E. Bartley, H.P. Babcock, R. Russell, T.J. Ha, D. Herschlag, and S. Chu, A single-molecule study of RNA catalysis and folding. Science 288 (2000) 2048.

[34]M. Duncan, J. Lee, and M. Warchol, Influence of surfactants on protein / peptide adsorption to pharmaceutical surfaces. Pharm. Res. 10 (1993) T6041.

[35]N.I. Ivanova, and E.D. Shchukin, Mixed adsorption of ionic and nonionic surfactants on calcium-carbonate, Elsevier Science Bv, 1993, pp. 109-113.

[36]S.L. Law, and C.L. Shih, Adsorption of calcitonin to glass. Drug. Dev. Ind. Pharm.. 25 (1999) 253-256.

[37]S. Welinklintstrom, A. Askendal, and H. Elwing, Surfactant and protein interactions on wettability gradient surfaces. J. Colloid Interface Sci. 158 (1993) 188-194.

[38]B. Huang, S. Kim, H. Wu, and R.N. Zare, Use of a mixture of n-dodecyl-beta-d-maltoside and sodium dodecyl sulfate in poly(dimethylsiloxane) microchips to suppress adhesion and promote separation of proteins. Anal. Chem. 79 (2007) 9145-9149.

[39]J.K. Luey, J. McGuire, and R.D. Sproull, The effect of ph and nacl concentration on adsorption of beta-lactoglobulin at hydrophilic and hydrophobic silicon surfaces. J. Colloid Interface Sci. 143 (1991) 489-500.

[40]J.H. Zhang, T.D.Y. Chung, and K.R. Oldenburg, A simple statistical parameter for use in evaluation and validation of high throughput screening assays. J. Biomol. Screen. 4 (1999) 67-73.

[41]G. Loving, and B. Imperiali, A versatile amino acid analogue of the solvatochromic fluorophore 4-N,N-dimethylamino-1,8-naphthalimide: A powerful tool for the study of dynamic protein interactions. J. Am. Chem. Soc. 130 (2008) 13630-13638.

[42]Z. Nikolovska-Coleska, R.X. Wang, X.L. Fang, H.G. Pan, Y. Tomita, P. Li, P.P. Roller, K. Krajewski, N.G. Saito, J.A. Stuckey, and S.M. Wang, Development and optimization of a binding assay for the xiap bir3 domain using fluorescence polarization. Anal. Biochem. 332 (2004) 261-273.

[43]Y.C. Cheng, and W.H. Prusoff, Realtionship between the inhibition constant (ki) and the concentration of inhibitor which cause 50 percent inhibition (ic50) of an enzymatic reaction Biochem. Pharmacol. 22 (1972) 3099-3108.

[44]R.C. Venema, H.S. Sayegh, J.D. Kent, and D.G. Harrison, Identification, characterization, and comparison of the calmodulin-binding domains of the endothelial and inducible nitric oxide synthases. J. Biol. Chem. 271 (1996) 6435-6440.

[45]M. Zhang, and H.S. Vogel, Charecterization of the calmodulin-binding domain of rat cerebellar nitric oxide synthase. J. Biol. Chem. 269 (1994) 981-985.

Chapter 5

Investigation of the autoinhibitory domain conformations of plasma membrane Ca^{2+}-ATPase

5.1 Introduction

Calmodulin (CaM) activates a diverse range of targets. Among these targets, plasma membrane Ca^{2+}-APTase (PMCA) is a well-characterized enzyme that helps maintain the low intracellular Ca^{2+} ion levels required for signal transduction in cells [1; 2; 3; 4]. In recent studies, PMCA has been reported to regulate other important roles in signal transductions processes [5]. Thus dysfunction of PMCA will result in serious functional and survival failure of the cell [6; 7]. For example, some physiologically relevant reactive oxygen species seem to alter PMCA in turn causing adverse effects on the function of the enzyme [8; 9; 10; 11; 12].

The mechanisms underlying the regulation of PMCA upon binding by CaM are poorly understood. It is clear from the recent results that the distribution of autoinhibitory domain conformations governs the response of PMCA to changes in Ca^{2+} levels [13; 14; 15]. Being a 134-kDa protein, PMCA contains 10 transmembrane segments and a large intracellular loop positioned between segments 4 and 5 (Figure 5.1). This intracellular loop contains binding sites for ATP and an aspartate residue where the phosphorylation occurs. The CaM binding domain of PMCA is located near the C-terminal domain of PMCA. This site also coincides with the autoinhibitory domain of PMCA, which plays a regulatory role for the function of the enzyme by

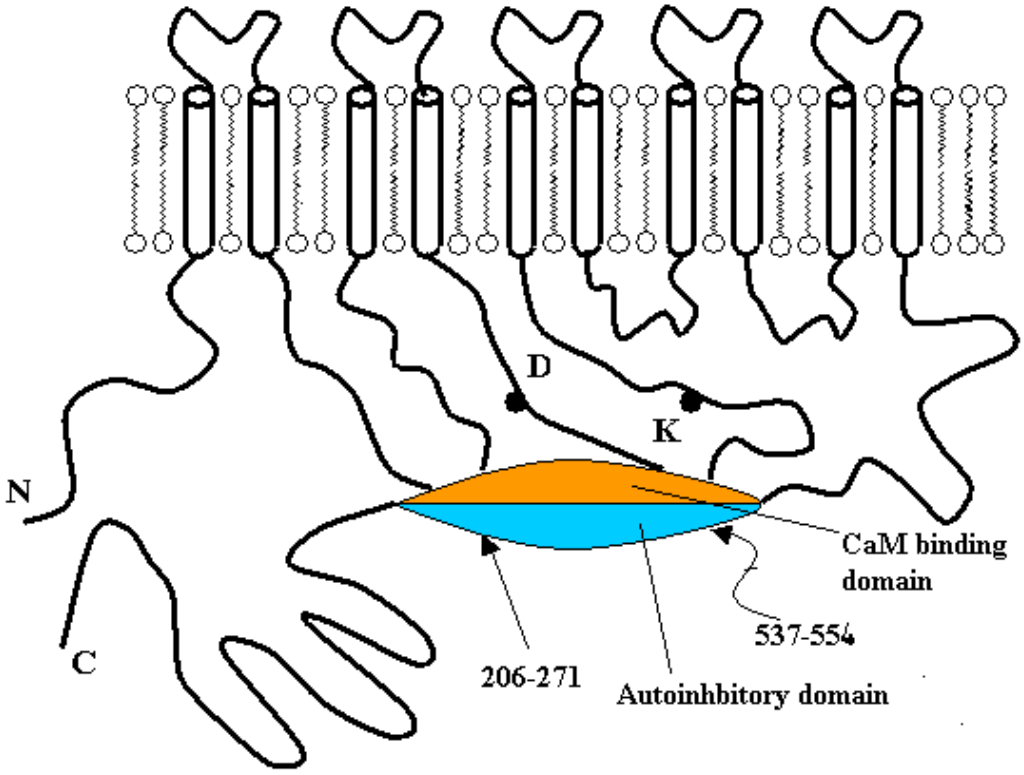

Figure 5.1 Schematic representation of the structure of PMCA elaborating the cytoplasmic domains (modified from [16]). These domains bear an aspartic residue (D), the sites for phosphorylation during enzymatic cycle, and the nucleotide-binding site (K). The C-terminal autoinhibitory domain interacts with residues 206-271 and 527-554, causing autoinhibition of the enzyme.

closely associating with the active site, thereby preventing binding or hydrolysis of ATP [17]. The autoinhibitory domain dissociates from the active site upon CaM binding allowing utilization of ATP to render the enzyme active. Although the fact that CaM binding releases the autoinhibitory domain from the active site of the enzyme is widely accepted, the dynamics of the structural changes in the enzyme during activation have not been well characterized in spite of several attempts.

Previous fluorescence anisotropy measurements on CaM bound to PMCA in native erythrocyte membranes, provide insight into an orientationally mobile state with a much faster rotational correlation time (80 ns) than that of PMCA in membrane (~ 100 μs) [18]. This information suggests that the autoinhibitory domain of PMCA is mobile upon binding to CaM at elevated Ca^{2+} levels. There has been a long-standing two state model for PMCA activation by CaM. This model describes that the pump stays inactive as long as the autoinhibitory domain is associated with the active site in the absence of CaM, and upon CaM binding to autoinhibitory domain it releases from the active site, conferring the activity to the enzyme [17; 19]. Biochemical kinetic measurements performed on PMCA have revealed that CaM has the ability to stay bound to inactive enzyme at low Ca^{2+} concentrations, giving the enzyme a memory from previous saturating Ca^{2+} levels [1]. It has also been reported that an inactive PMCA-CaM complex can respond to a transient increase in Ca^{2+} levels owing to the presence of CaM already bound to PMCA [20]. Osborn et al have put forward a three-state model for autoinhibitory domain dynamics based on the polarization modulation experiments at the single-molecule level [13; 21]. In this model, an intermediate state corresponding to CaM bound auto inhibitory domain without its release from the active site has been proposed.

They also have extended this single molecule approach to study the influence of oxidative modifications of CaM and PMCA on autoinhibitory domain dynamics upon changes in Ca^{2+} ion and ATP concentrations [22; 23].

Numerous efforts have been made to extract information about the structure and the dynamics of PMCA by attaching a fluorescent label directly to PMCA. Penniston and coworkers have sequenced the fluorescein isothiocyanate (FITC) binding site of PMCA by tryptic digestion and HPLC separation of fragments [24]. Fluorescence resonance energy transfer (FRET) studies of ologomerization of PMCA have been carried out using FITC and eosin isothiocyanate (EITC) labeled PMCA [25; 26]. These studies have shown that PMCA dimerization starts around 15 nM with a dissociation constant of 140 nM and the dimerization constitutes a mechanism protection from spontaneous denaturaton of PMCA [26; 27]. Fonseca et al used FITC attached close to the active site of PMCA along with fluorescence quenching experiments to study the solvent accessibility of the ATP binding pocket of the enzyme [27]. The location of important amino acid residues such as the autoinhibitory domain binding site, the labeling site for FITC (Lys 591), and the phosphorylation site (Asp 465) are shown in Figure 5.2. The conceptual basis for obtaining the distribution of single-molecule conformations of the autoinhibitory domain by single molecule FRET is demonstrated in Figure 5.3. Specific labeling of CaM at 34 site through site-directed mutagenesis and maleimide reactions of fluorophores is well established [22; 28].

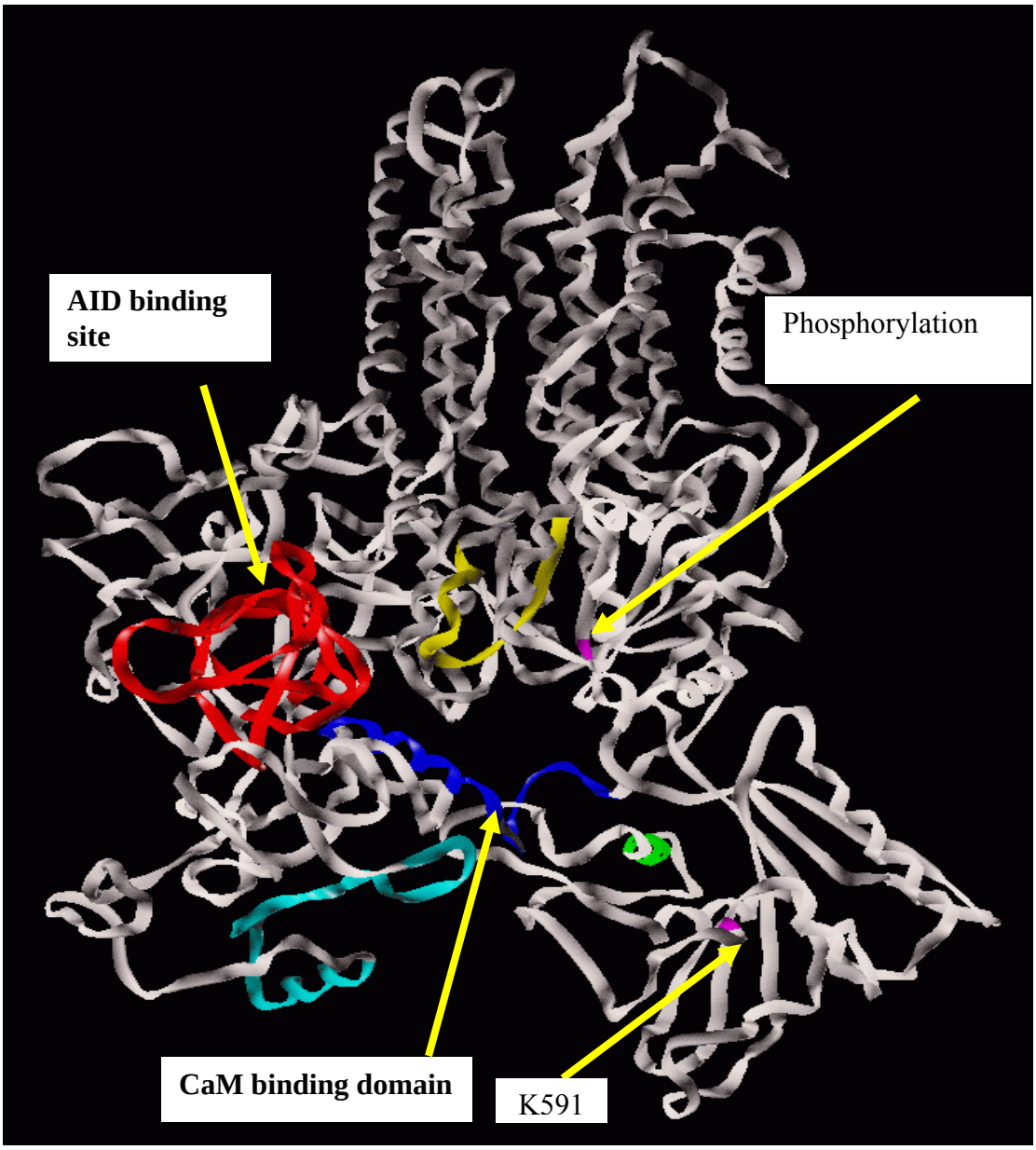

Figure 5.2 A model created for PMCA based on structurally homologous SERCA and biochemical studies. Inhibitory domain binding sites, red & green; CaM binding domain, blue; pKC , cyan; FSBA-reactive (ATP analog) binding site, yellow [29]. (Courtesy of G. Lushington)

(A)

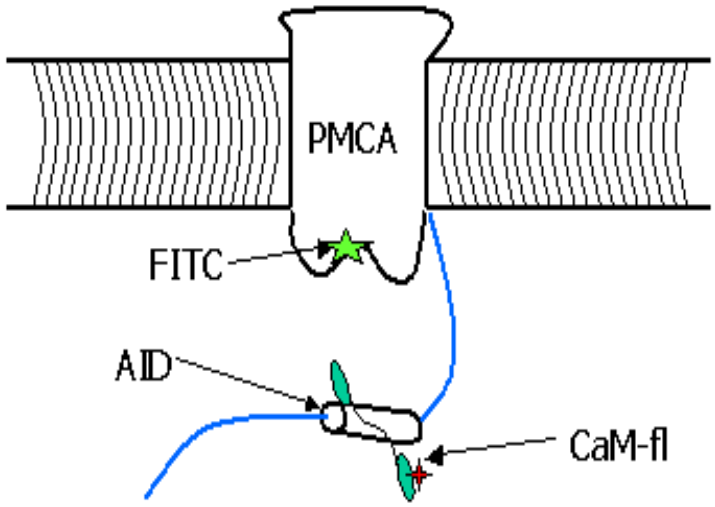

(B)

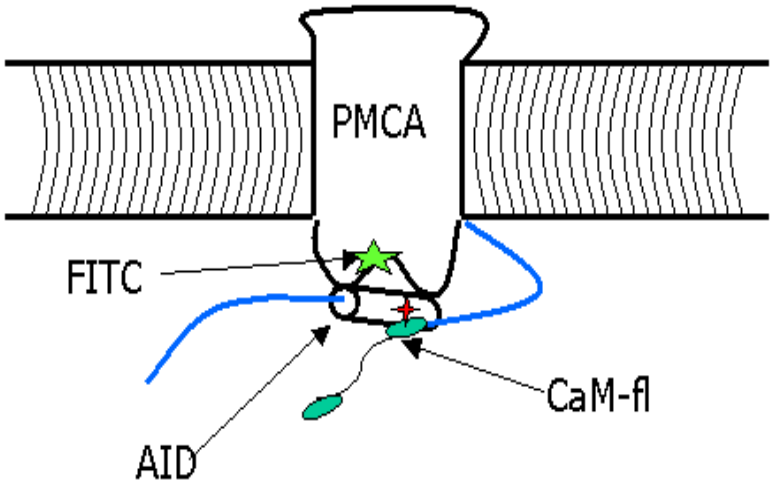

Figure 5.3 Schematics of the conformations of the autoinhibitory domain as applied to FRET experiments. The state (A) with a dissociated autoinhibitory domain gives rise to only a low FRET state, while state (B) where the autoinhibitory domain is closely associated with the catalytic core is responsible for the appearance of a high FRET state due to spatial proximity of the donor and the acceptor.

Single molecule spectroscopy has emerged as a powerful tool to characterize properties of heterogeneous distributions of macromolecules in biological systems [30; 31; 32; 33; 34]. In particular single-molecule detection methods are capable of distinguishing subpopulations of intermediate states that are hidden in bulk studies due to ensemble averaging over these subpopulations. Single molecule methods also follow time-dependent pathways of trajectories of biochemical events of non-equilibrated systems without requiring synchronization as in ensemble level experiments [33; 35]. FRET has also long been employed in biochemical and biophysical studies [36; 37]. In FRET the efficiency of energy transfer from an excited donor fluorophore to an acceptor fluorophore is measured and can be effectively used to measure distances in the range of tens of Angstroms [38]. The efficiency of the energy transfer, E, is given by

$$E = \frac{1}{1 + (R/R_0)^6} \tag{5.1}$$

where R is the distance between the donor and the acceptor and R_0 is the distance at which the probability of energy transfer is 50 %:

$$R_0 = 9.79 \times 10^3 (n^{-4} \kappa^2 \phi_d J)^{1/6} \tag{5.2}$$

where J is the spectral overlap of donor fluorescence and acceptor absorption, ϕ_d is the quantum yield of the donor in the absence of the acceptor, and κ^2 depends on the relative orientation of dipoles the donor and the acceptor. The κ^2 factor may take values ranging from 0 to 4, but in most cases it is approximated to 2/3 for interpreting distance distributions from energy transfer efficiencies assuming that the dipole moments of dyes are free to rotate in all directions at a much faster time scale than relative lifetimes of donor and acceptor [39]. Due to the strong distance dependence of FRET, it can be used

as a spectroscopic ruler where a small change in distance between two sites of a macromolecule bearing donor and acceptor molecules results in a significant change in *E*. So this is why we can use FRET to detect structural changes in biomolecules in the tens of Å regime [40].

During fluorescent burst measurements, fluorescently labeled molecules diffuse through the ~ 2 fL excitation volume of a focused laser beam and emit short bursts of fluorescence detected above the background noise level (see Figure 5.5). A schematic diagram of confocal fluorescence microscope is shown in Figure 5.4. Despite the fact that burst analysis is a simple technique, the stochastic nature of burst data demands sophisticated methods of data analysis. The burst data are dominated by shot noise since bursts often consist of less than 100 photons, and each molecule can take random paths through the excitation/collection volumes. This will result in a spatial dependency of excitation and collection efficiency leading to a range of burst widths and intensities [41]. Such transient signals are often analyzed by a method called burst analysis. Burst analysis is a processes involving counting of bursts, the quantification of the number of photons in a burst, the burst lengths, and calculating FRET efficiency.

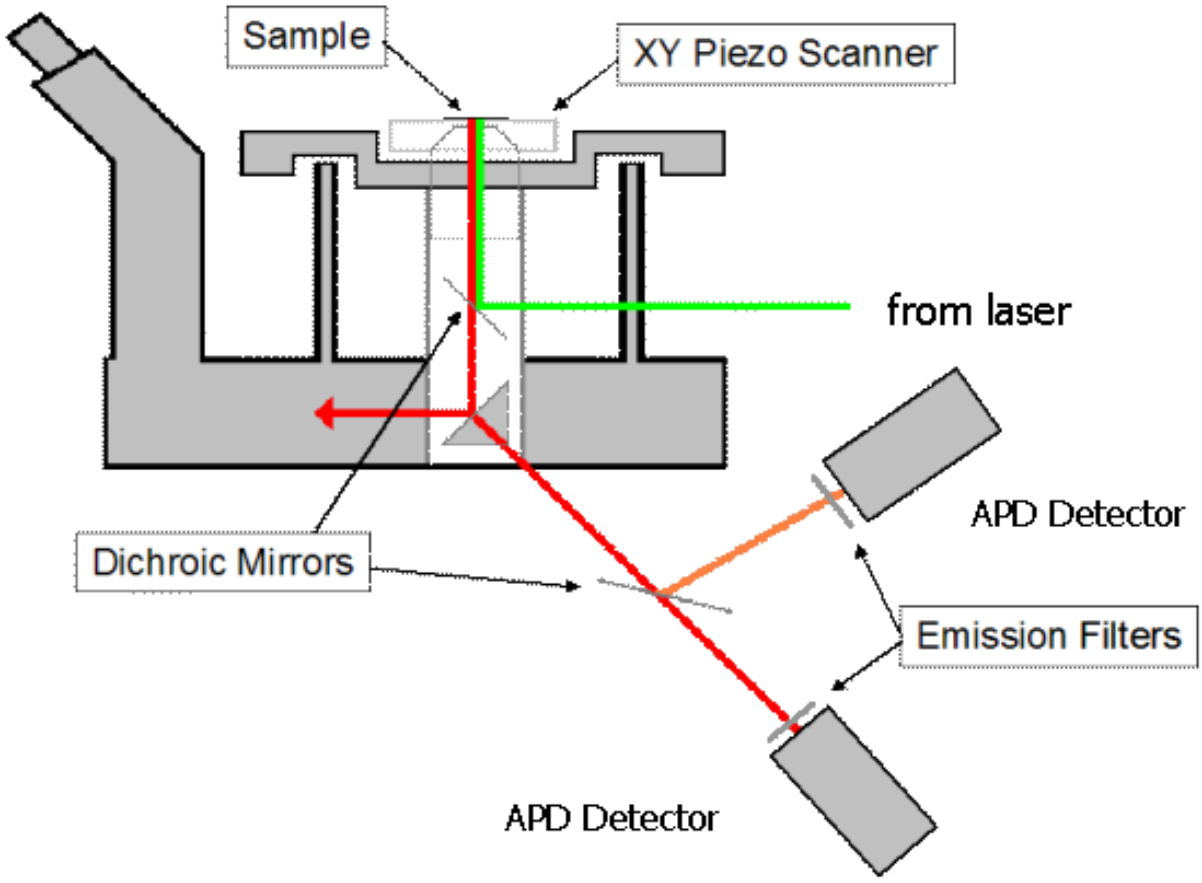

Figure 5.4 Schematic diagram of the inverted confocal fluorescence microscope used in burst measurements.

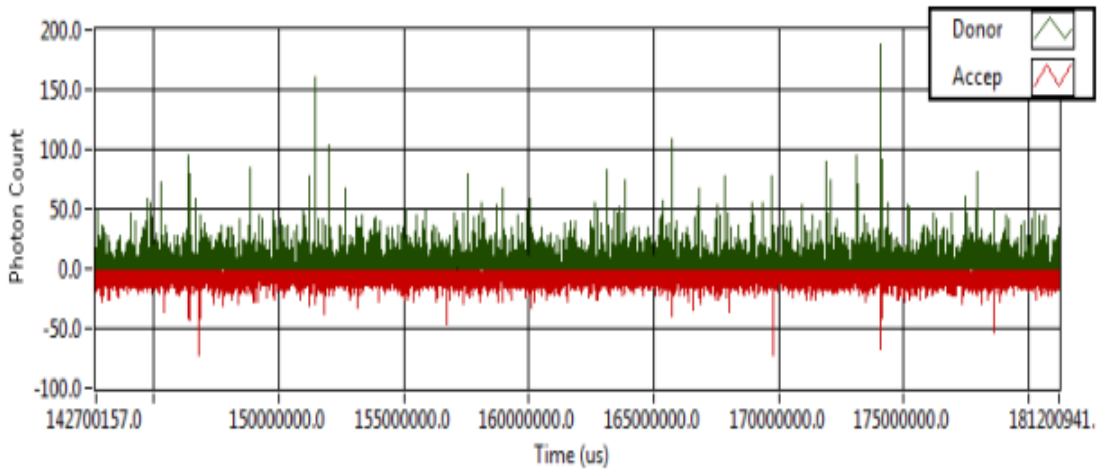

Figure 5.5 A burst trajectory showing bursts from single PMCA molecules labeled with FITC and CaM labeled with Texas Red passing through the focal volume of the excitation beam. In this trajectory, bursts are binned by 1 ms for the purpose of analysis.

5.2 Materials and methods

FITC labeling of PMCA was performed by following a protocol described by Kosk-Kosicka et al as follows [25]. Erythrocyte ghost membranes in HEPES buffer at pH 7.4 were incubated with a10-fold molar excess of FITC dissolved in dimethyl sulfoxide (DMSO) at 4 ^{0}C for 1 hour in the dark. The ghosts were washed several times to get rid of any unreacted dye before PMCA purification. Then the FITC-labeled ghost membrane was used to purify PMCA as described in the experimental section of Chapter One in this thesis.

A CaM-T34C mutant was expressed in *E. coli* as described in Chapter One of this thesis. Then the protein was purified using a phenyl sepharose affinity column according to the protocol described in Chapter One. CaM-T34C was then reacted with 10 fold molar excess of Texas Red dissolved in DMSO for one hour in the dark. The unreacted dye was separated from Texas Red labeled CaM using Sephadex G-25 size exclusion column. Glass coversilips were coated with BSA as follows to prevent nonspecific protein adsorption onto the surface of the coverslip. To coat coverslip, 40 μl of 2 mg/ml BSA was placed on a coverslip and incubated for 10 minutes. Then the coverslip was rinsed with water and air dried by blowing nitrogen over it. The final concentrations of 7 nM FITC-PMCA and 10 nM CaM-TR in solution were incubated for 15 minutes in either high or low Ca^{2+} HEPES buffer as required by the experiment. Then this solution was diluted 25 times right before taking burst measurement. The standard high Ca^{2+} buffer consists of 10 mM HEPES, 0.1 M KCl, 1 mM $MgCl_2$, 100 μM $CaCl_2$, pH 7.4, while low Ca^{2+} buffer consisted of 10 mM HEPES, 0.1 M KCl, 10 mM EGTA, 1.35 mM $MgCl_2$, 7.8 mM $CaCl_2$, pH 7.4.

Single molecule fluorescence bursts were collected using an inverted fluorescence microscope (Nikon TE2000) as previously described (Figure 4.4) [42; 43]. The 488 nm line of Ar^+ ion laser was directed to the back of a 1.2 NA, 60× water-immersion objective (Olympus) using a long pass dichroic mirror (Q505LP, Chroma Technologies). A drop of diluted PMCA-FITC and CaM-TR (~200 pM) was placed on a BSA-coated coverslip and 20 μW of laser power was used to excite the sample to collect single molecule bursts. For the control experiments CaM-TR was replaced with unlabeled CaM at both Ca^{2+} concentrations. The laser was focused onto the sample using the objective and the emitted fluorescence was collected back through the same objective. The focal region of the laser beam was set to 20 μm from the surface of the coverslip in order to reject fluorescence from immobilized molecules on the surface of the coverslip. The emission was then passed thorough the same dichroic mirror and filtered through a dichroic filter (565DCLP, Chroma Technologies) to separate donor and acceptor emission. The band-pass filters for donor (HQ525/50M, Chroma Technologies) and acceptor (HQ 620/75M, Chroma Technologies) channels were placed before each detector. The out-of-focus light was blocked by 75-μm pinholes before each channel. The fluorescence detection was performed using single-photon counting avalanche photodiodes (SPCM-ARQ-14, Perkin-Elmer). The fluorescence was collected into 300-μs time bins in each channel. Photon-mode data collection was used to acquire data in donor and acceptor channel with a PCI 6602 card (National Instrument) and a data acquisition program written in LabView (National Instruments).

Analysis of single-molecule FRET distributions. When fluorescent molecules diffuse through the focal volume of the microscope sudden bursts of fluorescence occur

above the noise level. Since the probability of a molecule occupying the focal volume at the concentrations required by the single molecule experiments is low, we need to set threshold signal levels to detect molecules in the focal volume. According to the previous cutoff methods used for single molecule burst analysis, the donor and the acceptor counts were required to be larger than 6 times the standard deviation of the background signal in each channel separately or the sum of donor and acceptor counts to be 6 times above the sum of the two channels' background [42; 43; 44]. Experimentally measured average donor bleed thorough (~10 %) was subtracted from the acceptor channel counts in order to avoid bins with false low FRET efficiency due to acceptor photobleaching. All the fluorescence bursts were binned into 1 ms time bins for data analysis.

After ensuring the bursts have enough counts by using threshold settings of donor and acceptor counts, the FRET efficiency for each bin was determined by substituting donor intensity I_D and acceptor intensity I_A to the following equation:

$$E = \frac{c(I_A - bI_D)}{c(I_A - bI_D) + I_D} \tag{5.3}$$

where c and b are correction factors for relative detection efficiency of the two channels and average bleed-through from donor to acceptor channel respectively. The correction factor c can be determined as follows.

$$I_A = g_A(F_A + cF_D) \tag{5.4}$$

where g_A is the acceptor channel detection efficiency, F_A number of acceptor photon from fluorescence, and F_D number of donor photons from fluorescence.

$$I_D = g_D F_D \tag{5.5}$$

E can be written as

$$E = \frac{F_A / \phi_A}{(F_A / \phi_A) + (F_D / \phi_D)} \tag{5.6}$$

where g_D is the donor channel detection efficiency, ϕ_A is the quantum yield of the acceptor and ϕ_D is the quantum yield of the donor. Substitution of eq. 5.4 in eq. 5.6 yields

$$E = \frac{\phi_{DA}\left[(I_A / g_A) - c(I_D c / g_D)\right]}{\phi_{DA}\left[(I_A / g_A - c(I_D c / g_D\right] + (I_D / g_D)} \tag{5.7}$$

where $\phi_{DA} = \phi_D / \phi_A$ and $G_{DA} = g_D / g_A$. Rearranging eq. 5.7 results in

$$E = \frac{\phi_{DA}\left[G_{DA} I_A - cI_D\right]}{\phi_{DA}\left[G_{DA} I_A - cI_D\right] + I_D} \tag{5.8}$$

The bleed-through correction, b can be obtained from a high concentration of donor-only sample:

$$b = \frac{I_A}{I_D} = \frac{g_A c F_D}{g_D F_D} = \frac{c}{G_{DA}} \tag{5.9}$$

Substituting the solution for c for in eq. 5.8 gives:

$$E = \frac{\phi_{DA} G_{DA}\left[I_A - bI_D\right]}{\phi_{DA} G_{DA}\left[I_A - bI_D\right] + I_D} \tag{5.10}$$

the value of $\phi_{DA}\, G_{DA}$ can be obtained by rearranging eq. 5.10;

$$\phi_{DA} G_{DA} = \frac{EI_D}{(I_A - bI_D)(1 - E)} \tag{5.11}$$

when bulk value for E can be measured to determine $\phi_{DA} G_{DA}$I.

5.3 Results

The labeling strategy we used to specifically label PMCA in this study is a well characterized and widely used method [26; 27; 45]. The labeling takes place at the lysine

591 residue of PMCA while it is intact in erythrocyte membrane, providing more control to the specific labeling reaction. Figure 5.6 shows the fluoresce emission spectrum of FITC-labeled PMCA. The single-molecule burst collections were performed by collecting fluorescence in the donor and the acceptor channels using the confocal setup described in the Materials and Methods section. In order to collect bursts only from single molecules, we maintain a spatially restricted excitation volume and low a picomolar concentration of labeled PMCA and CaM. Figure 5.5 shows a typical bust trajectory with bursts comprising high count levels for single molecules.

After selecting the criteria for single molecule bursts that can be deployed in calculating energy transfer efficiencies for single PMCA-CaM complex molecules, the energy transfer efficiencies were calculated for each bin. Since the single molecule measurements allow extracting information pertaining to the subpopulations of a heterogeneous environment, we were able to detect different distributions of energy transfer efficiencies. Figure 5.7 shows the energy transfer distributions for FITC-PMCA and CaM-TR (A) and FITC-PMCA and unlabeled CaM as the control (B) at high Ca^{2+} concentration (10 μM). The FRET distribution of FITC-PMCA and CaM-TR complex possesses only a minute population of a high FRET state at high Ca^{2+} level. Comparing this result to the control experiment where there is no acceptor fluorophore present on CaM reveals that this small population of FRET at high Ca^{2+} levels should come from the changes in donor acceptor distances. Since the donor bleed-through to the acceptor channel has been corrected, there should not be any significant contribution from donor bleed though to the high-FRET state. This is also clear from the control FRET distribution, which does not show any pseudo high FRET state. The inclusion of

unlabeled CaM in the control experiment makes sure that the conformations of PMCA remains the same in each instance without adding any complications to the interpretation of results. The similar population with a value of low energy transfer distribution of control and the case with FITC-PMCA and CaM-TR indicates that the seemingly low FRET state is not really a low FRET state but a no-FRET state coming from the donor only molecules.

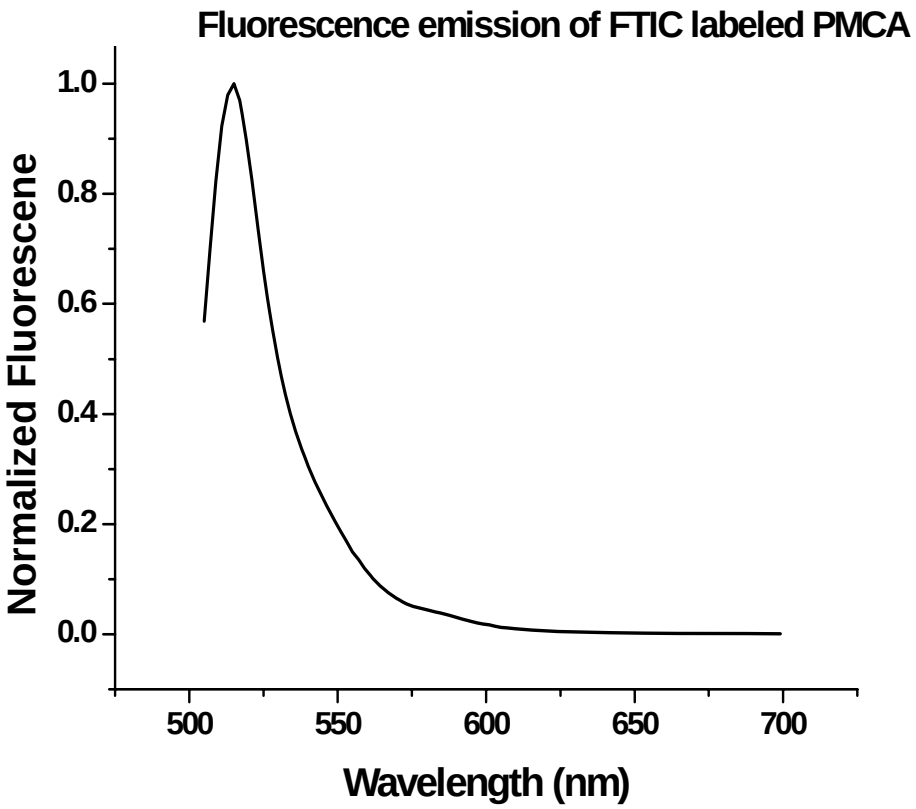

Figure 5.6 the fluorescence emission spectrum of FITC labeled PMCA showing the emission maximum similar to FITC. The emission spectrum was collected exciting FITC-PMCA at 480 nm.

This observation suggests that the FITC and Texas Red dye pair may not be capable of tracking the autoinhibitory domain when it is fully dissociated.

In contrast to the high Ca^{2+} level, at the low Ca^{2+} concentration (150 nM) the population with the high FRET state is very high (Figure 5.8). This close proximity of donor and acceptor fluorophores provides strong evidence for a closely associated state.

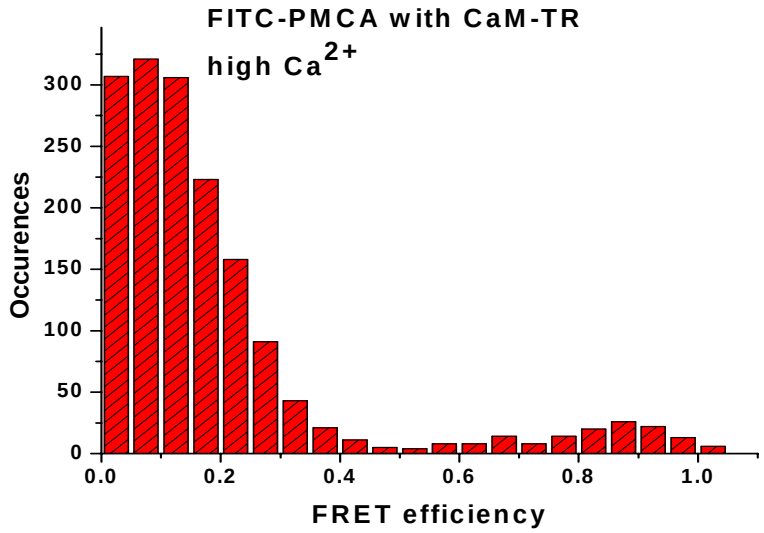

A

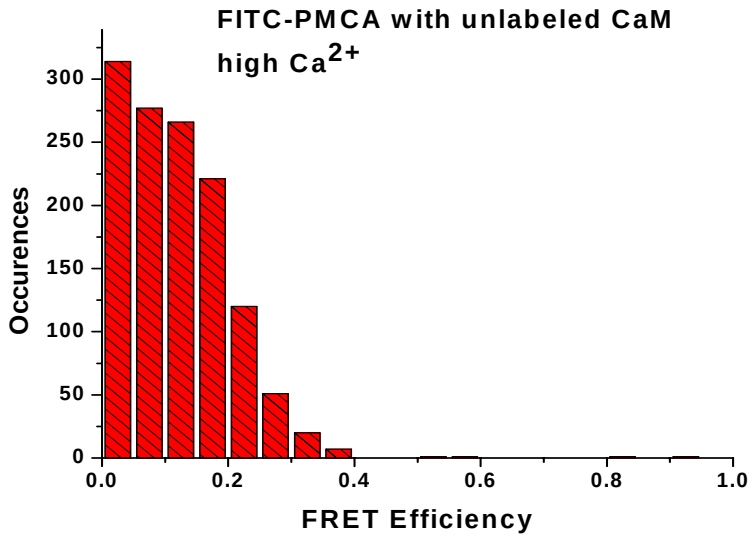

B

Figure 5.7 The populations showing energy transfer efficiency between FITC-PMCA and CaM-TR (A) and FITC-PMCA and unlabeled CaM (B) at High Ca^{2+} concentrations.

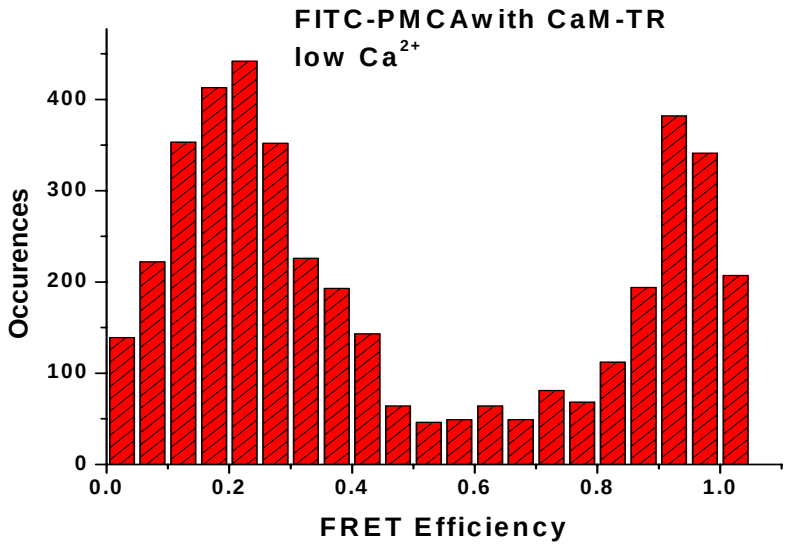

A

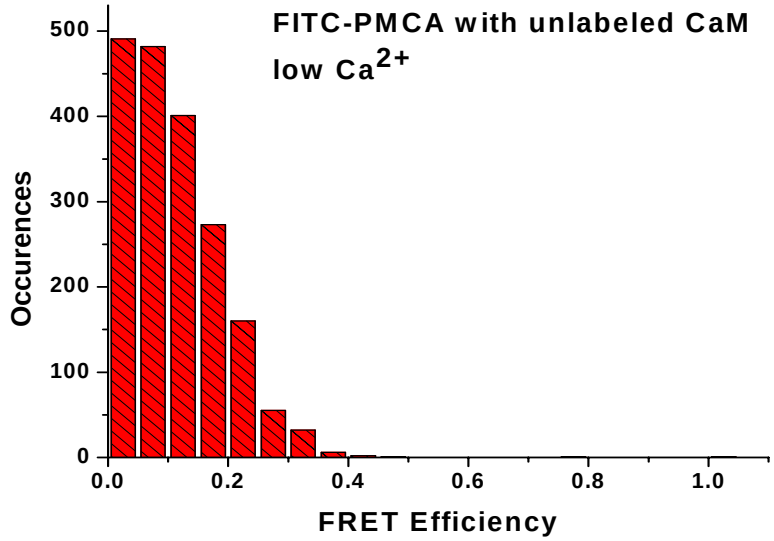

B

Figure 5.8 The populations showing energy transfer efficiency between FITC-PMCA and CaM-TR (A) and FITC-PMCA and unlabeled CaM (B) at low Ca^{2+} concentrations

5.4 Discussion

The importance and the roles of the autoinhibitory domain for the regulation of PMCA are worth studying since it may shed some light into the mechanism behind activation of PMCA. Although there is plenty of information about the function of P-type ATPases from the structurally homologous sarcoplasmic reticulum Ca^{2+}-ATPase (SERCA) [46], the lack of an autoinhibitory domain in SERCA keeps it from serving as a model for regulation of the enzyme. According to previous bulk studies of autoinhibitory domain dynamics, the autoinhibitory domain was supposed to play the role of an on-off switch to regulate the function of the enzyme proposing two-state model. Due to the inherent heterogeneity of biological systems, it is possible that a significant amount of information pertaining to the regulatory mechanism may have been hidden in bulk studies as result of averaging over many molecules in the population. If the traditional two-state model were correct, the decrease in Ca^{2+} concentration would simply lead to a decreased number of CaM molecules bound to PMCA without having any effect on the nature of the distributions. Based on the different populations of modulations depths reported at low and high Ca^{2+} levels, heterogeneous distribution of autoinhibitory domain conformations with differential interactions with the catalytic core of the enzyme may exist. Under these circumstances, the power of single molecule spectroscopy possessing the capability to reveal subpopulations of a heterogeneous distribution can play a major role in resolving theses intermediate conformations.

The particular approach we used in this study is based on the FRET measurements using bursts analysis. The burst collection-approach is more convenient and faster than methods based on scanning immobilized single molecules as we get

fluorescence burst from the molecules pass through the focal regions of the excitation beam. The desired resolution for collecting single molecule bursts were achieved by a combination of a confocal excitation volume defined by the features of the microscopic objective and maintaining low enough concentration (few hundred picomolar) to make sure the probability of finding two molecules simultaneously in the focal volume is extremely low.

There are some practical caveats we need to overcome in a single molecule approach for the study of autoinhibitory domain conformations. First of all, the loss of protein at very low concentrations due to adsorption onto the surface of the coverslip has detrimental effects on the measurement. The surface adsorption not only disturbs the equilibrium causing dissociation of bound complexes but also reduces the number of bursts that can be collected for a given sample. In order to prevent protein adsorption, the coverslips were treated with BSA to coat hydrophobic glass surface. The surface-treated glass coverslips worked well for reducing protein adsorption onto the surface.

Another limitation is that mixing PMCA and CaM at a picomolar level is not conducive for them to form a complex since the dissociation constant of PMCA-CaM complex is 7 nM. Since the concentration of each species is well below the dissociation constant, molecules in complex form are very rare. However, taking the advantage of a long off rate of CaM from the CAM-PMCA complex [47] we devised a strategy to mix CaM and PMCA at higher concentrations (~ 10 nM) and incubate the mixture for desired time followed by a rapid dilution to the desired picomolar level concentration right before taking burst measurements. Since the burst collection rather than scan method only takes a few minutes to collect fluorescence from hundreds of molecules, the probability of

finding CaM-PMCA complex molecules in the focal volume is still high because the off rate is longer than the time to record the burst trajectory. Therefore we were able to collect single molecule bursts of single CaM-PMCA molecules.

The photophysical properties of donor-acceptor pair also add certain limitations to successful implementation of the single molecule study: (a) FITC is a not a great single molecule-fluorophore because of its environmental sensitivity and fast photobleaching time. However, the specific labeling near the active site of enzyme with FITC is the only well-characterized approach to label PMCA. (b) The R_0 of the FITC-Texas Red dye pair is too short to track the conformations of dissociated autoinhibitory domain due to a greater distance between CaM binding domain and the active site upon dissociation from the active site of the enzyme. Therefore we need to exploit other dye pairs such as FITC and tetramethyl rhodamine (TMR), which has longer R_0 value than FITC and Texas Red in order to monitor the changes of dissociated autoinhibitory domain.

In order to make a strong case for the autoinhibitory domain conformations, we can put previous results bolstering the conformations of the autoinhibitory domain into context with the current findings. The observation that CaM triggers release of the autoinhibitory domain from the active site of the enzyme made by Enyedi et al [17] is further supported by measurement of the autocorrelation decay of single FITC-PMCA molecules. The decreased autocorrelation time of FITC when CaM is present is a result of enhanced solvent accessibility of FITC bound close to the active site [21]. The single-molecule fluorescence polarization modulation studies of the autoinhibitory domain conformations have suggested the existence of three-states for the autoinhibitory domain upon binding by CaM. The successful implementation of polarization modulation studies

to track the mobility states of autoinhibitory domain upon activation helps understand the mechanism behind the PMCA activation by CaM. According to the modulation depth distributions at low and high Ca^{2+} concentrations, the autoinhibitory domain adopts different conformations depending on the Ca^{2+} concentration. At low Ca^{2+} levels, there are two-modulation depth distributions reported for CaM-TMR bound to PMCA, providing evidence for the presence of two conformations of autoinhibitory domain. However, at high Ca^{2+} levels, there is only modulation depth distribution for CaM-TMR bound to PMCA indicating a single conformer of the autoinhibitory domain [13].

The previous results discussed above based on fluorescence polarization modulation experiments suggest that the autoinhibitory domain is not merely an on-off switch upon CaM binding and the regulatory mechanism of PMCA is more complex than previously predicted [13]. The results of the single molecule burst integrated FRET measurements we obtained for PMCA-FITC bound to CaM-TR further reinforce the existence of the three-state model for the regulatory mechanism of PMCA. The correlation between populations of low modulation depths and high FRET state at low Ca^{2+} level gives strong evidence for an associated autoinhibitory domain with the catalytic core of the enzyme (Figure 5.8). This state of the autoinhibitory domain as evidenced by the low mobility and high FRET state may represent an intermediate responsible for release and binding of autoinhibitory domain. The disappearance of the low-mobility and high-FRET state at elevated Ca^{2+} levels provides insight into a dissociated autoinhibitory domain. Very interestingly, at the low Ca^{2+} level, the possibility of an emerging low FRET state around energy transfer efficiency of 0.2 to 0.4 indicates a possible dissociated state of the autoinhibitory domain, yet wandering closely

around the active site. It is unlikely that this additional low FRET state is a result of some experimental artifact because it is a response only to change in Ca^{2+} concentration.

However, unambiguous distance determination of the dissociated autoinhibitory domain seems to be quite difficult with the current dye pair. In spite of this limitation, the single molecule FRET studies display a Ca^{2+} concentration dependence consistent with single molecule polarization modulation studies. These unprecedented results for Ca^{2+} dependency revealed by single molecule studies demonstrate the capability of single molecule techniques to distinguish the biologically crucial intermediates in the enzymatic cycle of PMCA.

5.5 Conclusion

With FITC as the donor in the vicinity of the active site of PMCA, the conformations of the autoinhibitory domain can be tracked with Texas Red labeled CaM. The concentration required for single-molecule bursts analysis was obtained by diluting a concentrated mixture of PMCA-FITC and CaM-TR right before taking the measurement. This ensures bursts coming from bound PMCA and CaM molecules. The distributions of FRET states at low and high Ca^{2+} levels are in agreement with previous single-molecule results based a model for the conformations of autoinhibitory domain. The appearance of two FRET state at low Ca^{2+} may provide evidence for the presence of more sub-states than we observed from polarization modulation experiments.

5.6 References

[1]A.J. Caride, A.R. Penheiter, A.G. Filoteo, Z. Bajzer, A. Enyedi, and J.T. Penniston, The plasma membrane calcium pump displays memory of past calcium spikes - differences between isoforms 2b and 4b. J. Biol Chem. 276 (2001) 39797-39804.

[2]F. Di Leva, T. Domi, L. Fedrizzi, D. Lim, and E. Carafoli, The plasma membrane Ca^{2+} - ATPase of animal cells: Structure, function and regulation. Arch. Biochem. Biophys 476 (2008) 65-74.

[3]H.J. Schatzmann, Depenence on calcium concentration and stoichiometry of the calcium pump in human red cells. J. Physiol 235 (1973) 551-569.

[4]E.E. Strehler, A.G. Filoteo, J.T. Penniston, and A.J. Caride, Plasma-membrane Ca^{2+} pumps: Structural diversity as the basis for functional versatility, Portland Press Ltd, 2007, pp. 919-922.

[5]J.C. Williams, A.L. Armesilla, T.M.A. Mohamed, C.L. Hagarty, F.H. McIntyre, S. Schomburg, A.O. Zaki, D. Oceandy, E.J. Cartwright, M.H. Buch, M. Emerson, and L. Neyses, The sarcolemmal calcium pump, alpha-1 syntrophin, and neuronal nitric-oxide synthase are parts of a macromolecular protein complex. J. Biol. Chem 281 (2006) 23341-23348.

[6]B.J. McCullough, J.C. Adams, D.J. Shilling, M.P. Feeney, K.C.Y. Sie, and B.L. Tempel, 3p-syndrome defines a hearing loss locus in 3p25.3. Hear. Res. 224 (2007) 51-60.

[7]V. Prasad, G.W. Okunade, M.L. Miller, and G.E. Shull, Phenotypes of serca and PMCA knockout mice. Biochem. Biophys. Res. Commun. 322 (2004) 1192-1203.

[8]S.N. Kip, and E.E. Strehler, Rapid downregulation of ncx and PMCA in hippocampal neurons following H_2O_2 oxidative stress. in: A. Herchuelz, M.P. Blaustein, J. Lytton, and K.D. Philipson, (Eds.), Blackwell Publishing, 2007, pp. 436-439.

[9]W.J. Pottorf, T.M. Johanns, S.M. Derrington, E.E. Strehler, A. Enyedi, and S.A. Thayer, Glutamate-induced protease-mediated loss of plasma membrane Ca^{2+} pump activity in rat hippocampal neurons. J. Neurochem. 98 (2006) 1646-1656.

[10]A. Zaidi, L. Barron, V.S. Sharov, C. Schoneich, E.K. Michaelis, and M.L. Michaelis, Oxidative inactivation of purified plasma membrane Ca^{2+}-ATPase by hydrogen peroxide and protection by calmodulin. Biochemistry 42 (2003) 12001-12010.

[11]A. Zaidi, J. Gao, T.C. Squier, and M.L. Michaelis, Age-related decrease in brain synaptic membrane Ca^{2+}-ATPase in f344/bnf1 rats. Neurobiol. Aging 19 (1998) 487-495.

[12]A. Zaidi, and M.L. Michaelis, Effects of reactive oxygen species on brain synaptic plasma membrane Ca^{2+}-ATPase. Free Radical Biol. Med. 27 (1999) 810-821.

[13]K.D. Osborn, A. Zaidi, A. Mandal, R.J.B. Urbauer, and C.K. Johnson, Single molecule dynamics of the calcium-dependent activation of plasma-membrane Ca^{2+}-ATPase by calmodulin. *Biophys. J.* 87 (2004) 1892-1899.

[14]R. Padanyi, K. Paszty, A.R. Penheiter, A.G. Filoteo, J.T. Penniston, and A. Enyedi, Intramolecular interactions of the regulatory region with the catalytic core in the plasma membrane calcium pump. J. Biol. Chem. 278 (2003) 35798-35804.

[15]A.R. Penheiter, E. Bajzer, A.G. Filoteo, R. Thorogate, K. Torok, and A.J. Caride, A model for the activation of plasma membrane calcium pump isoform 4b by calmodulin. Biochemistry 42 (2003) 12115-12124.

[16]E.E. Strehler, A.J. Caride, A.G. Filoteo, Y.N. Xiong, J.T. Penniston, and A. Enyedi, Plasma membrane Ca^{2+}-atpases as dynamic regulators of cellular calcium handling. Ann. N. Y. Acad. Sci. 1099 (2007) 226-236.

[17]A. Enyedi, T. Vorherr, P. James, D.J. McCormick, A.G. Filoteo, E. Carafoli, and J.T. Penniston, The calmodulin binding domain of the plasma-membrane Ca^{2+} pump interacts both with calmodulin and with another part of the pump. J. Biol. Chem. 264 (1989) 12313-12321.

[18]Y.H. Yao, J. Gao, and T.C. Squier, Dynamic structure of the calmodulin-binding domain of the plasma membrane Ca^{2+}-ATPase in native erythrocyte ghost membranes. Biochemistry 35 (1996) 12015-12028.

[19]R. Falchetto, T. Vorherr, J. Brunner, and E. Carafoli, The plasma-membrane Ca^{2+} pump contains a site that interacts with its calmodulin-binding domain. J. Biol. Chem. 266 (1991) 2930-2936.

[20]H.Y. Sun, and T.C. Squier, Ordered and cooperative binding of opposing globular domains of calmodulin to the plasma membrane Ca^{2+}-ATPase. J. Biol. Chem. 275 (2000) 1731-1738.

[21]K.D. Osborn, Single molecule studies of the interaction of calmodulin with the plasma membrane Ca^{2+}- ATPase, Chemistry, University of Kansas, Lawrence, KS, 2003, pp. 150.

[22]K.D. Osborn, R.K. Bartlett, A. Mandal, A. Zaidi, R.J.B. Urbauer, J.L. Urbauer, N. Galeva, T.D. Williams, and C.K. Johnson, Single-molecule dynamics reveal an altered conformation for the autoinhibitory domain of plasma membrane Ca^{2+}-

ATPase bound to oxidatively modified calmodulin. Biochemistry 43 (2004) 12937-12944.

[23]K.D. Osborn, A. Zaidi, R.J.B. Urbauer, M.L. Michaelis, and C.K. Johnson, Single-molecule characterization of the dynamics of calmodulin bound to oxidatively modified plasma-membrane Ca^{2+}-ATPase. Biochemistry 44 (2005) 11074-11081.

[24]J.T. Penniston, and A. Enyedi, Modulation of plasma membrane Ca^{2+} pump. J. Membrane. Biol. 165 (1998) 101-109.

[25]D. Kosk-kosicka, T. Bzdega, and A. Wawrzynow, Fluorescence energy-transfer studies of purified erythrocyte Ca^{2+} -ATPase - Ca^{2+}-regulated activation by oligomerization. *J. Biol. Chem.* 264 (1989) 19495-19499.

[26]V. Levi, J. Ross, P.R. Castello, and F.L.G. Flecha, Structural significance of the plasma membrane calcium pump oligomerization. Biophys. J. 82 (2002) 437-446.

[27]M.M. Fonseca, H.M. Scofano, P.C. Carvalho-Alves, H. Barrabin, and J.A. Mignaco, Conformational changes of the nucleotide site of the plasma membrane Ca^{2+}-ATPase probed by fluorescence quenching. Biochemistry 41 (2002) 7483-7489.

[28]M.W. Allen, R.J.B. Urbauer, and C.K. Johnson, Single-molecule assays of calmodulin target binding detected with a calmodulin energy-transfer construct. Anal. Chem. 76 (2004) 3630-3637.

[29]G.H. Lushington, A. Zaidi, and M.L. Michaelis, Theoretically predicted structures of plasma membrane Ca^{2+}-ATPase and their susceptibilities to oxidation. J. Mol. Graph. Model. 24 (2005) 175-185.

[30]H.P. Lu, L.Y. Xun, and X.S. Xie, Single-molecule enzymatic dynamics. Science 282 (1998) 1877-1882.

[31]W.E. Moerner, and M. Orrit, Illuminating single molecules in condensed matter. Science 283 (1999) 1670-1676.

[32]H. Noji, R. Yasuda, M. Yoshida, and K. Kinosita, Direct observation of the rotation of f-1-ATPase. Nature 386 (1997) 299-302.

[33]S. Weiss, Measuring conformational dynamics of biomolecules by single molecule fluorescence spectroscopy. Nature Structural Biology 7 (2000) 724-729.

[34]X.S. Xie, and J.K. Trautman, Optical studies of single molecules at room temperature. Annu. Rev. Phys. Chem. 49 (1998) 441-480.

[35]S. Weiss, Fluorescence spectroscopy of single biomolecules. Science 283 (1999) 1676-1683.

[36]T. Ha, T. Enderle, D.F. Ogletree, D.S. Chemla, P.R. Selvin, and S. Weiss, Probing the interaction between two single molecules: Fluorescence resonance energy transfer between a single donor and a single acceptor. Proc. Natl. Acad. Sci. USA 93 (1996) 6264-6268.

[37]P.R. Selvin, The renaissance of fluorescence resonance energy transfer. Nature Structural Biology 7 (2000) 730-734.

[38]L. Stryer, and R.P. Haugland, Energy transfer - a spectroscopic ruler. Proc. Natl. Acad. Sci. USA 58 (1967) 719-&.

[39]B.W. Van der Meer, G. Cocker, and S.Y. Chen, Resonance energy transfer: Theory and data, VCH, New York, 1994.

[40]T. Ha, Single-molecule fluorescence resonance energy transfer. Methods 25 (2001) 78-86.

[41]C. Gell, D. Brockwell, and A. Smith, Hand book of single molecule fluorescence spectroscopy, Oxford university press, 2006.

[42]B.D. Slaughter, M.W. Allen, J.R. Unruh, R.J.B. Urbauer, and C.K. Johnson, Single-molecule resonance energy transfer and fluorescence correlation spectroscopy of calmodulin in solution. J. Phys. Chem. B 108 (2004) 10388-10397.

[43]B.D. Slaughter, J.R. Unruh, M.W. Allen, R.J.B. Urbauer, and C.K. Johnson, Conformational substates of calmodulin revealed by single-pair fluorescence resonance energy transfer: Influence of solution conditions and oxidative modification. Biochemistry 44 (2005) 3694-3707.

[44]J.R. Grunwell, J.L. Glass, T.D. Lacoste, A.A. Deniz, D.S. Chemla, and P.G. Schultz, Monitoring the conformational fluctuations of DNA hairpins using single-pair fluorescence resonance energy transfer. J. Am. Chem. Soc. 123 (2001) 4295-4303.

[45]A.G. Filoteo, J.P. Gorski, and J.T. Penniston, The ATP-binding site of the erythrocyte-membrane Ca^{2+} pump - amino-acid-sequence of the fluorescein isothiocyanate-reactive region. J. Biol. Chem. 262 (1987) 6526-6530.

[46]C. Toyoshima, Structural aspects of ion pumping by Ca^{2+}-ATPase of sarcoplasmic reticulum. Arch. Biochem. Biophys. 476 (2008) 3-11.

[47]A.R. Penheiter, A.J. Caride, A. Enyedi, and J.T. Penniston, Tryptophan 1093 is largely responsible for the slow off rate of calmodulin from plasma membrane Ca^{2+} pump 4b. J. Biol. Chem. 277 (2002) 17728-17732.